ASTROMETRY AND ASTROPHYSICS, NO. 5, PROBLEMS OF ATMOSPHERIC OPTICS

Edited by I. G. Kolchinskiy

"Naukova Dumka" Press, Kiev, 1969

NATIONAL AERONAUTICS AND SPACE ADMINISTRATION • WASHINGTON, D. C. • JUNE 1970

ASTROMETRY AND ASTROPHYSICS, NO. 5, PROBLEMS OF ATMOSPHERIC OPTICS

Edited by I. G. Kolchinskiy

Translation of "Astrometriya i Astrofizika, 5,
Voprosy Atmosfernoy Optiki"
"Naukova Dumka" Press, Kiev, 1969

NATIONAL AERONAUTICS AND SPACE ADMINISTRATION

For sale by the Clearinghouse for Federal Scientific and Technical Information
Springfield, Virginia 22151 – CFSTI price $3.00

This collection considers problems of correcting for refraction in observation of objects within the Earth's atmosphere as well as investigations of the influence of atmospheric dispersion on photographic astrometry and problems related to research of the astroclimate (observations of the scintillation of stars and star images). It is intended for specialists in astronomy and also for geophysicists interested in the influence of the atmosphere on optical images. /4

TABLE OF CONTENTS

TABLES OF REFRACTION CORRECTIONS FOR OBSERVATION OF OBJECTS IN THE EARTH'S ATMOSPHERE

I.G. Kolchinskiy, A.N. Kur'yanova, Ye.B. Shmel'kina

ABSTRACT: Tables of refraction angles for atmospheric objects are given. Calculations are made for standard atmospheric conditions.

In the observation of objects located within the Earth's atmo- /7* sphere, it is necessary to allow for bending of the path of the light rays, i.e. for the effect of refraction. In geodesic and astronomical observations, refraction has been taken into account for a long time. In the first case, the paths of the light rays pass near the Earth's surface; in the second case, these paths pass beyond the limits of the Earth's atmosphere. Although methods for calculating refraction corrections have been evolved over the course of many years, investigation in this direction continues even now.

At the present it is especially important to determine refraction corrections for observation of objects located in the upper strata of the atmosphere. Meteoric particles and artificial Earth satellites are among such objects. In the observation of such objects from Earth, the values of their spatial coordinates are distorted by refraction. Similar distortion appears in aerial photographs of the Earth's surface, taken from very great heights.

In the propagation of various radiations through the Earth's atmosphere, especially those generated by laser sources, the effect of refraction on the distortion of the path of a light ray must be taken into account. Here it is necessary to solve problems analogous to those arising from the propagation of ultrashort radio waves in the atmosphere.

Practical requirements led to the appearance of a number of articles giving approximate formulas for the appropriate corrections, as well as tables of their values of various altitudes and zenith distances. A survey of these investigations is given in reference [1]. We are mainly concerned with elements of the path of light rays in the atmosphere. Such tables were calculated by F. Link and Z. Sekera [9]. These tables, using the argument of the visible zenith distance and the height above the Earth's surface, give the following elements characterizing the path of a ray in the atmosphere (Fig. 1): (1) the complete refraction r, i.e. the angle between the tangents to the ray through the point of observation A and the point of the object's position B; (2) the length of the arc s on the ray from the point of observation to the object; (3) the

---

* Numbers in the margin indicate pagination in the foreign text.

angle ϕ at the center of the Earth between the radii passing through the point of observation and the point of the object's position; (4) the angle i between the direction of the radius passing through a given point on the path P and the direction of the tangent to the ray at the same point. /8

The tables also give differential changes of r as a function of the zenith distance and the altitude. The tables are calculated according to data from aerological observations for several mean atmospheric conditions observed in Central Europe in the winter and summer.

For observations of objects located within the Earth's atmosphere, it is important to know the angles r_A and r_B (see Fig. 1), for which the equation

$$r_A + r_B = r. \qquad (1)$$

is valid. The angle r_A represents the difference between the true zenith distance of the object z and its visible zenith distance ζ, i.e.

$$r_A = z - \zeta.$$

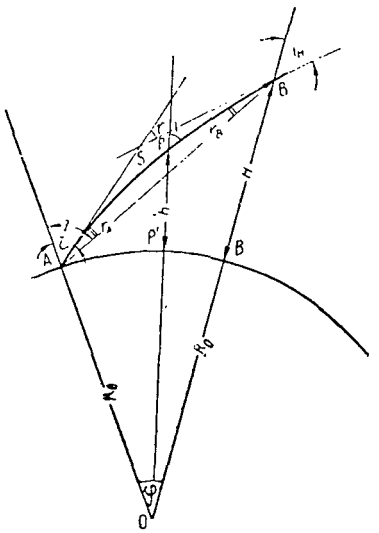

Fig. 1.

The angle r_B is sometimes called the photogrammetric angle of refraction, or the refraction parallax. Link and Sekera do not give any value for these angles in their tables. A small table of values for the angles r_A in the altitude range of 1 - 15 km and for zenith distances of 60 - 85° is calculated using approximate formulas by V. Numerova and presented in her article [2]. The values of r_A are given here with an accuracy of up to 0.1'.

The present article gives values for r_A and r_B calculated according to data on the Earth's atmosphere corresponding to the standard GOST (All-Union State Standard) 4401-64 atmosphere [3]. This atmosphere, in any case for the purpose of calculating refraction, can be considered practically coincident with the standard COSPAR atmosphere [10]. The initial values of air pressure and temperature on the Earth's surface for the GOST 4401-64 standard atmosphere are 1013.25 mb and 288.15° K. Table 1 gives certain data on the GOST 4401-64 atmosphere.

Calculation of angles r_A and r_B was carried out in the following manner. First of all, the angle ϕ was calculated according to formula (2), derived from the general refraction theory /9

$$\varphi = \int_{R_0}^{R_0+H} \tan i \frac{dR}{R}, \tag{2}$$

TABLE 1

Height H, km	Temperature T, °K	Relative Density	Height H, km	Temperature T, °K	Relative Density
0	288.15	1.0000	80	185.00	0.000017
11	216.66	0.29784	95	185.00	$1.16 \cdot 10^{-6}$
25	216.66	0.03316	115	294.97	$4.14 \cdot 10^{-8}$
46	274.00	0.00143	150	980.05	$1.4 \cdot 10^{-9}$
54	274.00	0.00054	200	1226.8	$2.9 \cdot 10^{-10}$

where tan i were determined according to the formula

$$\tan i = \frac{\frac{\mu_0 R_0}{\mu R} \sin\zeta}{\sqrt{1 - \left(\frac{\mu_0 R_0}{\mu R}\right)^2 \sin^2\zeta}}, \tag{3}$$

which follows from the dependence

$$\mu_0 R_0 \sin\zeta = \mu (R_0 + h) \sin i. \tag{4}$$

Here μ_0 and μ are the values of the refractive indices of the air at given conditions at the Earth's surface and at a height h; R_0 is the Earth's radius; i is the zenith distance of the ray at the height h; $R = R_0 + h$ ($h = PP'$). The values of μ_0 and μ were determined on the basis of the known formula of Gladstone and Dale

$$\mu = 1 + C_\lambda \rho, \tag{5}$$

where ρ is the density of the gas, being a function of the height h, C_λ is the constant for a given wavelength. The value of C_λ for dry air is determined by using the value of μ at a given temperature and air pressure. In formula (5) ρ symbolizes the value of the density with reference to a certain standard value ρ_0 at the Earth's surface, such that

$$\rho = \frac{\rho(h)}{\rho_0}.$$

If the value of ρ_0 corresponds to conditions where P_0 = 1013.25 mb, /10 T_0 = 288.15° K, then according to the tables of standard values in the "Spravochnik po geofizike" (Geophysics Handbook) [4] for a wavelength λ = 530 mμ in the case of dry air, C_λ = 0.00027824.

A 530 mμ wavelength is equal to the reference wavelength in Link and Sekera's tables. This is near the wavelength corresponding to the maximum sensitivity of the eye in daylight (550 mμ).

In calculating ϕ, a value of R_0 was taken equal to 6471.21 km. Then the value of the angle r_A was determined according to the formula

$$r_A = z - \zeta = \operatorname{arc\,tan} \frac{R \sin \varphi}{R \cos \varphi - R_0} - \zeta, \tag{6}$$

which can be derived on the basis of Figure 1.
The value of the angle r was determined from the formula

$$r = -\int_{R_0}^{R_0+H} \frac{\tan i \, d\mu}{\mu} = -C_\lambda \int_{R}^{R_0+H} \frac{\operatorname{tg} i}{1 + C_\lambda \rho} \cdot \frac{d\rho}{dR} dR. \tag{7}$$

The values of $\frac{d\rho}{dR}$ were determined from the differences between the values of ρ at the corresponding heights, according to the tables of the standard atmosphere. Then r_B was determined from formula (1). Calculations were carried out within the variational range of the zenith distances 1 - 88° and for the heights 5 - 40 km. The interval of change of ζ was 1°, and of H, 1 km. The integrals were calculated on an electronic computer according to the Simpson formula with a height interval every 0.5 km. Thus, the number of elementary strata contained in the integral varied with the height of the object above the Earth's surface from 10 to 80. The values of the derivatives $\frac{d\rho}{dR}$ for a height h were calculated from the values of the density at the points h + 0.25 km and h - 0.25 km, such that

$$\left(\frac{\Delta\rho}{\Delta h}\right)_h = \frac{\rho(h+0.25) - \rho(h-0.25)}{0.5}.$$

The terminal values of the angles were calculated with an accuracy of up to 0.01". The tables give the values rounded off to 0.1". The maximum error of the approximate integration, under the condition that the values of the air density and its derivative be exact values, at a zenith distance of 88° and at a height of 40 km, is approximately 2", i.e. approximately 0.2% of the value of the angle r. The values /11 of r_A, r_B and r are given in Tables 2, 3 and 4 respectively. In certain cases the equation $r = r_A + r_B$ is satisfied approximately, due to the fact that the values of r_B derived from the formula $r_B = r - r_A$ were obtained using values of r and r_A with an accuracy of up to 0.01", after which they were rounded off.

Comparison of the Tables Obtained with Other Tables

We shall compare the values of the angles of refraction obtained in our tables with the values presented by other authors.

Comparison of the values of the angle r with analogous values from Link and Sekera's tables. It is convenient to carry out this comparison using the values of r obtained by Link and Sekera for the summer period. These values were obtained using Gemfris' aerological data for Central Europe (up to 20 km) [5]. These correspond to an initial temperature of + 14.76°C (288°K) and to a mean pressure at sea level which can be considered equal to the initial pressure assumed by us for the standard atmosphere. Link and Sekera took a reference value of the refractive index equal to 1.000293 (for λ = 530 mμ at a temperature of 0°C, and a pressure of 760 mm). According to the tables presented in the "Geophysics Handbook", which we used, this value would be equal to 1.00029352. If the absolute temperature T and the air pressure P at the Earth's surface deviate from the standard, then from formula (5) on the basis of known laws for ideal gases

$$\frac{(\mu-1)_{T,P}}{(\mu-1)_{T_0,P_0}}=\frac{\rho_{T,P}}{\rho_{T_0,P_0}}=\frac{P}{P_0}\cdot\frac{T_0}{T}. \tag{8}$$

It can be considered (with sufficient accuracy for our comparison) that the refraction is proportional to values of μ-1 at different conditions, i.e.

$$\frac{r_{T,P}}{r_{T_0,P_0}}=\frac{P}{P_0}\cdot\frac{T_0}{T}. \tag{9}$$

Taking this into account and bearing in mind the small difference between the reference values μ-1, in order to make the transition from the refraction values in Link and Sekera's Tables to ours, it is necessary to multiply their data by the coefficient

$$K=\frac{288.0}{288.2}\cdot\frac{293.5}{293.0}\approx 1.001.$$

Allowing for this correction, the values of the refraction r according to Link and Sekera's data and according to our data are presented in Table 5. The resultant differences can be explained in part by differences in the assumed atmospheric conditions. The fact is that at a height of 1 km the relative density of Link and Sekera's atmosphere is 0.898, while the standard atmosphere has a density of 0.908. In the first case, the gradient of the decrease of density at a height of 0 - 1 km is equal to 0.102, in the second case it is 0.092. In the higher strata it is true that the difference in the

TABLE 2

ζ, Degrees	Height H, km																	
	5	6	7	8	9	10	11	12	13	14	15	16	17	18	19	20	21	22
1	0.2	0.2	0.3	0.3	0.4	0.4	0.4	0.4	0.4	0.5	0.5	0.5	0.6	0.6	0.6	0.6	0.6	0.6
2	0.4	0.5	0.6	0.6	0.7	0.8	0.8	0.9	0.9	1.0	1.0	1.0	1.1	1.1	1.2	1.2	1.2	1.3
3	0.6	0.8	0.9	1.0	1.0	1.1	1.2	1.3	1.4	1.4	1.5	1.6	1.6	1.7	1.8	1.8	1.9	1.9
4	0.9	1.0	1.1	1.3	1.4	1.5	1.6	1.7	1.8	1.9	2.0	2.1	2.2	2.3	2.3	2.4	2.5	2.5
5	1.1	1.3	1.4	1.6	1.7	1.9	2.0	2.2	2.3	2.4	2.5	2.6	2.7	2.8	2.9	3.0	3.1	3.2
6	1.3	1.5	1.7	1.9	2.1	2.3	2.4	2.6	2.7	2.9	3.0	3.2	3.3	3.4	3.5	3.6	3.7	3.8
7	1.5	1.8	2.0	2.2	2.4	2.7	2.8	3.0	3.2	3.4	3.6	3.7	3.9	4.0	4.1	4.2	4.4	4.5
8	1.7	2.0	2.3	2.6	2.8	3.0	3.3	3.5	3.7	3.9	4.1	4.2	4.4	4.6	4.7	4.8	5.0	5.1
9	2.0	2.3	2.6	2.9	3.2	3.4	3.7	3.9	4.2	4.4	4.6	4.8	5.0	5.2	5.3	5.5	5.6	5.8
10	2.2	2.6	2.9	3.2	3.5	3.8	4.1	4.4	4.6	4.9	5.3	5.3	5.6	5.7	5.9	6.1	6.2	6.4
1	2.4	2.8	3.2	3.6	3.9	4.2	4.5	4.8	5.1	5.4	5.6	5.9	6.1	6.3	6.5	6.7	6.9	7.0
2	2.6	3.0	3.5	3.9	4.2	4.6	4.9	5.3	5.6	5.9	6.2	6.4	6.7	6.9	7.1	7.3	7.5	7.7
3	2.9	3.3	3.8	4.2	4.6	5.0	5.4	5.7	6.1	6.4	6.7	7.0	7.2	7.5	7.8	8.0	8.2	8.4
4	3.1	3.6	4.1	4.5	5.0	5.4	5.8	6.2	6.5	6.9	7.2	7.5	7.8	8.1	8.4	8.6	8.8	9.0
5	3.3	3.8	4.4	4.9	5.3	5.8	6.2	6.6	7.0	7.4	7.7	8.1	8.4	8.7	9.0	9.2	9.5	9.7
6	3.6	4.1	4.7	5.2	5.7	6.2	6.7	7.1	7.5	7.9	8.3	8.7	9.0	9.3	9.6	9.9	10.2	10.4
7	3.8	4.4	5.0	5.6	6.1	6.6	7.1	7.6	8.0	8.5	8.8	9.2	9.6	9.9	10.2	10.5	10.8	11.1
8	4.0	4.7	5.3	5.9	6.5	7.0	7.5	8.0	8.5	9.0	9.4	9.8	10.2	10.5	10.9	11.2	11.5	11.8
9	4.2	5.0	5.6	6.3	6.8	7.5	8.0	8.5	9.0	9.5	10.0	10.4	10.8	11.2	11.5	11.9	12.2	12.5
20	4.5	5.2	5.9	6.6	7.2	7.9	8.4	9.0	9.5	10.0	10.5	11.0	11.4	11.8	12.2	12.5	12.8	13.2
1	4.7	5.5	6.3	7.0	7.6	8.3	8.9	9.5	10.1	10.6	11.1	11.6	12.0	12.5	12.8	13.2	13.6	13.9
2	5.0	5.8	6.6	7.4	8.1	8.8	9.4	10.0	10.6	11.2	11.7	12.2	12.7	13.1	13.6	13.9	14.3	14.6
3	5.2	6.1	7.0	7.7	8.5	9.2	9.9	10.5	11.1	11.7	12.3	12.8	13.3	13.8	14.2	14.6	15.0	15.4
4	5.5	6.4	7.3	8.1	8.9	9.6	10.3	11.0	11.6	12.3	12.9	13.4	14.0	14.4	14.9	15.3	15.7	16.1
5	5.8	6.7	7.6	8.5	9.3	10.1	10.8	11.6	12.2	12.7	13.5	14.1	14.6	15.1	15.6	16.1	16.5	16.9
6	6.0	7.0	8.0	8.9	9.7	10.5	11.3	12.1	12.8	13.5	14.1	14.7	15.3	15.8	16.3	16.8	17.2	17.7
7	6.3	7.3	8.3	9.3	10.2	11.0	11.8	12.6	13.4	14.1	14.8	15.4	16.0	16.5	17.1	17.5	18.0	18.4
8	6.6	7.6	8.7	9.7	10.6	11.5	12.4	13.2	13.9	14.7	15.4	16.0	16.7	17.3	17.8	18.3	18.8	19.2
9	6.8	7.9	9.0	10.1	11.0	12.0	12.8	13.7	14.5	15.3	16.0	16.7	17.4	18.0	18.6	19.1	19.6	20.1
30	7.1	8.3	9.5	10.5	11.5	12.5	13.4	14.3	15.1	15.9	16.7	17.4	18.1	18.7	19.3	19.9	20.4	20.9
1	7.4	8.6	9.8	10.9	12.0	13.0	13.9	14.9	15.7	16.6	17.4	18.1	18.8	19.5	20.1	20.7	21.2	21.8
2	7.7	9.0	10.2	11.4	12.5	13.5	14.5	15.5	16.4	17.3	18.1	18.8	19.6	20.3	20.9	21.5	22.1	22.6
3	8.0	9.3	10.6	11.8	12.9	14.0	15.1	16.1	17.0	17.9	18.8	19.6	20.3	21.0	21.7	22.3	22.9	23.5
4	8.3	9.6	11.0	12.3	13.4	14.6	15.7	16.7	17.7	18.6	19.5	20.4	21.1	21.9	22.6	23.2	23.8	24.4
5	8.6	10.0	11.4	12.8	14.0	15.1	16.2	17.3	18.4	19.4	20.3	21.1	21.9	22.7	23.4	24.1	24.8	25.3
6	8.9	10.4	11.9	13.2	14.5	15.7	16.8	18.0	19.1	20.1	21.0	21.9	22.8	23.6	24.3	25.0	25.7	26.3
7	9.3	10.8	12.1	13.7	15.0	16.3	17.5	18.6	19.7	20.8	21.8	22.7	23.6	24.4	25.2	26.0	26.6	27.3
8	9.6	11.2	12.8	14.2	15.6	16.9	18.1	19.4	20.5	21.6	22.6	23.6	24.5	24.5	26.2	26.9	27.6	28.3
9	10.0	11.6	13.2	14.7	16.1	17.5	18.8	20.0	21.2	22.4	23.4	24.4	25.4	26.3	27.1	27.9	28.6	29.3
40	10.3	12.0	13.7	15.3	16.7	18.1	19.4	20.8	22.0	23.1	24.3	25.3	26.3	27.2	28.1	28.9	29.6	30.4
1	10.7	12.4	14.2	15.8	17.3	18.8	20.2	21.5	22.8	24.0	25.1	26.2	27.2	28.2	29.1	29.9	30.7	31.4
2	11.0	12.9	14.7	16.4	17.9	19.4	20.8	22.3	23.6	24.8	26.0	27.1	28.3	29.2	30.1	31.0	31.8	32.6
3	11.4	13.4	15.2	16.9	18.6	20.2	21.6	23.1	24.4	25.7	27.0	28.1	29.2	30.2	31.2	32.1	32.9	33.7
4	11.9	13.8	15.7	17.5	19.2	20.9	22.4	23.9	25.3	26.6	27.9	29.1	30.2	31.3	32.3	33.2	34.1	34.9
5	12.2	14.3	16.3	18.2	19.9	21.6	23.2	24.7	26.2	27.6	28.9	30.1	31.3	32.4	33.5	34.4	35.3	36.2
6	12.7	14.8	16.9	18.8	20.6	22.4	24.0	25.6	27.1	28.6	29.9	31.2	32.4	33.6	34.6	35.6	36.6	37.4
7	13.1	15.4	17.5	19.5	21.4	23.2	24.9	26.5	28.1	29.6	31.0	32.3	33.6	34.8	35.9	36.9	37.9	38.8

TABLE 2 (cont'd)

ζ, Degrees	Height H, km																	
	23	24	25	26	27	28	29	30	31	32	33	34	35	36	37	38	39	40
1	0.6	0.7	0.7	0.7	0.7	0.7	0.7	0.7	0.7	0.7	0.7	0.7	0.8	0.8	0.8	0.8	0.8	0.8
2	1.3	1.3	1.3	1.4	1.4	1.4	1.4	1.4	1.5	1.5	1.5	1.5	1.5	1.5	1.6	1.6	1.6	1.6
3	1.9	2.0	2.0	2.0	2.1	2.1	2.2	2.2	2.2	2.2	2.2	2.3	2.3	2.3	2.3	2.3	2.4	2.4
4	2.6	2.6	2.7	2.7	2.8	2.8	2.8	2.9	2.9	3.0	3.0	3.0	3.0	3.1	3.1	3.1	3.1	3.2
5	3.2	3.3	3.4	3.4	3.5	3.5	3.6	3.6	3.6	3.7	3.7	3.8	3.8	3.8	3.9	3.9	3.9	4.0
6	3.9	4.0	4.0	4.1	4.2	4.2	4.3	4.4	4.4	4.5	4.5	4.5	4.6	4.6	4.7	4.7	4.7	4.7
7	4.5	4.6	4.7	4.8	4.9	5.0	5.0	5.1	5.1	5.2	5.3	5.3	5.3	5.4	5.4	5.5	5.5	5.6
8	5.2	5.3	5.4	5.5	5.6	5.7	5.8	5.8	5.9	6.0	6.0	6.1	6.1	6.2	6.2	6.3	6.3	6.4
9	5.9	6.0	6.1	6.2	6.3	6.4	6.5	6.6	6.6	6.7	6.8	6.8	6.9	7.0	7.0	7.1	7.1	7.2
10	6.5	6.7	6.8	6.9	7.0	7.1	7.2	7.3	7.4	7.5	7.6	7.6	7.7	7.8	7.8	7.9	7.9	8.0
1	7.2	7.3	7.5	7.6	7.7	7.8	7.9	8.0	8.2	8.2	8.3	8.4	8.5	8.5	8.6	8.7	8.8	8.8
2	7.9	8.0	8.2	8.3	8.5	8.6	8.7	8.8	8.9	9.0	9.1	9.2	9.3	9.3	9.4	9.5	9.6	9.7
3	8.6	8.7	8.9	9.0	9.2	9.3	9.4	9.6	9.7	9.8	9.9	10.0	10.1	10.2	10.2	10.3	10.4	10.5
4	9.2	9.4	9.6	9.8	9.9	10.0	10.2	10.3	10.4	10.5	10.7	10.8	10.9	11.0	11.0	11.1	11.2	11.3
5	9.9	10.1	10.3	10.5	10.6	10.8	10.9	11.1	11.2	11.3	11.4	11.6	11.6	11.8	11.9	11.9	12.0	12.1
6	10.6	10.8	11.0	11.2	11.4	11.6	11.7	11.8	12.0	12.2	12.3	12.4	12.5	12.6	12.7	12.8	12.9	13.0
7	11.3	11.5	11.8	11.9	12.2	12.3	12.5	12.6	12.8	12.9	13.1	13.2	13.3	13.4	13.5	13.6	13.7	13.8
8	12.0	12.2	12.5	12.7	12.9	13.1	13.3	13	13.6	13.7	13.9	14.0	14.2	14.3	14.4	14.5	14.6	14.7
9	12.8	13.0	13.2	13.5	13.7	13.9	14.1	14.2	14.4	14.6	14.7	14.9	15.0	15.1	15.3	15.4	15.5	15.6
20	13.4	13.7	14.0	14.2	14.4	14.7	14.8	15.0	15.2	15.4	15.6	15.7	15.8	16.0	16.1	16.2	16.3	16.5
1	14.2	14.5	14.8	15.0	15.2	15.5	15.7	15.9	16.1	16.2	16.4	16.6	16.7	16.8	17.0	17.1	17.2	17.4
2	15.0	15.3	15.6	15.8	16.1	16.3	16.5	16.7	16.9	17.1	17.3	17.4	17.6	17.8	17.9	18.0	18.2	18.3
3	15.7	16.0	16.3	16.6	16.8	17.2	17.4	17.6	17.8	18.0	18.2	18.3	18.5	18.6	18.8	18.9	19.1	19.2
4	16.5	16.8	17.1	17.4	17.7	18.0	18.2	18.4	18.6	18.8	19.0	19.2	19.4	19.6	19.7	19.9	20.0	20.2
5	17.2	17.6	18.0	18.2	18.5	18.8	19.1	19.3	19.5	19.7	20.0	20.2	20.3	20.5	20.7	20.8	21.0	21.1
6	18.0	18.4	18.8	19.1	19.4	19.7	19.9	20.2	20.4	20.6	20.8	21.0	21.2	21.4	21.6	21.8	21.9	22.0
7	18.8	19.2	19.6	19.9	20.2	20.5	20.8	21.1	21.3	21.6	21.9	22.0	22.2	22.	22.6	22.7	22.9	23.1
8	19.7	20.1	20.4	20.8	21.1	21.4	21.7	22.0	22.3	22.5	22.7	23.0	23.2	23.4	23.6	23.7	23.9	24.1
9	20.5	20.9	21.3	21.7	22.0	22.3	22.6	22.9	23.2	23.4	23.7	23.9	24.1	24.3	24.6	24.7	24.9	25.1
30	21.4	21.8	22.2	22.6	22.9	23.3	23.6	23.9	24.2	24.4	24.7	24.9	25.1	25.4	25.6	25.7	25.9	26.1
1	22.2	22.7	23.1	23.5	23.6	24.2	24.6	24.8	25.1	25.4	25.7	25.9	26.2	26.4	26.6	26.8	27.0	27.2
2	23.1	23.6	24.0	24.4	24.8	25.2	25.5	25.8	26.2	26.4	26.7	27.0	27.2	27.4	27.7	27.9	28.1	28.3
3	24.0	24.5	24.9	25.4	25.8	26.2	26.5	26.8	27.2	27.5	27.7	28.0	28.3	28.5	28.7	28.9	29.2	29.4
4	24.9	25.4	25.9	26.4	26.8	27.2	27.6	27.9	28.2	28.6	28.8	29.1	29.4	29.6	29.9	30.1	30.3	30.5
5	25.9	26.4	26.9	27.4	27.8	28.2	28.6	29.0	29.3	29.6	29.9	30.2	30.5	30.8	31.0	31.2	31.5	31.7
6	26.9	27.4	27.9	28.4	28.9	29.3	29.7	30.1	30.4	30.8	31.1	31.4	31.7	31.9	32.2	32.4	32.6	32.9
7	27.8	28.4	29.0	29.4	29.9	30.4	30.8	31.2	31.5	31.9	32.2	32.5	32.8	33.1	33.4	33.6	33.8	34.1
8	28.9	29.5	30.0	30.6	31.0	31.5	31.9	32.3	32.7	33.0	33.4	33.7	34.0	34.3	34.6	34.9	35.1	35.3
9	29.9	30.6	31.1	31.6	32.1	32.6	33.1	33.5	33.9	34.2	34.6	34.9	35.2	35.6	35.8	36.1	36.4	36.6
40	31.0	31.6	32.2	32.8	33.3	33.8	34.2	34.7	35.1	35.5	35.8	36.2	36.5	36.8	37.1	37.4	37.7	37.9
1	32.1	32.8	33.4	34.0	34.5	35.0	35.5	35.9	36.3	36.7	37.1	37.5	37.8	38.1	38.5	38.7	39.0	39.3
2	33.3	34.0	34.6	35.2	35.7	36.3	36.7	37.2	37.6	38.1	38.4	38.8	39.2	39.5	39.8	40.1	40.4	40.7
3	34.5	35.2	35.8	36.4	37.0	37.6	38.1	38.6	39.0	39.4	39.8	40.2	40.6	40.9	41.3	41.6	41.9	42.2
4	35.7	36.4	37.1	37.7	38.3	38.9	39.4	39.9	40.4	40.8	41.2	41.6	42.0	42.4	42.7	43.0	43.4	43.6
5	36.9	37.7	38.4	39.0	39.7	40.3	40.8	41.3	41.8	42.3	42.7	43.1	43.5	43.9	44.2	44.6	44.9	45.2
6	38.2	39.0	39.8	40.4	41.1	41.7	42.2	42.8	43.3	43.8	44.2	44.6	45.0	45.4	45.8	46.1	46.4	46.8
7	39.6	40.4	41.2	41.9	42.5	43.2	43.8	44.3	44.8	45.3	45.8	46.2	46.7	47.0	47.4	47.8	48.1	48.4

/14
/15

TABLE 2 (cont'd)

ζ Degrees	Height H, km																	
	5	6	7	8	9	10	11	12	13	14	15	16	17	18	19	20	21	22
48	13.6	15.9	18.1	20.2	22.1	24.0	25.8	27.4	29.1	30.6	32.1	33.5	34.8	36.0	37.2	38.2	39.2	40.1
9	14.1	16.5	18.7	20.8	22.9	24.9	26.7	28.4	30.1	31.7	33.2	34.7	36.0	37.3	38.5	39.6	40.6	41.6
50	14.6	17.0	19.4	21.6	23.7	25.7	27.6	29.4	31.2	32.9	34.4	35.9	37.3	38.6	39.8	41.0	42.1	43.1
1	15.2	17.7	20.1	22.4	24.6	26.7	28.6	30.5	32.3	34.1	35.7	37.2	38.7	40.0	41.3	42.5	43.6	44.6
2	15.7	18.3	20.8	23.2	25.4	27.7	29.7	31.6	33.5	35.3	37.0	38.6	40.1	41.5	42.8	44.0	45.2	46.3
3	16.2	19.0	21.6	24.0	26.4	28.6	30.7	32.8	34.7	36.6	38.3	40.0	41.5	43.0	44.4	45.6	46.8	47.9
4	16.8	19.7	22.4	25.0	27.4	29.7	31.9	34.0	36.0	37.9	39.8	41.4	43.1	44.6	46.0	47.3	48.6	49.7
5	17.4	20.4	23.2	25.9	28.4	30.8	33.1	35.3	37.3	39.3	41.2	43.0	44.7	46.2	47.7	49.0	50.4	51.6
6	18.1	21.2	24.1	26.9	29.5	32.0	34.4	36.6	38.8	40.9	42.8	44.6	46.4	48.0	49.5	51.0	52.3	53.5
7	18.8	22.0	25.1	27.9	30.6	33.2	35.7	38.0	40.2	42.4	44.4	46.4	48.1	49.8	51.4	52.9	54.3	55.6
8	19.5	22.8	26.0	29.0	31.8	34.5	37.0	39.5	41.8	44.0	46.1	48.1	50.0	51.8	53.4	54.9	56.4	57.6
9	20.3	23.7	27.0	30.1	33.0	35.8	38.5	41.0	43.5	45.8	48.0	50.0	52.0	53.8	55.5	57.1	58.6	60.0
60	21.1	24.6	28.1	31.3	34.4	37.3	40.1	42.7	45.2	47.6	49.9	52.1	54.1	56.0	57.8	59.4	61.0	62.4
1	22.0	25.7	29.3	32.6	35.8	38.9	41.7	44.5	47.1	49.6	52.2	54.2	56.4	58.3	60.2	61.9	63.5	65.0
2	22.9	26.8	30.5	34.0	37.4	40.5	43.5	46.4	49.1	51.7	54.2	56.5	58.7	60.8	62.7	64.5	66.2	67.8
3	23.9	27.9	31.8	35.5	38.9	42.2	45.4	48.4	51.2	54.0	56.5	59.0	61.3	63.4	65.4	67.2	69.0	70.7
4	25.0	29.2	33.2	37.1	40.6	44.1	47.4	50.5	53.5	56.3	59.0	61.6	64.0	66.2	68.3	70.2	72.1	73.8
5	26.2	30.6	34.8	38.8	42.6	46.2	49.6	52.8	55.9	58.9	61.8	64.4	66.9	69.2	71.4	73.5	75.4	77.2
6	27.4	32.0	36.4	40.6	44.6	48.3	51.9	55.3	58.6	61.7	64.7	67.4	70.0	72.5	74.8	76.9	78.9	80.8
7	28.7	33.6	38.2	42.6	46.8	50.7	54.4	58.0	61.4	64.7	67.8	70.7	73.4	76.0	78.4	80.6	82.8	84.7
8	30.1	35.3	40.1	44.7	49.1	53.2	57.2	60.9	64.5	67.9	71.2	74.2	77.1	79.8	82.3	84.7	86.9	89.0
9	31.7	36.8	42.2	47.0	51.6	56.0	60.1	64.0	67.8	71.8	74.8	78.0	81.1	83.9	86.6	89.0	91.4	93.5
70	33.4	39.0	44.5	49.6	54.4	59.0	63.3	67.5	71.5	75.3	78.9	82.3	85.4	88.4	91.2	93.8	96.3	98.6
1	35.3	41.3	47.0	52.4	57.5	62.4	66.9	71.3	75.6	79.6	83.3	86.9	90.3	93.4	96.4	99.1	101.7	104.1
2	37.3	43.7	49.8	55.5	60.9	66.0	70.8	75.5	80.0	84.2	88.2	92.0	95.5	98.9	102.0	104.9	107.6	110.2
3	39.7	46.5	52.9	59.0	64.7	70.2	75.3	80.2	85.0	89.5	93.7	97.7	101.5	105.0	108.3	111.4	114.3	117.0
4	42.3	49.5	56.4	62.8	68.9	74.7	80.2	85.4	90.5	95.2	99.8	104.0	108.0	111.8	115.3	118.6	121.6	124.5
5	45.2	52.9	60.2	67.1	73.7	79.8	85.7	91.3	96.7	101.8	106.6	111.1	115.4	119.4	123.1	126.6	129.9	133.0
6	48.6	56.8	64.7	72.1	79.1	85.7	92.0	98.0	103.7	109.2	114.4	119.2	123.8	128.1	132.1	135.8	139.3	142.6
7	52.4	61.4	69.8	77.8	85.3	92.5	99.2	105.7	111.9	117.7	123.3	128.5	133.4	138.0	142.3	146.3	150.1	153.6
8	56.9	66.5	75.7	84.3	92.5	100.2	107.5	114.5	121.2	127.5	133.5	139.2	144.4	149.4	154.1	158.4	162.4	166.2
9	62.2	72.6	82.6	92.0	100.9	109.3	117.2	124.8	132.1	139.0	145.5	151.6	157.4	162.8	167.8	172.5	176.9	181.0
80	68.4	80.0	90.9	101.2	111.0	120.2	128.8	137.2	145.1	152.6	159.7	166.4	172.7	178.6	184.1	189.2	194.0	198.5
1	75.9	88.6	100.7	112.2	122.9	133.1	142.7	151.8	160.6	168.8	176.7	184.0	190.9	197.4	203.4	209.0	214.3	219.2
2	85.3	99.6	113.2	125.9	137.9	149.2	159.9	170.0	179.8	189.0	197.6	205.8	213.4	220.5	227.2	233.4	239.2	244.6
3	97.2	113.4	128.8	143.1	156.7	169.4	181.4	192.8	203.7	214.0	223.7	232.8	241.3	249.2	256.7	263.6	270.1	276.1
4	112.7	131.4	148.9	165.4	180.8	195.4	209.0	221.9	234.3	246.0	256.9	267.2	276.8	285.7	294.1	301.9	309.1	315.9
5	133.8	155.7	176.2	195.4	213.3	230.4	245.8	260.8	274.9	288.3	300.8	312.5	323.4	333.6	343.1	351.9	360.2	367.8
6	164.3	190.6	215.0	237.7	258.9	278.6	297.1	314.4	330.9	346.3	360.8	374.3	386.8	398.5	409.4	419.5	428.9	437.7
7	210.5	242.8	272.6	300.1	325.5	349.1	370.9	391.4	410.7	428.8	445.6	461.2	475.8	489.3	501.9	513.5	524.4	534.6
88	288.1	328.8	365.7	399.4	430.2	458.6	484.6	508.8	531.5	552.6	572.3	590.5	607.4	623.1	637.6	651.2	663.8	675.6

TABLE 2 (cont'd)

ζ, Degrees	Height H, km								Height H, km									
	23	24	25	26	27	28	29	30	31	32	33	34	35	36	37	38	39	40
48	41.0	41.8	42.6	43.4	44.1	44.7	45.3	45.9	46.1	46.9	47.4	47.9	48.3	48.7	49.1	49.5	49.8	50.2
9	42.5	43.4	44.2	44.9	45.6	46.3	46.9	47.5	48.1	48.6	49.1	49.6	50.0	50.4	50.9	51.3	51.6	52.0
50	44.0	44.9	45.7	46.5	47.2	47.9	48.6	49.2	49.8	50.3	50.8	51.3	51.8	52.2	52.7	53.0	53.4	53.8
1	45.6	46.5	47.4	48.2	49.0	49.7	50.4	51.0	51.6	52.2	52.7	53.2	53.7	54.1	54.6	55.0	55.4	55.8
2	47.3	48.2	49.1	50.0	50.8	51.5	52.2	52.9	53.5	54.1	54.6	55.2	55.6	56.1	56.6	57.0	57.4	57.8
3	49.0	50.0	50.9	51.8	52.6	53.4	54.1	54.8	55.4	56.0	56.6	57.1	57.7	58.2	58.6	59.1	59.5	59.9
4	50.8	51.8	52.8	53.7	54.5	55.3	56.1	56.8	57.5	58.1	58.7	59.3	59.8	60.3	60.8	61.3	61.7	62.1
5	52.7	53.7	54.7	55.7	56.6	57.4	58.2	58.9	59.6	60.2	60.9	61.5	62.0	62.5	63.1	63.5	64.0	64.4
6	54.7	55.8	56.8	57.8	58.7	59.6	60.4	61.2	61.9	62.6	63.2	63.8	64.4	64.9	65.5	66.0	66.4	66.9
7	56.8	58.0	59.0	60.0	61.0	61.9	62.7	63.5	64.2	65.0	65.6	66.2	66.9	67.4	68.0	68.5	69.0	69.4
8	59.0	60.2	61.3	62.4	63.3	64.3	65.1	65.9	66.7	67.5	68.2	68.8	69.4	70.0	70.6	71.1	71.6	72.1
9	61.3	62.6	63.7	64.8	65.8	66.8	67.7	68.6	69.4	70.1	70.8	71.5	72.2	72.8	73.4	74.0	74.5	75.0
60	63.8	65.1	66.3	67.4	68.5	69.5	70.4	71.4	72.2	73.0	73.7	74.4	75.1	75.7	76.4	76.9	77.4	78.0
1	66.5	67.8	69.1	70.2	71.3	72.4	73.4	74.3	75.2	76.0	76.8	77.5	78.2	78.9	79.5	80.1	80.7	81.2
2	69.3	70.6	72.1	73.2	74.3	75.4	76.5	77.4	78.3	79.2	80.0	80.8	81.5	82.2	82.9	83.5	84.1	84.6
3	72.2	73.7	75.1	76.3	77.5	78.7	79.7	80.8	81.7	82.6	83.4	84.3	85.0	85.7	86.4	87.1	87.7	88.3
4	75.4	77.0	78.4	79.7	80.9	82.2	83.2	84.3	85.3	86.2	87.1	88.0	88.8	89.5	90.2	90.9	91.5	92.2
5	78.9	80.5	82.0	83.4	84.7	85.9	87.1	88.2	89.2	90.2	91.1	92.0	92.8	93.6	94.4	95.0	95.7	96.4
6	82.6	84.3	85.8	87.3	88.6	89.9	91.2	92.3	93.4	94.4	95.4	96.3	97.2	98.0	98.8	99.5	100.2	100.9
7	86.6	88.3	90.0	91.5	92.9	94.3	95.5	96.8	97.9	99.0	100.2	101.0	101.8	102.7	103.5	104.3	105.0	105.8
8	90.9	92.7	94.4	96.0	97.5	99.0	100.3	101.6	102.8	103.9	105.0	106.0	106.9	107.8	108.7	109.5	110.3	111.0
9	95.6	97.5	99.3	101.0	102.6	104.0	105.5	106.8	108.0	109.2	110.3	111.4	112.4	113.3	114.2	115.1	115.9	116.7
70	100.7	102.7	104.6	106.4	108.1	109.6	111.1	112.5	113.8	115.1	116.2	117.4	118.4	119.4	120.4	121.3	122.1	122.9
1	106.4	108.5	110.5	112.4	114.1	115.8	117.4	118.8	120.2	121.5	122.8	123.9	125.0	126.1	127.1	128.0	129.0	129.8
2	112.6	114.8	116.9	118.9	120.8	122.5	124.2	125.7	127.2	128.6	129.9	131.1	132.3	133.4	134.5	135.5	136.4	137.4
3	119.5	121.9	124.1	126.2	128.2	130.1	131.8	133.5	135.0	136.5	137.9	139.2	140.4	141.6	142.7	143.8	144.8	145.8
4	127.2	129.7	132.1	134.4	136.4	138.4	140.3	142.0	143.7	145.2	146.7	148.1	149.4	150.7	151.9	153.0	154.1	155.1
5	135.9	138.6	141.1	143.5	145.7	147.8	149.8	151.6	153.4	155.0	156.6	158.1	159.5	160.9	162.1	163.3	164.5	165.6
6	145.7	148.6	151.2	153.8	156.2	158.4	160.6	162.5	164.4	166.2	167.9	169.4	171.0	172.4	173.7	175.0	176.2	177.4
7	156.9	160.0	162.9	165.6	168.2	170.6	172.9	175.0	177.0	178.9	180.8	182.5	184.1	185.6	187.0	188.4	189.7	191.0
8	169.8	173.2	176.3	179.2	182.0	184.6	187.0	189.3	191.5	193.5	195.5	197.3	199.0	200.7	202.2	203.8	205.2	206.5
9	184.9	188.5	191.9	195.1	198.1	200.9	203.5	206.0	208.3	210.6	212.7	214.6	216.5	218.3	220.0	221.6	223.1	224.6
80	202.7	206.6	210.3	213.8	217.0	220.1	223.0	225.6	228.2	230.6	232.9	235.1	237.1	239.2	240.9	242.6	244.3	245.9
1	223.8	228.1	232.1	235.9	239.5	242.9	246.0	249.0	251.8	254.4	256.9	259.3	261.5	263.6	265.6	267.6	269.4	271.1
2	249.7	254.5	258.9	263.1	267.0	270.7	274.2	277.5	280.6	283.5	286.2	288.8	291.3	293.6	295.8	298.0	300.0	301.9
3	281.8	287.1	292.0	296.6	301.0	305.1	309.0	312.6	316.0	319.3	322.3	325.2	328.0	330.6	333.0	335.2	337.6	339.7
4	322.2	328.2	333.7	338.9	343.8	348.4	352.8	356.8	360.6	364.3	367.7	371.0	374.0	376.9	379.7	382.3	384.8	387.2
5	375.0	381.7	388.0	393.9	399.4	404.6	409.5	414.1	418.4	422.6	426.4	430.1	433.6	436.9	440.0	443.0	445.8	448.5
6	445.9	453.6	460.8	467.5	473.8	479.8	485.4	490.6	495.6	500.3	504.7	508.9	512.9	516.7	520.3	523.7	524.9	530.1
7	544.0	552.9	561.2	568.9	576.2	583.1	589.6	595.6	601.4	606.8	612.0	616.9	621.5	625.9	630.1	634.1	637.9	641.6
88	686.6	696.8	706.5	715.6	724.1	732.1	739.7	746.8	753.6	760.0	766.1	771.8	777.4	782.6	787.6	792.3	796.9	801.2

Note: The values of r_A are given in seconds of arc.

TABLE 3

Degrees	Height H, km																	
	5	6	7	8	9	10	11	12	13	14	15	16	17	18	19	20	21	22
1	0.2	0.2	0.2	0.3	0.3	0.3	0.3	0.3	0.3	0.4	0.4	0.4	0.4	0.4	0.3	0.3	0.3	0.3
2	0.4	0.4	0.4	0.5	0.5	0.6	0.6	0.6	0.7	0.7	0.7	0.7	0.7	0.7	0.7	07	0.6	0.6
3	0.6	0.6	0.7	0.8	0.8	0.9	0.9	1.0	1.0	1.0	1.0	1.0	1.0	1.0	1.0	1.0	1.0	1.0
4	0.7	0.8	1.0	1.0	1.1	1.2	1.2	1.3	1.3	1.3	1.4	1.4	1.4	1.3	1.3	1.3	1.3	1.3
5	0.9	1.0	1.2	1.3	1.4	1.4	1.5	1.6	1.6	1.7	1.7	1.7	1.7	1.7	1.6	1.6	1.6	1.6
6	1.1	1.3	1.4	1.5	1.6	1.7	1.8	1.9	2.0	2.0	2.0	2.0	2.0	2.0	2.0	2.0	1.9	1.9
7	1.3	1.5	1.6	1.8	1.9	2.0	2.1	2.2	2.3	2.3	2.4	2.4	2.4	2.4	2.3	2.3	2.2	2.2
8	1.5	1.7	1.9	2.0	2.2	2.3	2.4	2.5	2.6	2.7	2.7	2.7	2.7	2.7	2.6	2.6	2.6	2.5
9	1.6	1.9	2.1	2.3	2.4	2.6	2.7	2.8	2.9	3.0	3.0	3.0	3.0	3.0	3.0	3.0	2.9	2.8
10	1.8	2.1	2.4	2.6	2.7	2.9	3.0	3.2	3.3	3.3	3.2	3.4	3.4	3.4	3.3	3.3	3.2	3.2
1	2.0	2.3	2.6	2.8	3.0	3.2	3.3	3.5	3.6	3.7	3.7	3.8	3.8	3.7	3.7	3.6	3.6	3.5
2	2.2	2.6	2.8	3.1	3.3	3.5	3.6	3.8	4.0	4.0	4.1	4.1	4.1	4.1	4.0	4.0	3.9	3.8
3	2.4	2.8	3.1	3.3	3.6	3.8	3.9	4.1	4.3	4.4	4.5	4.5	4.5	4.4	4.4	4.'	4.2	4.2
4	2.6	3.0	3.3	3.6	3.9	4.1	4.3	4.5	4.6	4.7	4.8	4.8	4.8	4.8	4.7	4..	4.6	4.5
5	2.8	3.3	3.6	3.9	4.2	4.4	4.6	4.8	5.0	5.1	5.2	5.2	5.2	5.2	5.1	5.0	5.0	4.8
6	3.0	3.5	3.8	4.2	4.4	4.7	4.9	5.1	5.3	5.5	5.5	5.5	5.5	5.5	5.4	5.4	5.3	5.2
7	3.2	3.7	4.1	4.4	4.8	5.0	5.2	5.5	5.7	5.8	5.9	5.9	5.9	5.9	5.8	5.7	5.6	5.5
8	3.4	3.9	4.3	4.7	5.0	5.3	5.6	5.8	6.1	6.2	6.3	6.3	6.3	6.2	6.2	6.1	6.0	5.9
9	3.6	4.2	4.6	5.0	5.4	5.6	5.9	6.2	6.4	6.6	6.6	6.7	6.6	6.6	6.5	6.5	6.4	6.2
20	3.9	4.4	4.9	5.3	5.7	6.0	6.2	6.6	6 8	7.0	7.0	7.0	7.0	7.0	6.9	6.8	6.7	6.6
1	4.1	4.6	5.1	5.6	6.0	6.3	6.6	6.9	7.2	7.1	7.4	7.4	7.4	7.4	7.3	7.2	7.1	7.0
2	4.2	4.9	5.4	5.9	6.3	6.6	6.9	7.3	7.5	7.7	7.8	7.8	7.8	7.7	7.6	7.6	7.4	7.3
3	4.5	5.1	5.7	6.2	6.6	6.9	7.2	7.6	7.9	8.1	8.2	8.2	8.2	8.2	8.1	7.9	7.8	7.7
4	4.7	5.4	6.0	6.5	6.9	7.3	7.6	8.0	8.3	8.5	8.6	8.6	8.6	8.6	8.4	8.4	8.2	8.1
5	4.9	5.6	6.2	6.8	7.2	7.6	8.0	8.4	8.7	9.0	9.0	9.0	9.0	8.9	8.8	8.7	8.6	8,4
6	5.2	5.9	6.5	7.1	7.6	8.0	8.3	8.8	9.1	9.3	9.4	9.4	9.4	9.3	9.3	9.1	10.0	9.8
7	5.4	6.2	6.8	7.4	7.9	8.3	8.7	9.2	9.5	9.7	9.8	9.9	9.8	9.8	9.7	9.6	9.4	9.2
8	5.6	6.4	7.1	7.7	8.3	8.7	9.0	9.5	9.9	10.1	10.2	10.3	10.3	10.2	10.1	9.9	9.8	9.6
9	5.9	6.7	7.4	8.1	8.6	9.1	9.5	9.9	10.3	10.6	10.7	10.8	10.7	10.6	10.5	10.4	10.2	10.0
30	6.1	7.0	7.7	8.4	9.0	9.4	9.9	10.4	10.8	11.0	11.1	11.2	11.2	11.1	11.0	10.8	10.6	10.4
1	6.4	7.3	8.0	8.8	9.4	9.8	10.3	10.8	11.2	11.4	11.6	11.6	11.6	11.5	11.4	11.2	11.1	10.8
2	6.6	7.6	8.4	9.1	9.7	10.2	10.7	11.2	11 6	11.9	12.1	12.1	12.1	12.0	11.8	11.7	11.5	11.3
3	6.9	7.9	8.7	9.5	10.1	10.6	11.1	11.7	12.1	12.4	12.6	12.6	12.6	12.5	12.3	12.2	12.0	11.8
4	7.1	8.2	9.0	9.8	10.5	11.0	11.5	12.1	12.6	12.9	13.0	13.1	13 0	12.9	12 8	12.6	12.4	12.2
5	7.4	8.5	9.4	10.2	10.9	11.4	12.0	12.6	13.1	13.3	13.5	13.6	13.6	13.4	13.3	13.1	12.9	12.7
6	7.7	8.8	9.7	10.6	11.3	11.9	12.4	13.1	13.5	13.8	14.0	14.0	14.0	13.9	13.8	13.6	13.4	13.1
7	8.0	9.1	10.3	11.0	11.7	12.3	12.9	13 6	14.0	14.4	14.5	14.6	14.5	14.5	14.3	14.1	13.8	13.6
8	8.2	9.5	10.5	11.4	12.2	12.8	13.4	14.0	14.6	14.9	15.1	15.1	15.1	15.0	14.8	14.6	14.4	14.1
9	8.6	9.8	10.9	11.8	12.6	13.3	13.8	14.5	15.1	15.4	15.6	15.7	15.6	15.5	15.4	15.1	14 9	14.6
40	8.9	10.2	11.2	12.2	13.0	13.7	14.4	15.1	15 6	16.0	16.2	16.2	16.2	16.1	15.9	15.7	15.4	15.2
1	9.2	10.6	11.6	12.6	13.6	14.2	14.9	15.7	16.2	16.6	16.8	17.0	16.8	16.7	16.5	16.3	16.0	15.7
2	9.6	10.9	12.1	13.1	14.0	14.8	15.4	16.2	16.8	17.2	17.4	17.4	17.3	17.3	17.1	16.8	16.6	16.3
3	9.9	11.3	12.5	13.6	14.5	15.3	15.9	16.8	17.4	17.8	18.0	18.0	18.0	17.9	17.7	17.4	17.2	16.8
4	10.2	11.7	13.0	14.1	15.0	15.8	16.5	17.4	18.0	18.4	18.6	18.7	18.7	18.5	18 3	18.1	17.8	17.4
5	10.6	12.2	13.4	14.6	15.6	16.4	17.1	18.0	18.6	19.1	19.3	19.4	19.3	19.2	19.0	18,7	18.4	18.1
6	11.0	12.6	13.9	15.1	16.1	17.0	17.7	18.6	19.3	19.8	20.0	20.1	20.0	19.9	19.6	19.4	19.1	18.7
7	11.4	13.0	14.4	15.6	16.7	17.5	18.3	19.3	20.0	20.4	20.7	20.8	20.7	20.6	20.3	20.0	19.7	19.4

TABLE 3 (cont'd)

ζ, Degrees	Height H, km																	
	23	24	25	26	27	28	29	30	31	32	33	34	35	36	37	38	39	40
1	0.3	0.3	0.3	0.3	0.3	0.3	0.3	0.3	0.3	0.2	0.2	0.2	0.2	0.2	0.2	0.2	0.2	0.2
2	0.6	0.6	0.6	0.6	0.6	0.6	0.5	0.5	0.5	0.5	0.5	0.5	0.4	0.4	0.4	0.4	0.4	0.4
3	0.9	0.9	0.9	0.9	0.8	0.8	0.8	0.8	0.8	0.8	0.7	0.7	0.7	0.7	0.7	0.7	0.6	0.6
4	1.3	1.2	1.2	1.2	1.2	1.1	1.1	1.0	1.0	1.0	1.0	1.0	1.0	0.9	0.9	0.9	0.9	0.8
5	1.6	1.5	1.5	1.4	1.4	1.4	1.4	1.3	1.3	1.3	1.2	1.2	1.2	1.2	1.1	1.1	1.1	1.0
6	1.9	1.8	1.8	1.8	1.7	1.7	1.6	1.6	1.6	1.5	1.5	1.4	1.4	1.4	1.3	1.3	1.3	1.3
7	2.2	2.1	2.1	2.0	2.0	1.9	1.9	1.9	1.8	1.8	1.7	1.7	1.6	1.6	1.6	1.5	1.5	1.5
8	2.5	2.4	2.4	2.3	2.3	2.2	2.1	2.1	2.1	2.0	2.0	1.9	1.9	1.8	1.8	1.7	1.7	1.6
9	2.8	2.7	2.7	2.6	2.6	2.5	2.4	2.4	2.3	2.2	2.2	2.2	2.1	2.1	2.0	2.0	1.9	1.9
10	3.1	3.0	3.0	2.9	2.8	2.8	2.7	2.7	2.6	2.5	2.5	2.4	2.4	2.3	2.3	2.2	2.1	2.1
1	3.4	3.4	3.3	3.2	3.1	2.9	3.0	2.9	2.8	2.8	2.7	2.7	2.6	2.5	2.4	2.4	2.4	2.3
2	3.8	3.7	3.6	3.5	3.4	3.4	3.3	3.2	3.1	3.0	3.0	2.9	2.8	2.8	2.7	2.6	2.6	2.5
3	4.1	4.0	3.9	3.8	3.7	3.6	3.6	3.5	3.4	3.2	3.2	3.2	3.1	3.0	2.9	2.9	2.8	2.7
4	4.4	4.1	4.2	4.1	4.0	4.0	3.9	3.8	3.7	3.6	3.5	3.4	3.3	3.3	3.2	3.1	3.0	3.0
5	4.8	4.7	4.6	4.5	4.4	4.3	4.2	4.1	4.0	3.9	3.8	3.7	3.6	3.5	3.4	3.3	3.3	3.2
6	5.1	5.0	4.8	4.8	4.6	4.5	4.4	4.3	4.2	4.1	4.0	3.9	3.8	3.7	3.6	3.6	3.5	3.4
7	5.4	5.3	5.2	5.1	5.0	4.8	4.7	4.6	4.5	4.4	4.3	4.2	4.1	4.0	3.9	3.8	3.7	3.6
8	5.8	5.6	5.5	5.4	5.3	5.2	5.0	4.9	4.8	4.7	4.6	4.5	4.4	4.2	4.2	4.0	3.9	3.9
9	6.1	6.0	5.8	5.7	5.6	5.5	5.3	5.2	5.1	5.0	4.8	4.7	4.6	4.5	4.4	4.3	4.2	4.1
20	6.5	6.3	6.2	6.1	5.9	5.8	5.6	5.5	5.4	5.3	5.1	5.0	4.9	4.8	4.6	4.6	4.5	4.3
1	6.8	6.7	6.5	6.4	6.2	6.1	5.9	5.8	5.6	5.5	5.4	5.3	5.1	5.0	4.9	4.8	4.7	4.6
2	7.2	7.0	6.8	6.7	6.5	6.4	6.2	6.1	6.0	5.8	5.6	5.5	5.4	5.3	5.1	5.0	4.9	4.8
3	7.5	7.4	7.2	7.0	6.9	6.7	6.6	6.4	6.3	6.1	6.0	5.8	5.6	5.6	5.4	5.3	5.2	5.0
4	7.9	7.7	7.6	7.4	7.2	7.0	6.9	6.7	6.6	6.4	6.2	6.1	6.0	5.8	5.7	5.6	5.4	5.3
5	8.3	8.1	7.9	7.7	7.6	7.4	7.2	7.0	6.8	6.7	6.5	6.4	6.2	6.1	5.9	5.8	5.7	5.5
6	8.7	8.5	8.3	8.1	7.9	7.7	7.6	7.4	7.2	7.0	6.9	6.7	6.5	6.4	6.2	6.1	5.9	5.8
7	9.0	8.8	8.7	8.5	8.3	8.1	7.9	7.7	7.5	7.3	7.2	7.0	6.8	6.6	6.5	6.3	6.2	6.0
8	9.4	9.2	9.0	8.8	8.6	8.4	8.2	8.0	7.8	7.6	7.5	7.3	7.1	6.9	6.8	6.6	6.5	6.3
9	9.8	9.6	9.4	9.2	9.0	8.8	8.6	8.4	8.2	8.0	7.8	7.6	7.4	7.2	7.0	6.9	6.7	6.6
30	10.2	10.0	9.8	9.6	9.4	9.2	8.9	8.7	8.5	8.3	8.1	7.9	7.7	7.6	7.4	7.2	7.0	6.9
1	10.7	10.4	10.2	10.0	10.0	9.5	9.3	9.1	8.8	8.6	8.4	8.2	8.0	7.8	7.6	7.5	7.3	7.1
2	11.1	10.8	10.6	10.4	10.2	9.9	9.7	9.4	9.2	9.0	8.8	8.6	8.3	8.2	8.0	7.8	7.6	7.4
3	11.5	11.3	11.0	10.8	10.6	10.3	10.1	9.8	9.6	9.4	9.1	8.9	8.7	8.5	8.3	8.1	7.9	7.7
4	12.0	11.7	11.4	11.2	10.9	10.7	10.4	10.2	9.9	9.7	9.4	9.2	9.0	8.8	8.6	8.4	8.2	8.0
5	12.4	12.2	11.9	11.6	11.4	11.1	10.8	10.6	10.3	10.1	9.8	9.6	9.4	9.1	8.9	8.7	8.5	8.3
6	12.9	12.6	12.3	12.0	11.8	11.5	10.2	10.9	10.7	10.4	10.2	9.9	9.7	9.4	9.2	9.0	8.8	8.6
7	13.4	13.1	12.8	12.5	12.2	11.9	11.7	11.4	11.1	10.8	10.6	10.3	10.1	9.8	9.6	9.4	9.2	9.0
8	13.8	13.5	13.3	13.0	12.7	12.4	12.1	11.8	11.5	11.2	11.0	10.7	10.4	10.2	9.9	9.7	9.5	9.3
9	14.3	14.0	13.8	13.4	13.2	12.8	12.5	12.2	11.9	11.6	11.3	11.1	10.8	10.6	10.3	10.1	9.8	9.6
40	14.9	14.6	14.2	13.9	13.6	13.3	13.0	12.7	12.4	12.1	11.8	11.5	11.2	11.0	10.7	10.4	10.2	10.0
1	15.4	15.1	14.8	14.4	14.1	13.8	13.4	13.1	12.8	12.5	12.2	11.9	11.6	11.4	11.1	10.8	10.6	10.3
2	16.0	15.6	15.3	14.9	14.6	14.3	13.9	13.6	13.3	13.0	12.6	12.3	12.0	11.7	11.5	11.2	11.0	10.7
3	16.5	16.2	15.8	15.5	15.1	14.8	14.4	14.1	13.7	13.4	13.1	12.8	12.4	12.2	11.9	11.6	11.3	11.1
4	17.1	16.8	16.4	16.0	15.7	15.3	15.0	14.6	14.2	13.8	13.6	13.2	12.9	12.6	12.3	12.0	11.7	11.5
5	17.7	17.4	17.0	16.6	16.2	15.8	15.5	15.1	14.7	14.4	14.0	13.7	13.4	13.1	12.8	12.5	12.2	11.9
6	18.4	18.0	17.6	17.2	16.8	16.4	16.0	15.6	15.3	14.9	14.5	14.2	13.9	13.5	13.2	12.9	12.6	12.3
7	19.0	18.6	18.2	17.8	17.4	17.0	16.6	16.2	15.8	15.4	15.0	14.7	14.3	14.0	13.6	13.4	13.0	12.7

TABLE 3 (cont'd)

ζ, Degrees	Height H, km																	
	5	6	7	8	9	10	11	12	13	14	15	16	17	18	19	20	21	22
48	11.8	13.5	14.9	16.2	17.3	18.2	19.0	20.0	20.7	21.2	21.4	21.5	21.4	21.3	21.1	20.8	20.4	20.1
9	12.1	14.2	15.4	16.8	17.9	18.8	19.6	20.7	21.4	21.9	22.2	22.3	22.2	22.0	21.8	21.5	21.1	20.8
50	12.7	14.5	16.0	17.4	18.6	19.5	20.4	21.4	22.2	22.7	23.0	23.1	23.0	22.9	22.6	22.3	21.9	21.5
1	13.1	15.0	16.6	18.0	19.2	20.2	21.1	22.2	23.0	23.5	23.8	23.9	23.8	23.7	23.4	23.1	22.7	22.3
2	13.6	15.5	17.2	18.7	19.9	20.9	21.9	23.0	23.9	24.4	24.7	24.8	24.7	24.5	24.3	23.9	23.5	23.1
3	14.1	16.1	17.8	19.4	20.6	21.7	22.7	23.9	24.8	25.3	25.6	25.7	25.6	25.4	25.2	24.8	24.4	24.0
4	14.6	16.7	18.5	20.1	21.4	22.5	23.5	24.8	25.7	26.2	26.5	26.6	26.6	26.4	26.1	25.8	25.3	24.9
5	15.2	17.4	19.2	20.8	22.2	23.4	24.4	25.7	26.6	27.2	27.6	27.7	27.6	27.4	27.1	26.7	26.3	25.8
6	15.8	18.0	19.9	21.6	23.1	24.3	25.3	26.6	27.6	28.2	28.6	28.7	28.6	28.4	28.1	27.7	27.3	26.8
7	16.4	18.7	20.7	22.4	24.1	25.2	26.3	27.7	28.7	29.3	29.7	29.8	29.7	29.5	29.2	28.8	28.3	27.8
8	17.1	19.4	21.5	23.4	24.9	26.2	27.4	28.8	29.9	30.5	30.9	31.0	30.9	30.7	30.4	30.0	29.5	29.1
9	17.7	20.2	22.4	24.3	25.9	27.3	28.5	30.0	31.1	31.7	32.1	32.2	32.2	31.9	31.6	31.2	30.6	30.1
60	18.4	21.1	23.3	25.3	27.0	28.4	29.6	31.2	32.3	33.0	33.4	33.5	33.4	33.2	32.9	32.4	31.9	31.3
1	19.2	22.0	24.3	26.3	28.1	29.5	30.8	32.4	33.7	34.4	34.6	34.9	34.8	34.6	34.2	33.7	33.2	32.6
2	20.0	22.8	25.3	27.4	29.2	30.8	32.1	33.8	35.1	35.4	36.2	36.4	36.3	36.0	35.6	35.2	34.6	33.9
3	20.9	23.9	26.4	28.6	30.6	32.2	33.5	35.3	36.6	37.4	37.8	38.0	37.9	37.6	37.2	36.7	36.1	35.5
4	21.9	25.0	27.6	29.9	31.9	33.6	35.1	36.9	38.2	39.1	39.0	39.7	39.6	39.3	38.9	38.3	37.7	37.0
5	22.8	26.0	28.8	31.3	33.4	35.1	36.6	38.6	40.0	40.8	41.3	41.5	41.3	41.1	40.6	40.0	39.4	38.7
6	23.9	27.3	30.2	32.7	34.9	36.8	38.3	40.4	41.8	42.7	43.2	43.4	43.3	43.0	42.5	41.9	41.2	40.5
7	25.1	28.6	31.6	34.3	36.6	38.5	40.2	42.3	43.8	44.8	45.3	45.5	45.4	45.1	44.5	44.0	43.2	42.4
8	26.4	30.0	33.3	36.1	38.4	40.4	42.2	44.4	46.1	47.0	47.6	47.8	47.6	47.3	46.8	46.1	45.4	44.6
9	27.8	31.9	35.1	38.0	40.5	42.6	44.5	46.8	48.5	49.1	50.1	50.3	50.1	49.8	49.3	48.6	47.8	47.0
70	29.3	33.4	36.9	40.1	42.7	44.9	46.9	49.3	51.1	52.2	52.8	53.0	52.9	52.5	51.9	51.2	50.4	49.5
1	31.0	35.2	39.0	42.3	45.1	47.4	49.5	52.1	54.0	55.1	55.8	56.0	55.8	55.4	54.8	54.1	53.2	52.2
2	32.9	37.4	41.4	44.8	47.8	50.3	52.5	55.2	57.2	58.4	59.1	59.3	59.1	58.7	58.1	57.3	56.4	55.3
3	34.9	39.7	43.9	47.6	50.7	53.3	55.7	58.6	60.7	62.0	62.7	62.9	62.8	62.3	61.6	60.8	59.8	58.7
4	37.2	42.3	46.8	50.7	54.0	56.8	59.3	62.4	64.6	66.0	66.8	67.0	66.8	66.4	65.6	64.7	63.7	62.5
5	39.8	45.3	50.1	54.2	57.8	60.8	63.4	66.8	69.1	70.6	71.4	71.6	71.4	70.9	70.2	69.2	68.1	66.8
6	42.7	48.6	53.8	58.2	62.0	65.3	68.1	71.6	74.1	75.7	76.6	76.8	76.6	76.1	75.3	74.2	73.0	71.1
7	46.1	52.4	57.9	62.8	66.9	70.3	73.4	77.2	79.9	81.6	82.5	82.8	82.6	82.0	81.0	79.9	78.6	77.2
8	50.0	56.9	62.9	68.1	72.6	76.3	79.6	83.7	86.6	88.4	89.4	89.7	89.5	88.8	87.8	86.6	85.2	83.7
9	54.6	62.1	68.6	74.3	79.1	83.2	86.8	91.2	94.4	96.4	97.4	97.7	97.5	96.8	95.9	94.4	92.9	91.2
80	60.0	68.3	75.5	81.7	87.0	91.4	95.3	100.2	103.6	105.8	106.9	107.2	107.0	106.2	105.0	103.5	97.4	100.1
1	66.8	76.0	83.9	90.7	96.6	101.4	105.7	111.1	114.9	117.2	118.5	118.8	118.5	117.6	116.3	114.7	112.9	110.9
2	75.0	85.2	94.0	101.7	108.1	113.6	118.3	124.2	128.4	131.0	132.4	132.8	132.4	131.4	130.0	128.2	126.1	123.9
3	85.4	96.9	106.9	115.6	122.8	128.9	134.3	140.9	145.5	148.4	149.9	150.3	149.8	148.7	147.0	145.0	138.6	140.2
4	99.2	112.4	123.9	133.7	142.0	148.9	154.9	162.4	167.6	170.8	172.4	172.8	172.2	170.9	169.0	166.7	164.0	161.2
5	117.8	133.3	146.6	158.0	167.6	175.2	182.3	190.8	196.7	200.3	202.1	202.4	201.7	200.1	197.9	195.2	192.1	188.8
6	144.4	162.9	178.7	192.1	203.2	212.4	220.3	230.0	236.7	240.7	242.6	242.9	241.8	239.9	237.2	234.0	230.3	226.4
7	185.5	208.2	227.3	243.2	256.4	267.0	276.0	287.1	294.7	299.1	301.0	301.0	299.6	297.1	293.7	289.7	285.4	280.6
88	254.0	282.0	305.2	324.2	339.5	351.6	361.7	374.1	382.3	386.8	388.5	387.9	385.8	382.5	378.0	373.0	367.5	361.8

TABLE 3 (cont'd)

ζ, Degrees	Height H, km								Height H, km									
	23	24	25	26	27	28	29	30	31	32	33	34	35	36	37	38	39	40
48	19.7	19.3	18.8	18.4	18.0	17.6	17.2	16.8	16.4	16.0	15.6	15.2	14.8	14.5	14 2	13.8	13.5	13.2
9	20.4	20.0	19.5	19.1	18.7	18.2	17.8	17.4	16.9	16.5	16.1	15.7	15.4	15.0	14.6	14.3	14.0	13.7
50	21.1	20.7	20.2	19.8	19.4	18.9	18.5	18.0	17.6	17.1	16.7	16.3	15.9	15.6	15.2	14.8	14.5	14.2
1	21.8	21.4	20.9	20.5	20.0	19.6	19.1	18.6	18.2	17.7	17.3	16.9	16.5	16.1	15.7	15.4	15 0	14.7
2	22 6	22.2	21.7	21.2	20.8	20.3	19.8	19.3	18.8	18.4	18.0	17.5	17.1	16.7	16.3	15.9	15.6	15.2
3	23.5	23.0	22.5	22.0	21.6	21.0	20.5	20.0	19.6	19.1	18.6	18.2	17.7	17.3	16.9	16.5	16.2	15.8
4	24.4	23.9	23.4	22.8	22.3	21.9	21.3	20.8	20.3	19.8	19.3	18.8	18.4	18.0	17.5	17.1	16.7	16.3
5	25.3	24.8	24.3	23.7	23.2	22.6	22.1	21.6	21.0	20.6	20.1	19.6	19.1	18.7	18.2	17.8	17.4	17.0
6	26.3	25.7	25.1	24.6	24.0	23.5	22.9	22.4	21.8	21.3	20.8	20.3	19.8	19.4	18.9	18.4	18 0	17.6
7	27.3	26.7	26.1	25.5	25.0	21.4	23.8	23.2	22.7	22.1	21.6	21.1	20.6	20.1	19.6	19.2	18.7	18.3
8	28.4	27.8	27.2	25.6	26.00	25.4	24.8	24.2	23.6	23.0	22.5	22.0	21.4	20.9	20.4	20.0	19.5	19.1
9	29.)	28.9	28.2	27.6	27.0	26.4	25.8	25.2	24.6	24.0	23.4	22.8	22.3	21.8	21.2	20.7	20.3	19.8
60	30.7	30.0	29.4	28.8	28.1	27.5	26.8	26.2	25.6	24.9	24.3	23.7	23.2	22.6	22.1	21.6	21.1	20.6
1	32.0	31.3	30.6	29.9	29.3	28.6	27.9	27.2	26.6	25.9	25.3	24.7	24.1	23.5	23.0	22.5	22.0	21.4
2	33.3	32.6	31.7	31.2	30.5	29.8	29.1	28.4	27.7	27.0	26.4	25.7	25.1	24.5	24.0	23.4	22.9	22.4
3	34.8	34.0	33.3	32.6	31.8	31.1	30.4	29.6	28.9	28.2	27.5	26.9	26.3	25.6	25.0	24.5	23 9	23.4
4	36.3	35.5	34.8	34.0	33.3	32.5	31.7	31.0	30.2	29.5	28.8	28.1	27.4	26 8	26.2	25.6	25 0	24.4
5	37.9	37.1	36.3	35 6	34.8	34.0	33.2	32.3	31.6	30.8	30.1	29.3	28.6	28.0	27.3	26.7	26.1	25.5
6	39.7	38.9	38.0	37.2	36.4	35.5	34.7	33.9	33.1	32.3	31.5	30.7	30.0	29.3	28.6	28.0	27.3	26.7
7	41.6	40.8	39.9	39.0	38.1	37.3	36.4	35.5	34.7	33.8	32.8	32.2	31.5	30.7	30.0	29.3	28.6	28.0
8	43.7	42.8	41.9	41.0	40.1	39.1	38.2	37.3	36.4	35.5	34.6	33.8	33.0	32.3	31.5	30.8	30.1	29.4
9	46.0	45.1	44.1	43.2	42.2	41.2	40.2	39.3	38 3	37.4	36.5	35.6	34.8	34.0	33.2	32.4	31.7	31.0
70	48.5	47.5	46.5	45.5	44.4	43.4	42.4	41.4	40.4	39.4	38.5	37.6	36.7	35.8	35.0	34.2	33.4	32.7
1	51.2	50.1	49.1	48.0	47.0	45.2	44.8	43.7	42.7	41.6	40.6	39.7	38.8	37.8	37.0	36.1	35.3	31 6
2	54.3	53.1	52.0	50.9	49.7	48.6	47.5	46.3	45.2	44.1	43.1	42.1	41.0	40.1	39.2	38.3	37.4	36.6
3	57.6	56.4	55.2	54 0	52.8	51.6	50 4	49.1	48 0	46 8	45.7	44.6	43 6	42.6	41.6	40.6	39.7	38.9
4	61.3	60.0	58.8	57.5	56.2	54.9	53 6	52.4	51.1	49.9	48.7	47.6	46.4	45.4	44.3	43 3	42.4	41.4
5	65.5	64.2	62.8	61.4	60.1	58.7	57.4	56.9	54.7	53.4	52.1	50.9	49.7	48.5	47.4	46.4	45.3	44.4
6	70.2	68.8	67.4	65.9	64.5	63.0	61.6	60.1	58.7	57.3	55.9	54.6	53.4	52.1	51.0	49.8	48.7	47.6
7	75.7	74.2	72.6	71.0	69.5	67.9	66.3	64.8	63 2	61.7	60.3	58.9	57.5	56.2	54.9	53.7	52.5	51.4
8	82.1	80.4	78.7	77.0	75.3	73.6	71.9	70.2	68.6	67.0	65.4	63 9	62.4	61.0	59.6	58.3	57.0	55.8
9	87.8	87.6	85.7	83.9	82.1	80.2	78.4	76.6	74.8	73 0	71.2	69.7	68.1	66 6	65.1	63 6	62 3	60.9
80	98.1	96.1	94.1	92.1	90.1	88.1	86 0	84.1	82.1	80.2	78.4	76.6	74.8	73.0	71.6	70.0	68.5	67.1
1	103.7	106.5	104.3	102.1	99.9	97.7	95.5	93.3	91.2	89.1	87.0	85.1	83.2	81.4	79.6	77.9	76.2	74.6
2	121.5	119.0	116.6	114.2	111.7	109.3	106.8	104.4	102 0	99.7	97.5	95 3	93 2	91.2	89.2	87.3	85 5	83.7
3	137.5	134.8	132.0	129.3	126 6	123 8	121.1	118.4	115.7	113.2	110.6	108.2	105.9	103.6	101.4	99.5	97.3	95.4
4	158.2	155.0	151.9	148 8	145.7	142.6	139.5	136.5	133.5	130 6	127.8	125.1	122.4	119.9	117.4	115.1	112 8	110.6
5	185.3	181.7	178.1	174 6	171.0	167.5	163.9	160.5	157.1	153.8	150 6	147.6	144.4	141.5	138.8	136.0	133 4	130.9
6	222.4	218.2	213.9	209.8	205.7	201.6	197.4	193.4	189.5	185.7	182.0	178.4	174.9	171.6	168.3	165.2	164.2	159.3
7	275.7	270.8	265.7	260.9	256.0	251.1	246.2	241.5	236 9	232.4	228.0	223 8	219.7	215.7	212 0	208.3	204.3	201.4
88	355.8	349.7	343.6	337.7	331.7	325.8	320.0	314.3	308.8	303.4	298.1	293.1	288.1	283.4	278.8	274.4	270.2	266.1

Note: The values of the angle r_B are given in seconds of arc.

TABLE 4

ξ, Degrees	Height H, km																	
	5	6	7	8	9	10	11	12	13	14	15	16	17	18	19	20	21	22
1	0.4	0.4	0.5	0.6	0.6	0.7	0.7	0.7	0.8	0.8	0.8	0.9	0.9	0.9	0.9	0.9	1.0	1.0
2	0.8	0.9	1.0	1.1	1.2	1.3	1.4	1.5	1.6	1.6	1.7	1.7	1.8	1.8	1.8	1.9	1.9	1.9
3	1.2	1.4	1.6	1.7	1.9	2.0	2.1	2.2	2.4	2.4	2.5	2.6	2.7	2.7	2.7	2.8	2.8	2.8
4	1.6	1.9	2.1	2.3	2.5	2.7	2.8	3.0	3.1	3.3	3.4	3.5	3.6	3.6	3.7	3.7	3.8	3.8
5	2.0	2.3	2.6	2.9	3.1	3.3	3.5	3.7	3.9	4.1	4.2	4.3	4.4	4.5	4.6	4.7	4.7	4.7
6	2.4	2.8	3.1	3.4	3.7	4.0	4.2	4.5	4.7	4.9	5.1	5.2	5.3	5.4	5.5	5.6	5.6	5.7
7	2.8	3.2	3.6	4.0	4.4	4.7	5.0	5.2	5.5	5.7	5.9	6.1	6.2	6.3	6.4	6.5	6.6	6.7
8	3.2	3.7	4.2	4.6	5.0	5.3	5.7	6.0	6.3	6.6	6.8	7.0	7.1	7.3	7.4	7.5	7.6	7.6
9	3.6	4.2	4.7	5.2	5.6	6.0	6.4	6.8	7.1	7.4	7.6	7.8	8.2	8.2	8.3	8.4	8.5	8.6
10	4.0	4.7	5.2	5.8	6.2	6.7	7.1	7.5	7.9	8.2	8.5	8.8	8.9	9.1	9.3	9.4	9.5	9.6
1	4.5	5.1	5.8	6.4	6.9	7.4	7.8	8.3	8.7	9.1	9.4	9.6	9.9	10.0	10.2	10.3	10.5	10.6
2	4.9	5.6	6.3	7.0	7.6	8.1	8.6	9.1	9.5	9.9	10.2	10.5	10.8	11.0	11.2	11.3	11.4	11.5
3	5.3	6.1	6.9	7.6	8.2	8.8	9.3	9.9	10.4	10.8	11.1	11.4	11.7	11.9	12.1	12.3	12.4	12.5
4	5.7	6.6	7.4	8.2	8.8	9.5	10.0	10.7	11.2	11.6	12.0	12.4	12.6	12.9	13.1	13.3	13.4	13.5
5	6.1	7.1	8.0	8.8	9.5	10.2	10.8	11.4	12.0	12.5	12.9	13.3	13.6	13.8	14.1	14.2	14.4	14.5
6	6.6	7.6	8.5	9.4	10.2	10.9	11.6	12.2	12.9	13.4	13.8	14.2	14.5	14.8	15.0	15.2	15.4	15.6
7	7.0	8.1	9.1	10.0	10.8	11.6	12.3	13.1	13.7	14.3	14.8	15.1	15.5	15.8	16.0	16.2	16.4	16.6
8	7.4	8.6	9.6	10.6	11.5	12.3	13.1	13.9	14.6	15.2	15.7	16.1	16.5	16.8	17.0	17.3	17.5	17.6
9	7.9	9.1	10.2	11.3	12.2	13.1	13.9	14.7	15.4	16.1	16.6	17.1	17.4	17.8	18.1	18.3	18.5	18.7
20	8.3	9.6	10.8	11.9	12.9	13.8	14.7	15.6	16.3	17.0	17.6	18.0	18.4	18.8	19.1	19.4	19.6	19.8
1	8.8	10.2	11.4	12.6	13.6	14.6	15.5	16.4	17.2	17.7	18.5	19.0	19.4	19.8	20.1	20.4	20.6	20.8
2	9.2	10.7	12.0	13.2	14.3	15.4	16.3	17.3	18.1	18.8	19.5	20.0	20.5	20.8	21.2	21.5	21.7	21.9
3	9.7	11.2	12.6	13.9	15.1	16.1	17.1	18.2	19.0	19.8	20.5	21.0	21.5	21.9	22.3	22.6	22.8	23.0
4	10.2	11.8	13.2	14.6	15.8	16.9	18.0	19.0	20.0	20.8	21.5	22.0	22.6	23.0	23.4	23.7	24.0	24.2
5	10.7	12.3	13.9	15.3	16.5	17.7	18.8	19.9	20.9	21.8	22.5	23.1	23.6	24.1	24.5	24.8	25.1	25.3
6	11.2	12.9	14.5	16.0	17.3	18.5	19.7	20.8	21.9	22.8	23.5	24.2	24.7	25.2	25.6	25.9	26.2	26.5
7	11.6	13.5	15.1	16.7	18.1	19.4	20.5	21.8	22.8	23.8	24.6	25.2	25.8	26.3	26.7	27.1	27.4	27.7
8	12.2	14.1	15.8	17.4	18.9	20.2	21.4	22.7	23.8	24.8	25.6	26.3	26.9	27.4	27.9	28.3	28.6	28.9
9	12.7	14.7	16.5	18.2	19.7	21.1	22.3	23.7	24.8	25.9	26.7	27.4	28.1	28.6	29.1	29.5	29.8	30.1
30	13.2	15.3	17.2	18.9	20.5	21.9	23.3	24.7	25.9	26.9	27.8	28.6	29.2	29.8	30.3	30.7	31.0	31.3
1	13.7	15.9	17.9	19.7	21.3	22.8	24.2	25.7	27.0	28.0	29.0	29.8	30.4	31.0	31.5	31.9	32.3	32.6
2	14.3	16.5	18.6	20.5	22.2	23.7	25.2	26.7	28.0	29.2	30.1	31.0	31.7	32.3	32.8	33.2	33.6	33.9
3	14.8	17.2	19.3	21.2	23.0	24.7	26.2	27.7	29.1	31.5	31.3	32.2	32.9	33.5	34.0	34.5	34.9	35.2
4	15.4	17.8	20.0	22.1	23.9	25.6	27.2	28.8	30.3	31.5	32.5	33.4	34.2	34.8	35.4	35.8	36.3	36.6
5	16.0	18.5	20.8	22.9	24.8	26.6	28.2	29.9	31.4	32.7	33.7	34.7	35.5	36.1	36.7	37.2	37.6	38.0
6	16.6	19.2	21.6	23.8	25.8	27.6	29.3	31.0	32.6	33.9	35.0	36.0	36.8	37.5	38.1	38.6	39.0	39.4
7	17.2	19.9	22.4	24.7	26.7	28.6	30.4	32.2	33.8	35.2	36.3	37.3	38.2	38.9	39.5	40.1	40.5	40.9
8	17.9	20.7	23.2	25.6	27.7	29.7	31.5	33.4	35.0	36.4	37.7	38.7	39.6	40.3	41.0	41.5	42.0	42.4
9	18.5	21.4	24.1	26.5	28.7	30.8	32.6	34.6	36.3	37.8	39.0	39.1	41.0	41.8	42.5	43.0	43.5	43.9
40	19.2	22.2	24.9	27.4	29.8	31.9	33.8	35.8	37.6	39.2	40.4	41.5	42.5	43.3	44.0	44.6	45.1	45.5
1	19.9	23.0	25.8	28.4	30.8	33.0	35.0	37.2	39.0	40.6	41.9	43.0	44.0	44.9	45.6	46.2	46.7	47.2
2	20.6	23.8	26.8	29.5	31.9	34.2	36.3	38.5	40.4	42.0	43.4	44.6	45.6	46.5	47.2	47.8	48.4	48.8
3	21.3	24.7	27.7	30.5	33.1	35.4	37.6	39.8	41.8	43.5	45.0	46.2	47.2	48.1	48.9	49.5	50.1	50.6
4	22.1	25.5	28.7	31.6	34.3	36.7	38.9	41.2	43.3	45.0	46.5	47.8	48.9	49.8	50.6	51.3	51.9	52.4
5	22.9	26.4	29.7	32.7	35.5	38.0	40.3	42.7	44.8	46.6	48.2	49.5	50.6	51.6	52.4	53.1	53.7	54.2
6	23.7	27.4	30.8	33.9	36.7	39.3	41.7	44.2	46.4	48.3	41.9	51.3	52.4	53.4	54.3	55.0	55.6	56.2
7	24.5	28.3	31.7	35.1	38.0	40.7	43.2	45.8	48.1	50.0	51.7	53.1	54.3	55.3	56.2	56.0	57.6	58.2

TABLE 4 (cont'd)

ζ, Degrees	Height H, km																	
	23	24	25	26	27	28	29	30	31	32	33	34	35	36	37	38	39	40
1	1.0	1.0	1.0	1.0	1.0	1.0	1.0	1.0	1.0	1.0	1.0	1.0	1.0	1.0	1.0	1.0	1.0	1.0
2	1.9	1.9	1.9	1.9	2.0	2.0	2.0	2.0	2.0	2.0	2.0	2.0	2.0	2.0	2.0	2.0	2.0	2.0
3	2.9	2.9	2.9	2.9	2.9	3.0	3.0	3.0	3.0	3.0	3.0	3.0	3.0	3.0	3.0	3.0	3.0	3.0
4	3.8	3.9	3.9	3.9	3.9	3.9	3.9	3.9	4.0	4.0	4.0	4.0	4.0	4.0	4.0	4.0	4.0	4.0
5	4.8	4.8	4.8	4.9	4.9	4.9	4.9	5.0	5.0	5.0	5.0	5.0	5.0	5.0	5.0	5.0	5.0	5.0
6	5.8	5.8	5.8	5.9	5.9	5.9	5.9	5.9	5.9	6.0	6.0	6.0	6.0	6.0	6.0	6.0	6.0	6.0
7	6.7	6.8	6.8	6.8	6.9	6.9	6.9	6.9	7.0	7.0	7.0	7.0	7.0	7.0	7.0	7.0	7.0	7.0
8	7.7	7.7	7.8	7.8	7.9	7.9	7.9	7.9	8.0	8.0	8.0	8.0	8.0	8.0	8.0	8.0	8.0	8.0
9	8.7	8.7	8.8	8.8	8.9	8.9	8.9	9.0	9.0	9.0	9.0	9.0	9.0	9.0	9.0	9.0	9.0	9.1
10	9.6	9.7	9.8	9.8	9.9	9.9	9.9	10.0	10.0	10.0	10.0	10.0	10.0	10.0	10.1	10.1	10.1	10.1
1	10.6	10.7	10.8	10.8	10.9	10.9	11.0	11.0	11.0	11.0	11.0	11.1	11.1	11.1	11.1	11.1	11.1	11.1
2	11.6	11.7	11.8	11.8	11.9	11.9	12.0	12.0	12.0	12.0	12.1	12.1	12.1	12.1	12.1	12.1	12.1	12.2
3	12.6	12.7	12.8	12.9	12.9	13.0	13.0	13.0	13.1	13.1	13.1	13.1	13.1	13.2	13.2	13.2	13.2	13.2
4	13.6	13.7	13.8	13.9	13.9	14.0	14.0	14.1	14.1	14.1	14.2	14.2	14.2	14.2	14.2	14.2	14.2	14.3
5	14.7	14.8	14.8	14.9	15.0	15.1	15.1	15.1	15.2	15.2	15.2	15.2	15.3	15.3	15.3	15.3	15.3	15.3
6	15.7	15.8	15.9	16.0	16.0	16.1	16.2	16.2	16.2	16.2	16.3	16.3	16.3	16.3	16.4	16.4	16.4	16.4
7	16.7	16.8	16.9	17.0	17.1	17.2	17.2	17.3	17.3	17.3	17.4	17.4	17.4	17.4	17.4	17.4	17.4	17.5
8	17.8	17.9	18.0	18.1	18.2	18.2	18.3	18.4	18.4	18.4	18.5	18.5	18.5	18.5	18.5	18.5	18.5	18.6
9	18.8	19.0	19.1	19.2	19.3	19.4	19.4	19.4	19.5	19.5	19.6	19.6	19.6	19.6	19.6	19.7	19.7	19.7
20	19.9	20.0	20.2	20.3	20.4	20.4	20.5	20.6	20.6	20.6	20.7	20.7	20.7	20.7	20.8	20.8	20.8	20.8
1	21.0	21.1	21.3	21.4	21.5	21.6	21.6	21.7	21.7	21.8	21.8	21.8	21.8	21.9	21.9	21.9	21.9	21.9
2	22.1	22.3	22.4	22.5	22.6	22.7	22.8	22.8	22.9	22.9	22.9	23.0	23.0	23.0	23.0	23.1	23.1	23.1
3	23.2	23.4	23.5	23.6	23.7	23.8	23.9	24.0	24.0	24.1	24.1	24.1	24.2	24.2	24.2	24.2	24.2	24.3
4	24.4	24.5	24.7	24.8	24.9	25.0	25.1	25.1	25.2	25.2	25.3	25.3	25.4	25.4	25.4	25.4	25.4	25.4
5	25.5	25.7	25.8	26.0	26.1	26.2	26.3	26.3	26.4	26.4	26.5	26.5	26.6	26.6	26.6	26.6	26.6	26.6
6	26.7	26.9	27.0	27.2	27.3	27.4	27.5	27.5	27.6	27.7	27.7	27.7	27.8	27.8	27.8	27.8	27.8	27.9
7	27.9	28.1	28.2	28.4	28.5	28.6	28.7	28.8	28.8	28.9	28.9	29.0	29.0	29.0	29.0	29.1	29.1	29.1
8	29.1	29.3	29.4	29.6	29.7	29.8	30.0	30.0	30.1	30.1	30.2	30.2	30.3	30.3	30.3	30.3	30.4	30.4
9	30.3	30.5	30.7	30.9	31.0	31.1	31.2	31.3	31.4	31.4	31.5	31.5	31.6	31.6	31.6	31.6	31.6	31.7
30	31.6	31.8	32.0	32.2	32.3	32.4	32.5	32.6	32.7	32.7	32.8	32.8	32.9	32.9	32.9	32.9	33.0	33.0
1	32.9	33.1	33.3	33.5	33.6	33.7	33.8	33.9	34.0	34.0	34.1	34.2	34.2	34.2	34.3	34.3	34.3	34.3
2	34.2	34.4	34.6	34.8	35.0	35.1	35.2	35.3	35.4	35.4	35.5	35.5	35.6	35.6	35.6	35.6	35.7	35.7
3	35.5	35.8	36.0	36.2	36.3	36.5	36.6	36.7	36.7	36.8	36.9	36.9	37.0	37.0	37.0	37.0	37.1	37.1
4	36.9	37.2	37.4	37.6	37.7	37.9	38.0	38.1	38.2	38.2	38.3	38.3	38.4	38.4	38.4	38.5	38.5	38.5
5	38.3	38.6	38.8	39.0	39.2	39.3	39.4	39.5	39.6	39.7	39.8	39.8	39.8	39.9	39.9	39.9	40.0	40.0
6	39.8	40.0	40.2	40.5	40.6	40.8	40.9	41.0	41.1	41.2	41.2	41.3	41.3	41.4	41.4	41.4	41.5	41.5
7	41.2	41.5	41.8	42.0	42.1	42.3	42.4	42.5	42.6	42.7	42.8	42.8	42.9	42.9	42.9	43.0	43.0	43.0
8	42.7	43.0	43.3	43.5	43.7	43.8	44.0	44.1	44.2	44.3	44.4	44.4	44.4	44.5	44.5	44.6	44.6	44.6
9	44.3	44.6	44.9	45.1	45.3	45.5	45.6	45.7	45.8	45.9	46.0	46.0	46.1	46.1	46.1	46.2	46.2	46.2
40	45.9	46.2	46.5	46.7	46.9	47.1	47.2	47.4	47.5	47.5	47.6	47.7	47.7	47.8	47.8	47.8	47.9	47.9
1	47.5	47.9	48.1	48.4	48.6	48.8	48.9	49.1	49.2	49.3	49.3	49.4	49.4	49.5	49.5	49.6	49.6	49.6
2	49.2	49.6	49.9	50.1	50.4	50.5	50.7	50.8	50.9	51.0	51.1	51.2	51.2	51.3	51.3	51.3	51.4	51.4
3	51.0	51.3	51.6	51.9	52.1	52.3	52.5	52.6	52.7	52.8	52.9	53.0	53.0	53.1	53.1	53.2	53.2	53.2
4	52.8	53.2	53.5	53.8	54.0	54.2	54.4	54.5	54.6	54.7	54.8	54.8	54.9	55.0	55.0	55.0	55.1	55.1
5	54.7	55.0	55.4	55.6	55.9	56.1	56.3	56.4	56.5	56.6	56.7	56.8	56.9	56.9	57.0	57.0	57.0	57.1
6	56.6	57.0	57.3	57.6	57.9	58.1	58.3	58.4	58.6	58.7	58.7	58.8	58.9	59.0	59.0	59.0	59.0	59.1
7	58.6	59.0	59.4	59.7	59.9	60.2	60.3	60.5	60.6	60.7	60.8	60.9	61.0	61.0	61.1	61.1	61.2	61.2

TABLE 4 (cont'd)

Degrees	Height H, km																	
	5	6	7	8	9	10	11	12	13	14	15	16	17	18	19	20	21	22
48	25.4	29.4	33.0	36.3	39.4	42.2	44.7	47.4	49.8	51.8	53.5	55.0	56.2	57.3	58.2	59.0	59.6	60.2
9	26.3	30.4	34.2	37.6	40.8	43.7	46.3	49.1	51.6	53.6	55.4	56.9	58.2	59.3	60.3	61.1	61.8	62.4
50	27.2	31.5	35.4	39.0	42.3	45.2	48.0	50.9	53.4	55.6	57.4	59.0	60.3	61.5	62.4	63.3	64.0	64.6
1	28.2	32.6	36.7	40.4	43.8	46.9	49.7	52.7	55.3	57.6	59.5	61.1	62.5	63.7	64.7	65.6	66.3	66.9
2	29.3	33.8	38.0	41.9	45.4	48.6	51.6	54.7	57.4	59.7	61.6	63.3	64.8	66.0	67.1	67.9	68.7	69.4
3	30.3	35.1	39.4	43.4	47.0	50.4	53.4	56.7	59.5	61.9	63.9	65.6	67.1	68.4	69.5	70.4	71.2	71.9
4	31.5	36.4	40.9	45.0	48.8	52.2	55.4	58.8	61.7	64.2	66.3	68.1	69.6	71.0	72.1	73.1	73.9	74.6
5	32.6	37.8	42.4	46.7	50.6	54.2	57.5	61.0	64.0	66.6	68.8	70.6	72.2	73.6	74.8	75.8	76.6	77.4
6	33.9	39.2	44.0	48.5	52.6	56.2	59.7	63.3	66.4	69.1	71.4	73.3	75.0	76.4	77.6	78.7	79.6	80.3
7	35.2	40.7	45.7	50.4	54.6	58.4	62.0	65.7	69.0	71.7	74.1	76.2	77.9	79.4	80.4	81.7	82.6	83.4
8	36.6	42.3	47.5	52.3	56.7	60.7	64.4	68.3	71.7	74.5	77.0	79.1	80.9	82.4	83.8	84.9	85.8	86.6
9	38.0	44.0	49.4	54.4	59.0	63.1	67.0	71.0	74.5	77.5	80.1	82.3	84.1	85.7	87.1	88.3	89.2	90.1
60	39.6	45.8	51.4	56.6	61.4	65.7	69.7	73.9	77.5	80.7	83.3	85.5	87.5	89.2	90.6	91.8	92.9	93.8
1	41.2	47.6	53.6	59.0	63.9	68.4	72.6	76.9	80.8	84.0	86.8	89.2	91.2	92.9	94.4	95.6	96.7	97.6
2	43.0	49.7	55.8	61.5	66.6	71.3	75.6	80.2	84.2	87.6	90.4	92.9	95.0	96.8	98.4	99.7	100.8	101.7
3	44.8	51.8	58.2	64.1	69.5	74.4	78.9	83.7	87.8	91.3	94.4	96.9	99.1	101.0	102.6	104.0	105.1	106.1
4	46.8	54.1	60.8	67.0	72.6	77.7	82.4	87.4	91.7	95.4	98.5	101.2	103.5	105.5	107.2	108.6	109.8	110.8
5	49.0	56.6	63.6	70.0	75.9	81.2	86.2	91.4	95.9	99.8	103.0	105.8	108.2	110.3	112.0	113.5	114.8	115.9
6	51.3	59.3	66.6	73.4	79.5	85.1	90.3	95.7	100.4	104.4	107.9	110.8	113.3	115.5	117.3	118.8	120.2	121.3
7	53.8	62.2	69.9	76.9	83.4	89.2	94.6	100.3	105.3	109.5	113.1	116.2	118.8	121.1	123.0	124.6	126.0	127.2
8	56.5	65.3	73.4	80.8	87.5	93.7	99.4	105.4	110.6	115.0	118.8	122.0	124.8	127.1	129.1	130.8	132.3	133.6
9	59.5	68.7	77.2	85.0	92.1	98.6	104.6	110.8	116.3	121.0	124.9	128.3	131.2	133.7	135.8	137.6	139.2	140.5
70	62.7	72.5	81.4	89.6	97.1	103.9	110.2	116.8	122.6	127.5	131.7	135.3	138.3	140.9	143.2	145.0	146.6	148.0
1	66.2	76.6	86.0	94.7	102.6	109.8	116.5	123.4	129.5	134.7	139.1	142.9	146.1	148.8	151.2	153.2	154.9	156.4
2	70.2	81.1	91.1	100.3	108.7	116.3	123.3	130.7	137.2	142.6	147.3	151.3	154.7	157.6	160.1	162.2	164.0	165.5
3	74.6	86.2	96.8	106.5	115.4	123.5	131.0	138.8	145.6	151.4	156.4	160.6	164.2	167.3	169.9	172.2	174.1	175.7
4	79.5	91.8	103.2	113.5	123.0	131.6	139.5	147.8	155.1	161.3	166.5	171.0	174.9	178.1	180.9	183.3	185.3	187.1
5	85.0	98.2	110.3	121.4	131.5	140.6	149.1	158.0	165.8	172.4	178.0	182.8	186.8	190.3	193.3	195.8	198.0	199.8
6	91.3	105.5	118.4	130.3	141.1	151.0	160.6	169.6	177.9	184.9	190.9	196.0	200.4	204.2	207.3	210.0	212.4	214.3
7	98.5	113.8	127.8	140.6	152.2	162.8	172.6	182.8	191.7	199.3	205.8	211.3	216.0	220.0	223.4	226.3	228.8	230.8
8	106.9	123.4	138.6	152.4	165.0	176.5	187.1	198.1	207.8	215.9	222.9	228.8	233.9	238.2	241.9	245.0	247.7	250.0
9	116.7	134.8	151.2	166.3	180.0	192.5	204.0	216.1	226.5	235.4	242.9	249.4	254.9	259.5	263.5	266.9	269.8	272.2
80	128.5	148.3	165.4	182.9	197.9	211.6	224.2	237.3	248.7	258.4	266.7	273.7	279.6	284.7	289.1	292.7	295.9	298.5
1	142.7	164.6	184.6	202.9	219.5	234.5	248.4	262.9	275.4	286.1	295.2	306.6	301.4	315.0	319.7	323.7	327.2	330.1
2	160.3	184.8	207.2	227.6	246.0	262.8	278.2	294.3	308.2	320.0	330.0	338.5	345.8	351.9	357.1	361.5	365.3	368.5
3	182.6	210.4	235.7	258.7	279.5	298.3	315.6	333.6	349.2	362.4	373.6	383.0	391.1	397.9	403.7	408.6	412.8	416.3
4	211.8	243.8	272.8	299.0	322.8	344.2	363.9	384.3	401.9	416.8	429.3	440.0	449.0	456.6	463.1	468.6	473.2	477.1
5	251.6	289.0	322.8	353.4	380.9	405.6	428.2	351.6	471.7	488.6	502.9	514.9	525.1	533.7	541.0	547.1	552.2	556.6
6	308.7	353.4	393.7	429.8	462.1	491.0	517.3	544.4	567.6	587.0	603.4	617.1	628.7	638.4	646.6	653.5	659.3	664.2
7	396.0	451.0	493.9	543.3	581.9	616.1	647.0	678.6	705.4	727.8	746.6	762.2	775.4	786.4	795.6	803.3	809.8	815.2
88	542.1	610.8	670.9	723.6	769.7	810.2	846.3	882.9	913.9	939.5	960.8	978.4	993.2	1005.4	1015.7	1024.2	1031.3	1037.3

TABLE 4 (cont'd)

ζ, Degrees	Height H, km																		
	23	24	25	26	27	28	29	30	31	32	33	34	35	36	37	38	39	40
48	60.7	61.1	61.5	61.8	62.1	62.3	62.5	62.6	62.8	62.9	63.0	63.1	63.1	63.2	63.3	63.3	63.3	63.4
9	62.9	63.3	63.7	64.0	64.3	64.5	64.7	64.9	65.0	65.1	65.2	65.3	65.4	65.5	65.5	65.6	65.6	65.6
50	65.1	65.6	66.0	66.3	66.6	66.8	67.0	67.2	67.4	67.5	67.6	67.7	67.7	67.8	67.9	67.9	67.9	68.0
1	67.5	67.9	68.3	68.7	69.0	69.2	69.4	69.6	69.8	69.9	70.0	70.1	70.2	70.2	70.3	70.4	70.4	70.4
2	69.9	70.4	70.8	71.2	71.5	71.8	72.0	72.2	72.3	72.5	72.6	72.7	72.7	72.8	72.9	72.9	73.0	73.0
3	72.5	73.0	73.4	73.8	74.1	74.4	74.6	74.8	75.0	75.1	75.2	75.4	75.4	75.5	75.5	75.6	75.5	75.7
4	75.2	75.7	76.1	76.5	76.9	77.1	77.4	77.6	77.7	77.9	78.0	78.1	78.2	78.3	78.3	78.4	78.4	78.5
5	78.0	78.5	79.0	79.4	79.7	80.0	80.3	80.5	80.6	80.8	80.9	81.0	81.1	81.2	81.3	81.3	81.4	81.4
6	81.0	81.5	82.0	82.4	82.8	83.1	83.3	83.5	83.7	83.9	84.0	84.1	84.2	84.3	84.3	84.4	84.4	84.5
7	84.1	84.6	85.2	85.6	86.0	86.3	86.5	86.8	86.9	87.1	87.2	87.3	87.4	87.5	87.6	87.6	87.7	87.8
8	87.4	88.0	88.5	88.9	89.3	89.6	89.9	90.1	90.3	90.5	90.6	90.8	90.9	90.9	91.0	91.1	91.1	91.2
9	90.8	91.4	92.0	92.4	92.9	93.2	93.5	93.7	93.9	94.1	94.2	94.4	94.4	94.6	94.6	94.7	94.7	94.8
60	94.5	95.2	95.7	96.2	96.6	97.0	97.2	97.5	97.7	97.9	98.0	98.2	98.3	98.4	98.4	98.5	98.6	98.6
1	98.4	99.1	99.6	100.2	100.6	101.0	101.3	101.5	101.8	101.9	102.1	102.2	102.3	102.4	102.5	102.6	102.6	102.7
2	102.6	103.3	103.8	104.4	104.8	105.2	105.6	105.8	106.0	106.2	106.4	106.5	106.6	106.7	106.8	106.9	107.0	107.0
3	107.0	107.7	108.4	108.9	109.4	109.8	110.1	110.4	110.6	110.8	111.0	111.1	111.3	111.4	111.4	111.5	111.6	111.6
4	111.7	112.5	113.1	113.7	114.2	114.6	115.0	115.3	115.5	115.7	115.9	116.0	116.2	116.3	116.4	116.5	116.5	116.6
5	116.8	117.6	118.3	118.9	119.4	119.9	120.2	120.5	120.8	121.0	121.2	121.3	121.5	121.6	121.7	121.8	121.8	121.9
6	122.3	123.1	123.8	124.5	125.0	125.5	125.8	126.2	126.4	126.7	126.8	127.0	127.1	127.3	127.4	127.4	127.5	127.6
7	128.2	129.1	129.8	130.5	131.1	131.5	131.9	132.3	132.6	132.8	133.0	133.1	133.3	133.4	133.5	133.6	133.7	133.7
8	134.6	135.5	136.3	137.0	137.6	138.1	138.5	138.9	139.2	139.4	139.6	139.8	140.0	140.1	140.2	140.3	140.4	140.4
9	141.6	142.6	143.4	144.1	144.7	145.2	145.7	146.1	146.4	146.6	146.8	147.0	147.2	147.3	147.4	147.5	147.6	147.7
70	149.2	150.2	151.1	151.9	152.5	153.1	153.5	153.9	154.2	154.5	154.7	154.9	155.1	155.2	155.4	155.5	155.5	155.6
1	157.6	158.6	159.6	160.4	161.1	161.6	162.1	162.5	162.9	163.2	163.4	163.6	163.8	163.9	164.1	164.2	164.3	164.4
2	166.8	167.9	168.9	169.8	170.5	171.1	171.6	172.0	172.4	172.7	173.0	173.2	173.4	173.5	173.7	173.8	173.9	174.0
3	177.1	178.3	179.3	180.2	181.0	181.6	182.2	182.6	183.0	183.3	183.6	183.8	184.0	184.2	184.3	184.4	184.6	184.6
4	188.5	189.8	190.9	191.8	192.7	193.4	193.9	194.4	194.8	195.2	195.4	195.7	195.9	196.0	196.2	196.3	196.4	196.5
5	201.4	202.7	203.9	204.9	205.8	206.5	207.1	207.6	208.1	208.4	208.7	209.0	209.2	209.4	209.6	209.7	209.8	209.9
6	216.0	217.4	218.7	219.8	220.7	221.5	222.1	222.6	223.1	223.5	223.8	224.1	224.3	224.5	224.7	224.8	225.0	225.1
7	232.7	234.2	235.5	236.7	237.7	238.5	239.2	239.8	240.3	240.7	241.0	241.3	241.6	241.8	242.0	242.1	242.3	242.4
8	251.9	253.5	254.9	256.8	257.3	258.2	258.9	259.5	260.1	260.5	260.9	261.2	261.5	261.7	261.9	262.0	262.2	262.3
9	272.7	276.1	277.6	279.0	280.1	281.1	281.9	282.6	283.1	283.5	284.0	284.3	284.6	284.9	285.1	285.3	285.4	285.5
80	300.8	302.7	304.4	305.9	307.1	308.1	309.0	309.8	310.4	310.9	311.3	311.7	312.0	312.2	312.4	312.7	312.8	312.9
1	332.5	334.6	336.5	338.1	339.4	340.5	341.5	342.3	342.9	343.5	344.0	344.4	344.7	345.0	345.2	345.4	345.6	345.7
2	371.2	378.5	375.5	377.3	378.7	380.0	381.0	381.9	382.6	383.2	383.7	384.1	384.5	384.8	385.1	385.3	385.5	385.6
3	419.3	421.8	424.0	425.9	427.6	428.9	430.0	431.0	431.8	432.4	433.0	433.4	433.8	434.2	434.5	434.7	434.9	435.1
4	480.4	483.2	485.6	487.8	489.6	491.0	492.3	493.3	494.2	494.9	495.5	496.0	496.4	496.8	497.1	497.4	497.6	497.8
5	560.3	563.4	566.5	568.5	568.4	572.1	573.5	574.6	575.5	576.3	577.0	577.6	578.0	578.4	578.8	579.0	579.3	579.5
6	668.3	671.7	674.7	677.3	679.5	681.3	682.8	684.1	685.1	686.0	686.7	687.3	687.8	688.2	688.6	688.9	689.2	689.4
7	819.8	823.6	826.9	829.8	832.2	834.2	835.8	837.1	838.3	839.2	840.0	840.6	841.2	841.6	842.1	842.4	842.6	842.9
88	1042.3	1046.5	1050.1	1053.2	1055.8	1057.9	1059.7	1061.1	1062.4	1063.4	1064.2	1064.9	1065.5	1066.0	1066.4	1066.7	1067.0	1067.3

Note: The values of the angle r are given in seconds of arc.

/36

TABLE 5

ζ, Degrees	Data		Difference
	Link and Sekera	Main Astron. Observ. Ukr. Acad. of Sciences SSR	
75	212.6″	209.9″	+ 2.7″
80	317.1	312.9	+ 4.2
83	439.6	435.1	+ 4.5
85	587.4	579.5	+ 7.9
86	699.1	689.4	+ 9.7
87	857.7	842.9	+14.8
88	1088.3	1067.3	+21.0

gradients is significantly less and may become positive as well as negative. At identical initial conditions at the Earth's surface, the difference in the value of $\frac{\Delta\rho}{\Delta h}$ at the 0 - 1 km stratum leads to a change in r of approximately

$$(\mu_0 - 1)\tan\zeta\cdot\Delta\rho \approx 3\cdot10^{-4}\cdot10^{-2}\tan\zeta \approx 3\cdot10^{-6}\tan\zeta,$$

which corresponds to 0.6″ tan ζ.

At a zenith distance of 75° the increase of refraction according to Link and Sekera in comparison to that obtained by the Main Astronomical Observatory of the Academy of Sciences of the Ukrainian SSR would be 2.2″, while at 88° it would be 17.4″, which corresponds approximately to the data in Table 5.

A Comparison of the Obtained Tables with the Pulkovo Refraction Tables. For comparison with the Pulkovo refraction tables we must allow for several corrections.

Correction for change in wavelength. It is considered that /37
the Pulkovo refraction tables correspond to λ = 575 mμ [8]. From the tables in [6] it can be learned that $\mu_{530} - \mu_{575} \approx 86\cdot10^{-8}$ at T = 288° K, P = 1013.25 mb. The appropriate correction for making the transition from our tables to the Pulkovo tables at not too great values of ζ can be computed by the formula

$$\Delta_1 r = (\mu_{575} - \mu_{530})\tan\zeta \approx -9\cdot10^{-7}\tan\zeta \approx -0.18''\tan\zeta.$$

Correction for atmospheric height. In calculating our tables we took the maximum height of an object to be equal to 40 km. In practice, in calculating astronomical refraction, one can ignore strata above 300 km. In fact, even at a height of 200 km, the

relative density of the air is equal to $3 \cdot 10^{-10}$, so that the influence of superincumbent strata on the refraction integral can be considered negligible. The correction for atmospheric height can be roughly accounted for by using the formula

$$\Delta_2 r = (\mu_{40} - \mu_{300}) \tan \zeta \approx 9 \cdot 10^{-7} \tan \zeta,$$

where μ_{40} and μ_{300} are the refractive indices at a height of 40 and 300 km, equal to $\mu_{40} = 1.0000009$, $\mu_{300} = 1$.

Correction for air moisture. Our tables were calculated for dry air, but the Pulkovo tables were calculated for moist air with a water vapor pressure of 5.5 mb. Moisture reduces refraction; the refractive index of the air decreases due to moisture by $6 \cdot 10^{-8}$ for every millibar of water vapor pressure. The appropriate correction can be estimated according to the formula

$$\Delta_3 r = -0.066'' \tan \zeta.$$

The combined correction for making the transition from our tables to the Pulkovo tables would be equal to

$$\Delta r = \Delta_1 r + \Delta_2 r + \Delta_3 r = [(\mu_{575} - \mu_{530}) + (\mu_{40} - \mu_{300}) - 0.066''] \tan \zeta \approx -0.07'' \tan \zeta.$$

(the subscripts 40 and 300 indicate height in kilometers).

In sum, the following differences are obtained between the refraction values according to the Pulkovo tables and ours (obtained in Golosyevo):

ζ	10	20	30	40	50	60	70	80-85
Difference Pulkovo Goloseyevo	0.00"	0.00"	0.00"	+0.03"	+0.01"	+0.01"	+0.00"	-0.06"to-0.17"

As we see, the differences are fairly small.

Calculation of Values of the Angle r_A at Heights Greater than 40 km. /38

It was possible to calculate the angle r_A at heights greater than 40 km in the same manner as at smaller heights, i.e. by extending the integration in formula (2) to heights greater than 40 km and by then calculating r_A according to formula (6). Here, in view of the fact that the density in the atmospheric strata under consideration is very small, it is feasible to increase the integration interval, i.e. the thickness of the unit stratum. Since our calculations were carried out on an electronic computer, this caused certain inconveniences, and we used a different procedure, in which the path

of the ray in strata above 40 km was considered to be a straight line, i.e. the angle of refraction r in these strata was assumed to be equal to zero. Link [11] applied the same method in his turn. We calculate the approximate value of the angle ϕ. From Figure 1 it is evident that

$$\varphi_H = \zeta + r_H - i_H, \tag{10}$$

where the subscript H indicates that the corresponding angles are taken at the height of the object located on the ray. We shall restrict ourselves to consideration of the case when 40 km $\leq H \leq$ 300 km. The angle r_H must be determined according to formula (7), and i_H by the formula

$$\sin i_H = \frac{\mu_0}{\mu_H} \cdot \frac{R_0}{R_H} \sin \zeta, \tag{11}$$

where

$$R_H = R_0 + H.$$

If we ignore refraction at $H > 40$ km, we must obviously assume $\mu_H \approx \mu_{40}$ in formula (11) and calculate the appropriate rough values for the ray's angle of emergence which we now designate by i'_H. It is obvious that $i'_H < i_H$, since $\mu_{40} > \mu_H$. On the other hand, in formula (10), instead of r_H we can substitute the value r_{40}, while $r_{40} < r_H$. Thus, the errors in r and i will compensate for one another to a certain degree, reducing the error of ϕ. From formula (11) it follows that

$$\sin i'_H - \sin i_H \approx (\mu_H - \mu_{40}) \frac{R_0}{R_H} \sin \zeta \tag{12}$$

or, since i'_H differs little from i_H, that /39

$$i'_H - i_H \approx \frac{(\mu_H - \mu_{40}) \frac{R_0}{R_H} \sin \zeta}{\cos i_H}. \tag{13}$$

For a rough estimate, if we assume $i_H \approx \zeta$ and $\frac{R_0}{R_H} \approx 1$, then it is evident from formula (13) that

$$i'_H - i_H \approx (\mu_H - \mu_{40}) \tan \zeta < 0.$$

The error of the equation $r_H \approx r_{40}$ at not too great values of ζ (< 80°) can be estimated according to the formula

$$\Delta r \approx (\mu_{40} - \mu_{H}) \tan \zeta. \tag{14}$$

Thus, in the approximation used by us, the effect of error in i and r on the value of the angle ϕ roughly compensates for itself. Since the angle r under normal conditions is less than 0.6°, with an error of less than 1°, the equation

$$\zeta - i \approx \varphi. \tag{15}$$

would be valid.

The value of ϕ (as follows, for instance, from Link's tables) at H = 300 km and ζ = 88° is equal to 15.6°, while at ζ = 80°, it is 9.9°. The effect of error in the values of the angle ϕ on the error of z or of z_A can be estimated by differentiating formula (6) over ϕ. In this manner we obtain

$$\frac{dz}{d\varphi} = \frac{(1 + \varepsilon \cos\varphi - \cos\varphi)\cos^2 z}{(\cos\varphi - 1 + \varepsilon)^2}, \tag{16}$$

where

$$\varepsilon = \frac{H}{R_0 + H}.$$

In formula (16) we can assume $z = \zeta$. Then at small values of ϕ we obtain

$$\frac{dz}{d\varphi} \approx \frac{R_0 + H}{H} \cos^2 \zeta,$$

and

$$\Delta z \approx \left(\frac{dz}{d\varphi}\right) \Delta\varphi. \tag{17}$$

From formulas (16) and (17) it is evident that at small values of ζ and H, $\frac{dz}{d\phi}$ will be so large that the error in determining the angle /40
z can be ten times greater than the error in the angle ϕ, and this fact must be allowed for in the calculations. Computation of the error in the values of Δi according to formula (13) and of Δr according to formula (14), as well as allowing for $\frac{dz}{d\phi}$ by means of formula (16) permits us to estimate the error in calculations of r_A, by substituting a straight path for the curved path of the light ray in the height range from 60 to 300 km in the following manner:

ζ, Deg.	10	30	45	60	70	80	88
Error Less than	0.05″	0.1″	0.2″	0.3″	0.5″	1″	3″

In calculating these values we assumed $\phi \approx \zeta - i$, but in formula (14) $\mu_{40} \approx 9 \cdot 10^{-7}$ and $\mu_H = \mu_{300} = 1$ for all heights, such that

$$\Delta r \approx 0.18'' \tan \zeta.$$

The values of Δr at $\zeta = 88°$ were calculated by multiplying 0.18" by the ratio $\frac{r_{83}}{r_{45}}$, which at $H = 40$ km is equal to 18.7.

The values of the angles r_A, calculated by the indicated method, for the standard z atmosphere are given in Table 6.

TABLE 6

ζ.Deg.	Height H, km						
	60	80	100	150	200	250	300
10	8.9"	9.2"	9.4"	9.6"	9.7"	9.8"	9.8"
20	18.4	19.0	19.3	19.8	20.1	20.2	20.3
30	29.0	30.0	30.6	31.4	31.8	32.0	32.2
40	41.9	43.4	44.3	45.5	46.1	46.5	46.7
50	59.2	61.4	62.7	64.4	65.3	65.8	66.2
60	85.4	88.7	90.6	93.2	94.5	95.3	95.9
70	134.1	139.3	142.4	146.6	148.7	150.0	150.8
75	180.2	187.2	191.5	197.1	200.0	201.7	202.9
76	193.0	200.6	205.1	211.2	214.2	216.1	217.4
77	207.6	215.7	220.6	227.2	230.5	232.5	233.9
78	224.4	233.2	238.4	245.5	249.1	251.3	252.8
79	243.9	253.4	259.2	266.9	270.8	273.2	274.9
80	266.9	277.2	283.5	292.0	296.3	299.0	300.8
81	294.2	305.6	312.5	321.8	326.7	329.7	331.7
82	327.2	339.8	347.5	358.0	363.4	366.8	369.1
83	367.8	382.7	390.6	402.5	408.7	412.6	415.3
84	418.9	434.9	444.8	458.5	465.8	470.3	473.5
85	484.6	503.1	514.6	530.8	539.4	544.9	548.8
86	571.8	593.6	607.2	626.7	637.4	644.2	649.1
87	691.2	717.5	734.4	758.7	772.3	781.1	787.5
88	861.6	894.6	916.1	948.0	966.1	978.1	986.8

Values of r_A for various heights and for zenith distances of 10°, 50°, 88° are plotted as graphs in which the height in kilometers corresponds to the x-axis while the y-axis corresponds to values of the angle r_A in angular seconds. Values of r_A for heights $H < 40$ km are plotted on these graphs (Fig. 2). In progressing past $H = 40$ km, the values of r_A change fairly smoothly for all ζ. We note that the ratio $\frac{r_A}{r}$ at a given ζ increases in proportion to the increase in height of the object. This ratio is given in Table 7 for various ζ and H. At a height of 5 km, $\frac{r_A}{r}$ changes from the value 0.55 at $\zeta =$ 10° to the value 0.53 at $\zeta = 88°$. Obviously, at heights less than 5 km the value of $\frac{r_A}{r}$ approaches 0.5, which agrees with a common assumption in geodesy, when the path of a ray near the Earth's surface is taken for part of the circumference. At great heights the value of $\frac{r_A}{r}$ approaches unity as is to be expected.

/41

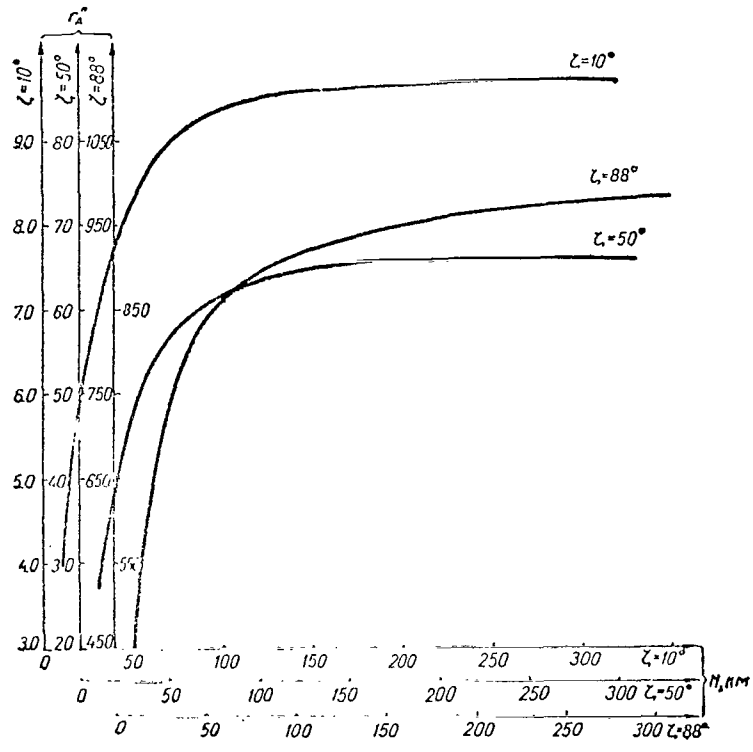

Fig. 2.

TABLE 7

/42

ζ, Degrees	Height H, km										
	5	10	15	20	25	30	35	40	100	200	300
10	0.55	0.57	0.60	0.65	0.69	0.73	0.77	0.79	0.93	0.96	0.97
20	0.54	0.57	0.60	0.65	0.69	0.73	0.76	0.79	0.92	0.96	0.97
30	0.54	0.57	0.60	0.65	0.69	0.73	0.76	0.79	0.92	0.96	0.97
40	0.54	0.57	0.60	0.65	0.69	0.73	0.76	0.79	0.92	0.96	0.97
50	0.53	0.57	0.60	0.65	0.69	0.73	0.76	0.79	0.92	0.96	0.97
60	0.53	0.57	0.60	0.65	0.69	0.73	0.76	0.79	0.92	0.96	0.97
70	0.53	0.57	0.60	0.65	0.69	0.73	0.76	0.79	0.91	0.95	0.97
80	0.53	0.57	0.60	0.65	0.69	0.73	0.76	0.78	0.90	0.94	0.96
88	0.53	0.57	0.60	0.64	0.69	0.73	0.73	0.75	0.85	0.90	0.92

Comparison of the obtained values of r_A with values calculated by other authors. For zenith distances less than 75°, ignoring the curvature of the Earth, we can derive an approximate formula for calculating the angle r_A:

$$r_A = (\mu_0 - 1)\left[1 - \frac{l(H)}{H}\right] \tan \zeta. \qquad (18)$$

Here the value of μ_0 is taken for conditions at the point of observation, H is the height of the object above the Earth's surface,

$l(H)$ is expressed by the integral

$$l(H)=\int_0^H \frac{\rho(h)}{\rho_0}\,dh, \tag{19}$$

where $l(H)$ is a height analogous to the height of the uniform atmosphere for a stratum of thickness H. Formula (18) was first presented in V. Numerova's article [2]. It was also used in Dufour's article [12].

For the standard atmosphere $l(H)$ has the values given in Table 8. Using these values of $l(H)$ and a value of μ_0 - 1 equal to /43

TABLE 8

Height H, km	$l(H)$, km	Height H, km	$l(H)$, km	Height, H, km	$l(H)$, km	Height H, km	$l(H)$, km
1	0.95	6	4.51	15	7.43	50	8.43
2	0.82	7	5.02	20	7.98	60	8.44
3	2.60	8	5.47	25	8.23	80	8.44
4	3.30	9	5.87	30	8.34	100	8.44
5	3.94	10	6.23	40	8.41	—	—

0.00027824 (for a wavelength assumed by us to be λ = 530 mμ), we obtain values of r_A which are compared in Table 9 to those we computed. The maximum discrepancy at ζ = 70° is approximately 2″. The

TABLE 9

ζ, Deg.	Height H, km											
	10			20			40			100		
	1	2	3	1	2	3	1	2	3	1	2	3
10	3.8″	3.8″	0.0″	6.1″	6.1″	0.0″	8.9″	8.0″	0.0″	9.3″	9.4″	−0.1″
20	7.9	7.9	0.0	12.5	12.5	0.0	16.5	16.5	0.0	19.1	19.3	−0.2
30	12.6	12.5	+0.1	19.9	19.9	0.0	26.2	26.1	+0.1	30.4	30.6	−0.2
40	18.3	18.0	+0.3	28.9	28.9	0.0	38.0	37.9	+0.1	44.1	44.3	−0.2
50	26.0	25.7	+0.3	41.0	41.0	0.0	54.0	53.8	+0.2	62.7	62.7	0.0
60	37.8	37.3	+0.5	59.6	59.4	+0.2	78.5	78.0	+0.5	90.1	90.6	−0.5
70	59.9	59.0	+0.9	94.6	93.8	+0.8	121.6	122.9	+1.7	144.5	142.4	+2.1

Notes; (1) shows the values calculated according to an approximate formula; (2) shows the values obtained by numerical integration; (3) shows the difference between the first two values.

greatest deviation from the table of values for r_A calculated by V. Numerova on the basis of formula (18), correcting for the difference between the initial conditions, is approximately 3″ at a height of 15 km and ζ = 80°. This divergence can be attributed in part to the difference in density at a height of 15 km in the atmospheric models used.

Now let us compare our data with the values of r_A calculated on the basis of Veis' formula [13]. According to Veis, the difference between the angles r_∞ and r_A in the case of a very distant object is determined by the formula

$$r_\infty - r_A = 435.0'' \tan\zeta \frac{}{H}(1 - e^{-0.1385H}), \qquad (20)$$

where H is expressed in kilometers, while the coefficient corresponds to the conditions: temperature of 0°C and pressure of 760 mm Hg. Veis' formula is derived for the condition $\zeta < 45°$. We assumed that r_∞ under these conditions is expressed by the formula /44

$$r_\infty = 60.2'' \tan\zeta.$$

Reducing the values of r_A found by us to these conditions (which is equivalent to increasing them by 5%) we obtain the values given in Table 10.

TABLE 10

H, km	ζ, Degrees											
	10			20			30			40		
	1	2	3	1	2	3	1	2	3	1	2	3
10	4.9″	4.0″	−0.1″	10.1″	8.3″	+1.8″	16.0″	13.1″	+2.9″	23.2″	19.0″	+4.2″
40	8.7	8.4	+0.2	18.0	17.3	+0.7	28.5	27.4	+1.1	41.4	39.8	+1.3
100	9.8	9.9	−0.1	20.3	20.3	0.0	32.2	32.1	+0.1	46.9	46.5	+0.6
200	10.2	10.2	0.0	21.1	21.1	0.0	33.5	33.4	+0.1	48.7	48.4	+0.4
300	10.4	10.3	+0.1	21.4	21.3	+0.1	33.9	33.8	+0.1	49.3	49.0	+0.3

Notes: (1) shows the values calculated according to Veis' formula; (2) shows the values obtained at the Main Astronomical Observatory of the Academy of Sciences of the Ukrainian SSR; (3) shows the difference of these two values.

Values of the Angle r_B at Heights Greater than 40 km

Let us consider what values of the angle r_B are obtained at heights greater than 40 km. Approximate values of the angles can be obtained from the formula $r_B = r_H - r_A$. We obtain approximate values for r_H by adding the value $\Delta r = (\mu_{40} - \mu_H) \tan\zeta$ to r_{40}. We considered that at $H \geq 60$ km, $\mu_H - 1 = 0$. (Actually $\mu_{60} - 1 = 9 \cdot 10^{-8}$, while $\mu_{40} - 1 = 9 \cdot 10^{-7}$.) Allowing for these corrections and using our tables for finding r_{40} and Table 2 for r_A, we find the values of the angle r_B (Table 11).

Table 12 gives the results of comparing the values of r_B with the data of other authors for an object at a height H = 100 km. It can be seen from the table that the values computed by the authors of the present article agree very well with those given by I.F. Kushtin [7, 8], calculated according to formula (21) at H = 100 km:

TABLE 11

H, km	ζ, Degrees									
	10	20	30	40	50	60	70	80	85	88
100	0.7″	1.6″	2.5″	3.7″	5.5″	8.3″	13.7″	30.5″	66.9″	156.4″
200	0.4	0.8	1.3	1.9	2.9	4.4	7.4	17.7	42.1	106.4
300	0.3	0.6	0.9	1.3	2.0	3.0	5.3	13.2	32.7	85.6

TABLE 12

/45

Author	ζ, Degrees						
	10	20	30	40	50	60	70
I.G. Kolchinskiy et al.	0.7″	1.6″	2.5″	3.7″	5.5″	8.3″	13.7″
I.F. Kushtin	0.8	1.7	2.7	3.9	5.5	8.0	12.8
Difference: Kolchinskiy-Kushtin	-0.1	-0.1	-0.2	-0.2	0.0	+0.3	+0.9
Jones	--	--	7.3	--	10.1	--	16.1
Barrow	--	--	3.2	--	6.7	--	15.4
Kabeláč	0.9	1.9	3.1	4.6	6.1	8.6	

$$r_B = \frac{465''}{H} \tan \zeta. \qquad (21)$$

This approximate formula corresponds to conditions of the standard atmosphere. The values given by Kabeláč [14] agree satisfactorily with ours, while those of Barrow [15] and especially Jones [16] are greatly exaggerated.

Thus, taking into account the good agreement of our data with the data of all the authors who calculated the angles r_A and r_B by approximate formulas, and our remarks on the accuracy of our calculations, we must consider the values obtained by us for the angles in the entire range of zenith distances 0-88° and of heights 5-300 km sufficiently reliable for practical use under conditions similar to conditions of the standard atmosphere.

The problem of corrections for deviations from these conditions will be analyzed in another article. Here we note only that for rough estimates at not too great values of ζ in the case of fairly high objects, we can make the transition from the values $r_A(P_{st}, T_{st})$, corresponding to standard conditions, to the values of P and T at the point of observation using the formula

$$r_A(P, T) = r_A(P_{st}, T_{st}) \cdot \frac{P}{P_{st}} \cdot \frac{T_{st}}{T}, \qquad (22)$$

just as is done in the approximate theory of astronomical refraction. For more precise calculations of the angle r_A we must carry out numerical integration over the results of sounding in each separate case or use the values of the angles calculated according to the average seasonal results of sounding. /46

References

1. Kolchinskiy, I.G.: Refraktsiya sveta v zemnoy stmosfere (Refraction of Light in the Earth's Atmosphere). "Naukova dumka" Press, Kiev, 1967.
2. Numerova, V.: Byull. Astron. in-ta. No. 35, pp. 249-254, 1934.
3. Tablitsa standartnoy atmosfery, Gost 4401-64 (Table of the Standard Atmosphere, All-Union State Standard 4401-64), Standards Press, Moscow, 1964.
4. Spravochnik po geofizike (Geophysics Handbook). "Nauka" Press, Moscow, 1964.
5. Gemfris, V.: Fizika vozdukha (The Physics of Air). United Scientific and Technical Presses, Moscow, Leningrad, 1936.
6. Tablitsy refraktsii Pulkovskoy observatorii (Refraction Tables of the Pulkovo Observatory). Academy of Sciences USSR Press, Moscow, Leningrad, 1956.
7. Kushtin, I.F.: Izv. vuzov. "Geodeziya i aerofotos'yemka", No. 4, pp. 89-100, 1966.
8. Kushtin, I.F.: Geodeziya i kartografiya, No. 11, pp. 45-52, 1966.
9. Link, F. and Z. Sekera: Dioptrische Tafeln der Erdatmosphäre (Dioptric Tables of the Earth's Atmosphere). Prague, 1940.
10. Cospar International Reference Atmosphere Amsterdam, 1961.
11. Link, F.: Extension des tables dioptriques de l'atmosphère terrestre (Extension of the dioptric Tables of the Earth's Atmosphere). Prague, 1947.
12. Dufour, H.M.: Bull. Géodésique, Vol. 73, pp. 217-229, 1964.
13. Veis, G.: Space Sciences Review, Vol. 2, p. 2, 1963.
14. Kabelac, J.: Wiss. Zeitschr. der Techn. Univ. Dresden, Vol. 14, No. 3, pp. 675-678, 1965.
15. Barrow, C.H.: Photogramm Engineering, Vol. 26, No. 5, pp. 798-804, 1960.
16. Jones, B.L.: J. Geophys. Res., Vol. 66, No. 4, pp. 1135-1138, 1961.

OBSERVATIONS OF ASTRONOMICAL REFRACTION AT GREAT ZENITH DISTANCES MADE IN GOLOSEYEVO (KIEV SUBURB)

N.A. Vasilenko

ABSTRACT: The results of observations of astronomical refraction near the horizon taken on a 2-second multipurpose instrument are given. The maximum deviation of the measured refraction from the calculated refraction on the basis of the Pulkovo tables reaches 1' at a zenith distance of 89.5°. In some cases the measured refraction was compared with that obtained by the method of numerical integration of atmospheric sounding data. The measured refraction was less than that calculated. The deviations are 3 - 4 percent of refraction value, which is difficult to explain by human or instrumental observational errors.

The accuracy with which it is possible to correct for refraction in observation of heavenly bodies has always concerned astronomers. For instance, according to F. Bessel's estimates given in [1], the probability of the deviation of the actual refraction from the tables in the case of zenith distances from 70 to 90° may reach values of /47

70°	80°	85°	88°	89°	89.5
±0.5″	±0.9″	±1.7″	±7.7″	±16.8″	±20.0″.

Astronomers have carried out observations of heavenly bodies at zenith distances greater than 80° comparatively infrequently. Information on investigations for determining true astonomical refraction near the horizon is given in I.G. Kolchinskiy's survey [2].

Observations of celestial bodies near the horizon for the purpose of determining the amount of refraction, which have been carried out up to the present, in the majority of cases were sporadic and of short duration, and therefore were unable to furnish sufficient material for the problem under investigation [3-5 et al.]. The problem of the deviation of true refraction from that calculated from tables has not yet been sufficiently clarified.

Systematic observations of celestial bodies near the horizon were carried out in 1867 - 1868 by the Pulkovo astronomer V. Ye. Fuss [2,9]. He observed the Sun and the Stars with the aid of vertical Repsold transit circle.

TABLE 1

Date of Observation	Heavenly Body	Zenith Distance	Deviation of Measured from Calculated Refraction	Temperature, °C	Pressure, mm
1868,Mar 16	Sun	89°26'	+ 79"	- 4.2	771.9
1868,Oct 7	β Tauri	89 29	+ 79	+ 4.8	765.0
1868,Oct 5	β Tauri	89 48	+105	+ 1.1	770.0
1868,Oct 5	β Orionis	89 50	+259	+ 2.0	769.5
1868,Mar 17	Sun	89 59	+150	- 2.4	764.4
1867,Aug 31	Sun	90 01	+110	+10.8	757.0

As an example, Table 1 presents several results of his observations, from which it is evident that for Pulkovo true refraction near the horizon, even at normal meteorological conditions, can exceed the refraction calculated according to Gulden's theory by up to 4'. /48

According to observations of the Sun near the horizon carried out by V. Kh. Buynitskiy in the Arctic in 1938-39 on the icebreaker "Sedov" with the aid of Hildebrandt and Kern multipurpose instruments [5], the increase of the measured refraction over the refraction calculated according to the Pulkovo tables reached 16' at a zenith distance of 89°54'.

As a result of the swift development of cosmic geodesy, investigation of the deviation of the true refraction from the calculated refraction at all zenith distance has attracted great interest. In connection with this, the Main Astronomical Observatory of the Academy of Sciences of the Ukrainian SSR has carried out observation of bodies near the horizon for the purpose of determining the true astronomical refraction.

For this purpose we used heavenly bodies whose equatorial coordinates can be considered to be known fairly precisely, in any case with an error no greater than 0.1". The luminosity of the bodies had to be great enough for them to be observed at the horizon. Such bodies are, for instance, the Sun, the planet Jupiter and the bright stars (no weaker than the first magnitude) α Orionis, α Canis Minoris, α Boötes, α Lyrae, α Canis Majoris, β Tauri, β Orionis.

If at a determined moment of time S the visible zenith distance of a body ζ is measured, and its true value z is computed, then the refraction will be equal to

$$r = z - \zeta$$

On the other hand, having determined the temperature, the pressure and the humidity of the air at the instrument's lens at the moment of observation, it is possible, by using, for instance, the Pulkovo

refraction tables, to obtain the value of the refraction r_p for a given ζ.

For zenith distances $0° < \zeta < 80°$, as is known, it is possible to consider with sufficient approximation, that

$$z - \zeta - r_p = 0. \qquad (1)$$

At $\zeta \geq 80°$, equation (1) ceases to be valid and we can write

$$z - \zeta - r_p = \Delta r. \qquad (2)$$

For instance, according to Bessel, at $\zeta = 80°$, the value Δr can reach several tenths of a second.

For the purpose of determining the values of Δr for zenith distances $80° < \zeta < 90°$, observations of bright objects near the horizon were begun in 1965 at Goloseyevo from a specially constructed tower (see figure). The basic task which we formulated was that /49

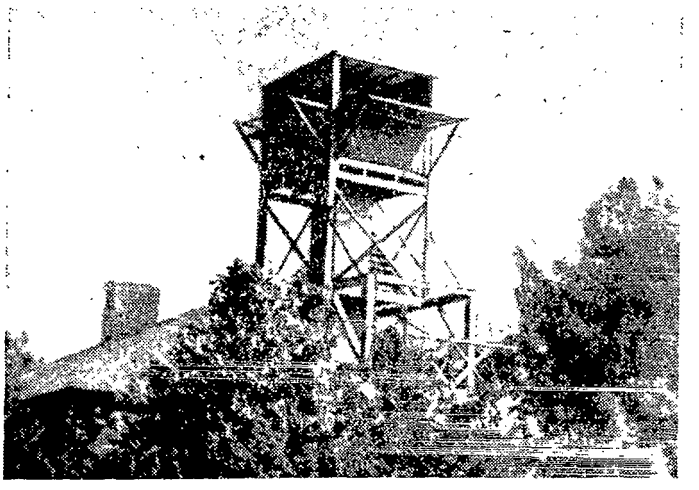

of determining the order of magnitude of the deviation of the measured refraction from that calculated from tables. Furthermore, we calculated the astronomical refraction on the basis of aerological data for moments close to the moments of observation; the astronomical refraction was compared to the true and the table refraction.

Instruments, Methods and Accuracy of the Observations

For the observations we used a two-second multipurpose instrument UV 2″/2″ EOMZ TsNIIGAiK, which is characterized by the following parameters. The main tube is a broken line, centrally located, with a focal length of 450 mm, an objective lens diameter of 55 mm, a field of vision of 54′ and a magnifying power of 45 - 56. The vertical circle has a diameter of 220 mm, with the smallest graduations of the micrometer-microscope drum at 2″ and with a recording accuracy of 0.2″. The levels are: at the alidade of the vertical

circle with a scale value of 1.3", a Talcott level with a scale value of 1.6" and a level laid on the horizontal axis of the instrument with a scale value of 2.4".

Before beginning the observations the instrument was investigated under laboratory conditions. It appeared to be completely satisfactory for purposes of measuring the zenith distance of heavenly bodies. /50

With the aid of a recording chronograph, we determined the moment of passage of the image of a heavenly body through three central horizontal cross-hairs of a telescope by the "eye-key" method; we took readings from the micrometer-microscope of the vertical circle and from the level at the frame of the microscopes. At the beginning and end of the observations, signals of the exact time to the second were taken orally on the stellar chronometer with an error of ± 0.05 sec. The chronograph tape at the beginning and end of the observation was attached to the time information furnished by the chronometer. Contact breaking in registering the moment of passage through one cross-hair was carried out with an error of ± 0.1 sec. The error in registering the moment of passage through the central cross-hair of the telescope, correcting for signal reception, was equal to ± 0.08 sec.

At the beginning and end of the observations we determined the zenith location ZL of the vertical circle with respect to the Pole star. The oscillation of ZL in the course of an evening did not exceed 2". At the moment of measuring the ζ of a heavenly body, we recorded the readings on two thermometers with an accuracy of ± 0.1° and on an aneroid barometer with an accuracy of ± 0.1 mm. Allowing for differences in the thermometer readings, as they were located in different places in the shed, in practice the error in determining the temperature of the lowest stratum of air (at the objective) was equivalent on the average to approximately ± 0.3°.

The error of vertically positioning the instrument's telescope is composed of several basic errors: (1) errors of sighting in on a delineation of the limb and of reading from the micrometer drum, whose total error may be assumed to be equal to ± 1", but if the process is repeated four times, the error will be reduced to ± 0.5": (2) random errors in determining the diameters of the limb, which can be assumed to be equal to ± 0.5"; (3) systematic errors in determining the limb's diameters, uncompensated for in this method of observation, which may be assumed on the average not to exceed ± 0.5"; (4) errors in calculating its inclination, equal to ± 0.5". On the basis of these data, we shall find the mean square error of reading off the vertical circle to be m_0 = 1.0".

Systematic error in measuring ζ, due to the bent shape of the telescope, is not excluded from the results. Due to the lack of solid supports for installing collimators, there was no opportunity to determine the coefficients of the bending of the telescope with

any reliability. From approximate determinations based on the stars at the meridian it was established that the vertical bending of the telescope at $\zeta = 89°$ did not exceed $\pm 1.5''$. Since with the broken path of the ray in the telescope the error due to the bending was basically caused by the suspension of the lens part, the value of ζ was constantly reduced, while as a result of varying the moment of observation, z increased, and consequently the measured refraction proved to be somewhat exaggerated. /51

Thus, the strictly instrumental error in measuring the zenith distance of a heavenly body was approximately $\pm 1.5''$ at $\zeta = 80°$ and $\pm 2.5''$ at $\zeta = 89°$. Due to atmospheric dispersion and flickering of the images, at $\zeta = 88 - 89°$ the errors of measurement could reach $6 - 8''$.

The results of the observations were rounded off to tenths of a second before being processed.

Concerning the Errors of Calculating True Zenith Distances and Refraction According to Tables

We calculated the true zenith distances z for a given moment of observation of a heavenly body s according to the known formula

$$\cos z = \sin \varphi \sin \delta + \cos \varphi \cos \delta \cos t. \tag{3}$$

In this equation, the zenith distance z and the hour angle $t = s - \alpha$ vary, but the latitude for a given location and the declination of the heavenly body remain constant. The latitude of the place of observation was known with an error of $\pm (0.1 - 0.2'')$. The equatorial coordinates of the body α and δ for a given moment of observation were interpolated using the "astronomicheskiy yezhegodnik" (Astronomical Yearbook) with errors not exceeding $\pm 0.2''$; we did not allow for the terms of the short-period nutation. The moment of passage through the central cross-hairs s, and consequently, the hour angle t as well, were known with an error of $\Delta t = \pm 0.08$ sec.

Taking into account the errors in the values of ϕ, α, δ and t, which figure in equation (3), the total error of calculating z in the most unfavorable case (at the first vertical circle) reached $1''$.

In calculating the refraction r_p from the Pulkovo tables, we did not correct for the humidity of the air and for the spectral class of the heavenly bodies. At a mean value of the relative air moisture of Goloseyevo of 80% and with extreme values of the temperature at the moment of observation at +20° and -20°, the corrections may reach a magnitude of from $0.5''$ at $\zeta = 80°$ to $1.8''$ at $\zeta = 88°$.

In neglecting corrections for the spectral class of the heavenly bodies in calculating refraction, we allowed for an error of up to 0.5″ at $\zeta = 88°$. Due to an error of determining the temperature of the lowest stratum of air at the moment of observation of $\Delta t°C = \pm 0.3°$, on the average we allowed an error in calculating the refraction from ± 0.4″ at $\zeta = 80°$ to ± 2.0″ at $\zeta = 88°$. We allowed, /52 on the average, a total error in calculating the refraction from tables equal to ± 1″ at $\zeta = 80°$ and ± (2-3″) at $\zeta = 88°$; under the most unfavorable conditions this error could reach 4″.

The values of Δr for single observations were obtained on the average with errors of ± (2-3″) for $\zeta = 80°$ and 5-7″ for $\zeta = 88°$. Under the most unfavorable conditions, the error in the value of Δr for a single observation could reach 10-12″ at $\zeta = 88 - 89°$. In all tables, the results of calculating z, r_p and Δr are given rounded off to tenths of a second.

Observational Results

In our research we analyzed the results of observations from 37 evenings. Certain individual observational results are presented in Table 2. During the period under consideration, the observations were carried out in a temperature range from +27 to -23°C and at pressures of 742 - 757 mm at an altitude of 200 m above sea level.

Table 2 clearly shows the decrease in the true refraction for Goloseyevo with reference to the refraction calculated from tables; this discrepancy sometimes reaches several tens of seconds at the

TABLE 2

Date, Heavenly Body	Local Sidereal Time s	Visible Zenithe Distance ζ	$\Delta r = z - \zeta - r_p$	Air Pressure, mm	Air Temperature at the Objective 0_C
5—6. IV 1965 a Canis Majoris	13h07m31s.3	81°01′57″.6	+ 1″.7	751.5	— 3.8
	13 17 31 .7	82 36 30 .0	— 0 .1	—	—
	13 22 35 .0	83 24 07 .8	— 3 .1	—	—
	13 27 46 .5	84 12 50 .8	— 5 .3	—	—
	13 32 37 .7	84 58 04 .3	— 2 .4	—	—
	13 37 32 .6	85 43 46 .7	— 6 .0	—	—
	13 42 46 .4	86 31 39 .8	— 9 .1	—	—
	13 47 28 .6	87 14 18 .6	—15 .5	—	—
	13 52 21 .6	87 57 38 .1	—14 .0	751.5	— 4.0
6. IV 1965 Sun	6 50 05 .4	83 03 57 .3	— 4 .2	751.4	+ 7.6
	6 58 09 .2	84 19 18 .3	— 4 .7	—	—
	7 05 38 .2	85 28 40 .1	— 8 .2	—	—
	7 13 22 .1	86 39 20 .2	— 1 .2	—	—
	7 20 37 .9	87 44 15 .2	—10 .6	—	—
	7 28 14 .5	88 50 06 .9	—26 .8	—	—
	7 33 30 .0	89 19 44 .3	—44 .5	751.5	+ 6.0

TABLE 2 (Cont'd)

Date, Heavenly Body	Local Sidereal Time s	Visible Zenithe Distance ζ	$\Delta r = z - \zeta - r_p$	Air Pressure, mm	Air Temperature at the Objective 0c
6—7.IV 1965 Jupiter	10h27m53s.6	83°09'54".4	— 6".2	751.5	+ 3.0
	10 32 58 .4	83 54 10 .1	—10 .2	—	—
	10 42 35 .6	85 16 46 .4	—14 .3	—	—
	10 47 29 .6	85 58 01 .0	—16 .0	—	—
	10 52 36 .6	86 40 21 .2	—15 .4	—	—
	10 57 47 .6	87 22 25 .3	—17 .7	—	—
	11 05 17 .5	88 21 29 .9	—31 .2	751.5	+ 3.0
7.IV 1965 Sun	6 51 36 .1	82 26 48 .2	— 3 .2	748.1	+ 9.8
	6 59 02 .8	83 36 40 .4	— 5 .8	—	—
	7 17 54 .7	86 30 51 .0	— 7 .6	—	—
	7 24 16 .7	87 28 00 .6	— 7 .6	—	—
	7 31 54 .5	88 34 41 .8	—21 .2	748.2	+ 8.5
12.IV 1965 Sun	7 21 06 .6	82 31 36 .0	+ 3 .1	753.6	+ 6.7
	7 25 42 .4	83 45 57 .9	— 1 .6	—	—
	7 32 50 .2	84 52 02 .3	— 2 .3	—	—
	7 40 00 .2	85 57 43 .2	— 9 .0	—	—
	8 03 36 .0	89 08 29 .7	—23 .6	753.6	+ 4.7
13—14. VII 1965 a Scorpii	18 17 36 .2	80 26 00 .9	— 0 .9	747.1	+18.5
	18 28 13 .7	81 10 07 .1	— 0 .4	—	—
	18 37 36 .2	81 52 06 .4	— 3 .4	—	—
	18 47 48 .6	82 40 40 .8	— 6 .0	—	—
	18 58 08 .5	83 32 53 .8	—10 .0	—	—
	19 08 06 .9	84 25 49 .9	— 4 .3	—	—
	19 18 06 .2	85 21 25 .9	— 9 .6	—	—
	19 28 23 .1	86 20 48 .1	— 9 .1	—	—
	19 38 18 .0	87 19 49 .8	—14 .1	747.1	+18.0
13—14. VII 1965 a Boötis	21 12 25 .9	83 54 39 .7	— 8 .6	747.6	+17.0
	21 23 47 .0	85 31 15 .6	—10 .3	—	—
	21 34 04 .4	86 56 17 .5	—19 .9	—	—
	21 45 17 .7	88 24 44 .5	—24 .6	747.6	+17.0
25—26. IX 1965 Jupiter	22 13 51 .0	87 45 40 .6	—40 .8	752.8	+11.6
	22 20 31 .1	86 55 40 .0	+ 0 .5	—	—
	22 27 19 .4	86 03 16 .6	— 1 .1	—	—
	22 35 56 .0	84 55 07 .3	— 1 .7	—	—
	22 43 48 .3	83 51 14 .1	— 0 .2	—	—
	22 50 50 .7	82 53 02 .3	+ 1 .5	—	—
	22 57 46 .8	81 54 50 .9	+ 2 .2	—	—
	23 04 50 .3	80 54 51 .4	+ 0 .4	—	—
	23 10 38 .8	80 04 52 .8	+ 0 .1	752.8	+11.0

TABLE 2 (Cont'd)

/54

Date, Heavenly Body	Local Sidereal Time s	Visible Zenithe Distance ζ	$\Delta r = z - \zeta - r_p$	Air Pressure, mm	Air Temperature at the Objective 0_C
28—29. IX 1965	$21^h24^m48^s.8$	85°39'47".4	— 3".4	751.4	+12.6
a Boötis	21 29 45 .4	86 20 54 .0	—12 .3	—	—
	21 38 33 .4	87 32 07 .3	—19 .9	751.5	+12.2
29—30. XI 1965	0 27 47 .9	82 36 22 .6	+ 0 .2	745.1	— 0.6
a Piscis	0 37 47 .3	83 10 10 .0	— 0 .1	—	—
Australis	0 48 21 .5	83 49 18 .9	— 1 .0	—	—
	0 58 22 .1	84 29 26 .0	— 0 .3	—	—
	1 08 28 .4	85 12 51 .1	— 2 .7	—	—
	1 18 16 .3	85 57 27 .0	— 3 .8	—	—
	1 28 10 .3	86 44 48 .9	— 6 .0	745.3	— 1.1
27—28. III 1966	6 01 55 .3	84 21 06 .9	— 4 .6	742.4	+ 5.1
Sun	6 07 14 .4	85 10 23 .9	+ 3 .1	—	—
	6 11 00 .6	86 00 50 .3	— 2 .2	—	—
	6 19 19 .1	87 01 13 .0	+ 3 .5	—	—
	6 26 01 .8	88 01 26 .2	—12 .6	—	—
	6 32 57 .2	89 11 25 .4	—31 .2	—	—
	6 37 40 .9	89 40 44 .5	—68 .2	742.5	+ 4.0
27—28. III 1966	8 26 10 .8	87 23 01 .4	—11 .8	742.6	+ 1.9
a Lyrae	8 32 41 .4	87 01 08 .7	—11 .4	—	—
	8 40 58 .4	86 31 22 .2	— 9 .1	—	—
	8 48 43 .2	86 01 36 .7	— 5 .6	—	—
	9 03 08 .3	85 01 32 .2	— 2 .0	—	—
	9 16 43 .0	83 59 36 .8	— 2 .6	—	—
	9 29 28 .5	32 56 50 .1	— 2 .0	—	—
	9 41 59 .6	81 51 12 .3	— 6 .0	—	—
	9 49 13 .2	81 11 27 .3	— 3 .1	742.6	+ 1.0
27—28. III 1966	10 26 06 .2	82 44 43 .8	+ 3 .8	742.6	+ 0.6
a Canis	10 36 11 .1	84 01 21 .2	— 0 .6	—	—
Majoris	10 44 01 .1	85 01 48 .5	— 3 .5	—	—
	10 51 43 .4	86 01 47 .9	— 1 .2	—	—
	10 59 21 .3	87 01 39 .0	—11 .4	—	—
	10 07 04 .5	88 01 40 .0	— 9 .5	742.7	+ 0.1
12. VII 1966	23 45 07 .4	87 41 39 .6	—11 .1	748.6	+17.2
Sun	23 51 37 .5	86 54 00 .8	— 4 .0	—	—
	23 59 09 .4	86 01 14 .7	— 3 .3	—	—
	00 06 33 .3	84 54 10 .0	— 2 .0	—	—
	00 13 22 .8	84 01 13 .7	— 1 .2	—	—
	00 20 31 .5	83 01 18 .2	— 1 .8	—	—
	00 27 33 .8	82 01 12 .6	+ 0 .6	748.5	+17.8

horizon. Thus, in an observation of the setting of the Sun on April 6, 1965, at ζ = 89° 20′, Δr = -44.5″; in an observation of the setting of Jupiter on September 25 - 26, 1965, at ζ = 87° 46′, Δr = - 40.8″; in an observation of the setting of the Sun on March 27, 1966, at ζ = 89° 41′, Δr = -68.2″. As is evident from the tables, the maximal values of Δr in all cases were obtained at a positive temperature. /55

TABLE 3

ζ, Degrees	Number of Evenings	$\Delta\bar{r}$	Δr_{max}	
			from	to
80 - 81	15	- 0.8″	- 4.2″	+ 4.7″
81 - 82	25	- 1.2	- 5.3	+ 5.9
82 - 83	32	- 1.6	- 7.4	+ 3.4
83 - 84	37	- 2.8	-10.6	+ 7.8
84 - 85	33	- 2.6	- 9.8	+ 4.7
85 - 86	35	- 3.4	-11.3	+ 3.1
86 - 87	33	- 5.0	-11.3	+ 0.6
87 - 88	28	- 6.6	-40.8	+ 3.0
88 - 89	16	-10.4	-26.8	+ 8.5
89 - 89°41′	5	-39.4	-68.2	+23.6

All the observational results were divided into 10 groups, corresponding to the zenith distance intervals: 80 - 81°, 81 - 82°, 88 - 89°, 89 - 89°41′. Table 3 gives the mean values of the differences $\Delta\bar{r}$ for the indicated observational period. It is evident from the table that the mean value of $\Delta\bar{r}$ for all ζ has a negative sign; it increases with the zenith distance from 0.76″ (80 - 81°) to 19.41″ (88 - 89°), while in the range 89 - 89°41′ it reaches 39.4″.

Analysis of the Results of the Observations and Comparison with Aerological Data

If we compare Tables 1 and 2, it follows that for the maximum deviations at Pulkovo the true refraction was greater than the calculated refraction, i.e., the values of Δr in equation (2) are positive, while in Goloseyevo the true refraction proves to be less than that calculated from the tables, and the values of Δr in the maximum deviations are negative. It is also interesting that the maximum deviations of the measured refraction from the table refraction at Pulkovo and at Goloseyevo were obtained at normal air temperatures for the moment of observation. For six cases of maximum deviation at Pulkovo and Goloseyevo, the temperature of the lowest air stratum was in the range from -4 to +12°C, while the pressure in all six cases was higher than normal at both Pulkovo and Goloseyevo. For certain evenings the Δr deviations obtained for single observations were near zero at all ζ from 80 to 88°, and infrequently had positive values. It is almost impossible to establish any sort /56

of dependence of the changes Δr on the temperature and pressure of the lowest air stratum at the moment of observation: we do not have a sufficient number of observations on record to do this.

The mean values of Δr in Table 3 are negative. If we corrected for the bending of the telescope, then the values of Δr in Table 3 would increase by some absolute value.

For eleven cases of maximal deviation of Δr, we calculated the refraction values by the method of numerical integration of aerological data on 15 atmospheric soundings which were very close in time to the observations. The calculations were carried out on an electronic computer by A.N. Kur'yanova using a technique evolved by I.G. Kolchinskiy. In seven cases we used data of atmospheric soundings carried out from 0.9 to 3.4 hrs. after the moment of observation, in the four other cases we used data of soundings before the moment of observation and after it from -1.6 to +5.1 hrs. The atmosphere was sounded up to a height of 30 - 32 km. Density variation curves were extrapolated up to 40 km in accordance with the shape of density changes for the standard atmosphere [8].

We calculated the refraction integral by totaling over strata 0.5 km thick according to the Simpson formula; we divided the atmosphere up to a height of 40 km into 80 layers of uniform density. The data on the temperature and the pressure were taken for the middle of each layer. The refractive indices of the air were calculated for a wavelength of λ = 530 mμ. The correction for the additional thickness of the layer of air from 40 - 300 km was calculated according to the approximate formula

$$\Delta r_H = (\mu_{40} - \mu_{300})K, \tag{4}$$

where $K = \frac{r_\varepsilon}{r_{45^*}}$ is the ratio of the mean refraction for the measured ζ to the mean refraction for $\zeta = 45°$, μ_{40} and μ_{300} are the refractive indices at heights of 40 and 300 km. We ignored air strata above 300 km, since their density is practically equal to zero. The correction for the difference of the effective wavelengths was calculated according to the approximate formula /57

$$\Delta r_\lambda = (\mu_i - \mu_{530})K, \tag{5}$$

where μ_i is the refractive index of the air for the effective wavelength corresponding to a determined spectral class of heavenly body [6], μ_{530} is the refractive index of the air for a wavelength of 530 mμ, which we used in calculating the refraction integral. (Corrections for Δr_H and Δr_λ by chance proved to be identical in absolute value). Corrections for the difference in the heights of the lowest air stratum of the observation and of the sounding (200

and 170 m) were determined according to a formula analogous to (4),

$$\Delta r_h = (\mu_{200} - \mu_{170}) K.$$

The calculated values of the refraction were corrected for the difference of the temperature and the air pressure of the lowest stratum at the moment of observation and at the moment of sounding, according to an approximate formula which is actually used by astronomers in calculating the reduction for the temperature and the air pressure at the point of observation, for instance [8, p. 185].

$$r_{\text{calc } (T, P_2)} = r_{\text{calc } (T, P_1)} \frac{P_2 T_1}{P_1 T_2}.$$

Here T_1, P_1 and T_2, P_2 are the temperature on the Kelvin scale and the pressure of the lowest air stratum at the moment of sounding and observation respectively.

The refraction calculated from aerological data of two adjacent probes for a given ζ was linearly integrated for the moment of observation, and then compared with the measured and table refraction; in the case of a single sounding, it was directly compared with the others.

Table 4 presents the values of the measured refraction, the refraction calculated according to the Pulkovo tables and that determined by numerical integration of atmospheric sounding data. Here the values of the table refraction are corrected for the spectral class of the heavenly bodies and the air moisture.

The differences of the measured refractions and those calculated using the sounding data, and of the measured refractions and those according to the tables, as can be seen from Table 4, are negative and reach an absolute value of 75 and 70″. In only one case, when the variational curve of the relative density ρ/ρ_0 of the two adjacent probes noticeably differs from the other thirteen, does the difference $r_{\text{meas}} - r_{\text{calc}}$ have a positive value. The convergence of the refractions calculated from the Pulkovo tables and from the /58 atmospheric sounding data is illustrated in Table 5.

In six cases out of eleven, the refraction calculated from the atmospheric sounding data agrees very well with the refraction calculated from the Pulkovo tables with difference variations from +1.5 to +5.8″. In one case where a noticeable deviation of the density/height curve is observed, the difference $r_p - r_{\text{calc}}$ has a result which clearly diverges from the others. (We must point out that the true curves of the variation of density with height were not known to us at the moment of observation). In the other four cases we observe deviations of the calculated refraction from the table refraction reaching 30″, i.e. approximately 2% refraction.

TABLE 4

Correction for the Wavelength Difference	Correction for the Height of the Air Stratum (40 - 300 km)	Correction for the Height of the Lowest Stratum (200 - 170 m)	Complete Calculated Refraction	Measured Refraction	Differences $r_{meas}-r_{calc}$	Differences $r_{meas}-r_{tabl}$	Date of Observation	Local Sidereal Time s	Measured Zenith Distance of the Heavenly Body	(Pulkovo) Table Refraction with Corrections for Air Moisture and the Spectral Class of the Heavenly Body	Local Sidereal Time of Sounding	Refraction Calculated from Aerological Data for λ=530 m. and H=40 km	Corrections for the Difference of T and P at the moment of Observation and of Sounding
−5.0″	+5.0″	−4.4″	1597.4″	1569.5″	−27.9″	−30.4″	29.III 1965	6h 45m	89°13′00″	1599.9″	8h 00m	1609.5″	−7.7″
−5.8	+5.8	−5.2	1836.5	1783.8	−52.7	−69.8	27.III 1966	6 38	89 40 44	1853.6	7 51	1842.2	− 0.5
−3.5	+3.5	−3.1	1127.7	1118.3	− 9.4	−10.9	28 III 1966	11 07	88 01 40	1129.2	13 52	1125.6	+ 5.2
−3.8	+3.8	−3.4	1277.6	—	—	—	4.IV 1965	11 03	88 19 37	1265.5	8 23	1262.5	+18.5
			1279.0	1244.6	−34.4	−20.9							
−3.8	+3.8	−3.4	1280.4	—	—	—	5.IV 1965	11 03	88 19 37	1265.5	14 24	1285.1	− 1.3
−3.8	+3.8	−3.4	1272.1	—	—	—	5.IV 1965	10 24	88 17 50	1248.6	8 27	1261.4	+14.1
			1267.6	1242.9	−24.7	−5.7							
−3.8	+3.8	−3.4	1256.4	—	—	—	6.IV 1965	10 24	88 17 50	1248.6	15 28	1258.0	+ 1.8
−5.2	+5.2	−4.6	1668.2	1594.0	−74.2	−46.0	6.IV 1965	7 34	89 19 44	1640.0	8 31	1681.3	− 8.5
−3.9	+3.9	−3.4	1228.3	1200.9	−27.4	−32.1	6—7.IV 1965	11 05	88 21 30	1233.0	14 32	1234.8	− 3.1
−4.1	+4.1	−3.6	1269.3	1247.4	−21.9	−24.1	7.IV 1965	7 32	88 34 42	1271.5	8 35	1278.4	− 5.5
−4.9	+5.0	−4.3	1550.7	1531.1	−19.6	−24.8	12.IV 1965	8 03	89 08 30	1555.9	8 55	1568.1	−13.2
−2.9	+3.0	−2.6	900.5	—	—	—	26.IV 1965	12 14	87 18 27	908.1	9 50	890.3	+12.7
			902.3	887.0	−15.3	−21.1							
−2.9	+3.0	−2.6	905.6	—	—	—	27.IV 1965	12 14	87 18 27	908.1	15 51	912.9	− 4.9
−3.1	+3.1	−2.8	914.5	—	—	—	28.IX 1965	21 39	87 32 07	953.1	20 01	905.4	+11.9
			922.9	932.7	+9.8	−20.4							
−3.1	+3.1	−2.8	946.1	—	—	—	29.IX 1965	21 39	87 32 07	953.1	2 02	948.4	−2.3

TABLE 5

Pulkovo (Table) Refraction r_p	Refraction Calculated from Aerological Data r_{calc}	r_p-r_{calc}	Pulkovo (Table) Refraction r_p	Refraction Calculated from Aerological Data r_{calc}	r_p-r_{calc}
1853.6″	1836.5″	+17.1″	1248.6	1267.6	−19.0
1640.0	1668.2	−28.2	1233.0	1228.3	+ 4.7
1599.9	1597.4	+ 2.5	1129.2	1127.7	+ 1.5
1555.9	1550.7	+ 5.2	953.1	922.9	+30.2
1271.5	1269.3	+ 2.2	908.1	902.3	+ 5.8
1265.5	2279.0	−13.5			

It is difficult to explain such deviation by instrumental error. /60

The fact is that, in calculating refraction by strata by the method of numerical integration, we essentially assumed that the density distribution of the air which we obtained for the point of observation remains constant over a fairly large territory, or else that strata of equal density are concentric spheres. In actuality, this assumption is only roughly satisfied. Especially large deviations, obviously, can arise at large values of ζ. Furthermore, a source of substantial errors in calculating refraction can be the fact that the sounding and the astronomical observations are taken at different times. It is quite possible that allowing for change in meteorological conditions along the path of the ray could lead to less deviation of the observed refraction from that calculated from aerological data.

From the present article it can be concluded that even at large zenith distances the deviation of the calculated refraction from the observed refraction is comparatively small at Goloseyevo. It is possible that this is a result of the comparatively stable meteorological conditions under which the observations were carried out.

V. Ye. Fuss carried out observations under the climatic conditions of the littoral of the Baltic Sea. Here the measured refraction in most cases, and especially under unusual conditions, as is shown in Table 1, proved greater than the refraction calculated from tables not infrequently exceeding it by 100 seconds and more.

Although in Goloseyevo such great deviations were not detected, a certain decrease of the observed refraction with respect to that calculated from the Pulkovo tables and from atmospheric sounding data was observed. Therefore, in order to reach more general conclusions, it would be expedient to organize observations of astronomical refraction near the horizon at the greatest possible number of points with varying meteorological conditions.

References

1. Fogel', R.: Kurs sfericheskoy astronomii (Course in Spherical Astronomy). Kiev, p. 257, 1910.
2. Kolchinskiy, I.G.: Refraktsiya sveta v zemnoy atmosfere (Refraction of Light in the Earth's Atmosphere). "Naukova dumka" Press, Kiev, 1968.
3. Mazayev, A.V.: Vestnik voyenno-inzhenernoy akademii im. V.V. Kuybysheva (Handbook of the V.V. Kuybysheva Military Engineering Academy) No. 88, pp. 87-107, 1955.
4. Fesenkov, V.T.: Russk. astr. zhurn., Vol. 4, No. 1, pp. 37-43, 1927.
5. Buynitskiy, V. Kh.: Problemy Arktiki (Problems of the Arctic). No. 3, pp. 72-78, 1949.
6. Kolchinskiy, I.G.: Publikatsii Kievskoy astronomicheskoy observatorii (Publications of the Kiev Astronomical Observatory). No. 2, pp. 81-90, 1948.
7. Blazhko, S.N.: Kurs sfericheskoy astronomii (Course in Spherical Astronomy). Gostekhizdat, Moscow, Leningrad, 1948. /61
8. Tablits a standartnoy atmosfery GOST 4401-64 (All-Union State Standard 4401-64 Table of the Standard Atmosphere). Standards Press., Moscow, 1964.
9. Fuss, V.: Memoires de L'Acad. Imp. des Sciences de St. Petersb., St. Petersbourg, Vol. VII, Series 18, p. 3, 1871.

THE ATMOSPHERE DISPERSION AND THE LUMINOSITY FUNCTION FOR THE 400-mm ASTROGRAPH OF THE MAIN ASTRONOMICAL OBSERVATORY OF THE ACADEMY OF SCIENCES OF THE UKRAINIAN SSR

A.B. Onegina

ABSTRACT: The results of determining the atmospheric dispersion and the magnitude equation on plates taken with the 400-mm astrograph are given. The value obtained for the atmospheric dispersion constant is 0.17 ± 0.03" for stars whose color indices differed by one magnitude at a zenith distance of 45 . The magnitude equation obtained is ± 0.014" in x and 0.015" in y for one magnitude difference. Probable errors are ± 0.003" in both coordinates.

The results of a number of articles gave a basis for assuming /62 that due to atmospheric dispersion the relative positions of stars of various spectral classes obtained on the plates of the 400-mm astrograph of the Goloseyevo observatory are subject to a systematic error.

Thus, B.I. Kozarenko [1], having investigated the luminosity function for this astrograph, came to the conclusion that it is mainly due to the effect of atmospheric dispersion, since the most distinct luminosity function is observed on the y-coordinate and depends on the zenith distance.

The author of [2,3] attempted to estimate the quantitative value of atmospheric dispersion, but the results obtained could not be used to determine the numerical value of the corrections to the measured coordinates of the stars. However, in finding the relative coordinates of heavenly bodies it sometimes becomes advisable to introduce such corrections. They are especially necessary in determining the relative positions of the components of multiple stars of various spectral classes.

Atmospheric dispersion and the luminosity function are determined on the one hand by the properties of the objective lens (a constant component of errors), and on the other hand, by the meteorological conditions of observation (this error component can change substantially from day to day). Both errors are closely related to one another. Therefore it is desirable to determine them jointly. The present article describes the results of research on determining the constant component of the luminosity function and atmospheric dispersion errors, which is produced by the objective. These errors distort the position of objects on all the plates obtained with this particular instrument.

Since the majority of observations are carried out at moderate zenith distances with exposures ranging from several minutes to several tens of minutes, investigation of the errors under consideration must be carried out on plates obtained under the same conditions so as to be able subsequently to apply the results obtained for correcting the measured coordinates on the conventional plates. Furthermore, in taking photographs at great zenith distances, where the atmospheric dispersion and the magnitude equation are greater than at moderate zenith distances, flickering of the images greatly increases, which can result in an increase of the random error of the measurement and of the final result. /63

For our investigation we selected area V of the Catalog of Photographic, Photovisual and Photored Magnitudes of 22,000 Stars [4] ($20^h47^m + 44°30'$), which coincides with the fortieth area of Kapteyn. In this area it was possible to select stars up to 13.5^m with known magnitudes and color indices. The area being photographed was located in the constellation Cygnus; when passing through the meridian it is near the zenith. In order to obtain photographs of this area at zenith distances of 30 - 40°, the observations were carried out at large hour angles.

Eleven plates of the region selected were measured in all; basic data on them are given in Table 1. (The abbreviations in the

TABLE 1

No. of Plates	Data	z	Hour Angle	Position of Telescope	t°C	P, mm	Observer
			h m				
2810	1963 July 22	9,0	−0 49.9	E	+17	750	A. O.
2835	1963 July 26	7,9	−0 31.2	W	+22	751	E. C.
2898	1963 August 28	8,1	−0 35.4	E	+21	751	E. C.
2918	1963 September 11	6,5	−0 22.0	W	+19	748	A. O.
2919	1963 September 11	15,3	+0 07.0	W	+19	748	A. O.
2921	1963 September 11	21,5	+2 05.0	W	+18	748	A. O.
2932	1963 September 16	10,0	+0 50.0	W	+15	755	A. O.
2933	1963 September 16	20,0	+2 01.4	W	+14	755	A. O.
2934	1963 September 17	34,5	+3 25.0	W	+12	755	A. O.
2935	1963 September 17	44,2	+4 28.2	W	+12	755	A. O.
2936	1963 September 17	47,8	+4 58.1	W	+12	755	A. O.

last column indicate: A.O. is A. Onegina, E.S. is E. Sereda). All photographs were taken with an exposure time of 20 minutes. An objective grid with constants a (distance between bands) and b (width of the bands) equal to 5.0 mm and 1.2 mm respectively was used in photographing. The grid is generally set up in such a manner that its direction of dispersion is perpendicular to the diurnal motion and that the secondary diffraction companions of bright stars are located to the north and south of the central image. At 20 min exposures these secondary companions around stars of up to 10^m can be measured. Such measurements are carried out on a KIM-3 gauging machine for two positions of the plate differing by 180°, in order to exclude any human error.

The rectangular coordinates of stars thus obtained differ from the tangential coordinates due to the inaccuracy of the scale, the divergence of the reference points, the errors of orientation. /64
Furthermore, they are also subject to systematic errors dependent on the luminosity of the star, its spectral class and on the observational conditions, which generally can be expressed

$$x = x_1 + \sum_{i=1}^{N_i} d_i (m - m_0)^i + \sum_{j=1}^{N_j} l_j (C - C_0)^j + \sum_{k=1}^{N_k} \rho_k \tan^k z \sin p, \qquad (1)$$

where x is the value of the coordinate found by the process of measuring; x_1 is the value which the measured coordinate would have had if there were no magnitude and spectral class equations and atmospheric dispersion; m is the stellar magnitude; C is the color index; z is the zenith distance; p is the parallactic angle; d_i, l_j, ρ_k are unknown coefficients which specifically may be functions of m and C. (An analogous equation can be written for y.). It is impossible to define all the coefficients of equation (1), and we shall restrict ourselves to the linear terms only:

$$\begin{aligned} x &= x_1 \pm d(m - m_0) \pm l(C - C_0) + \rho_1 \tan z \sin p, \\ y &= y_1 \pm d'(m - m_0) \pm l'(C - C_0) + \rho_1 \tan z \cos p. \end{aligned} \qquad (2)$$

Here the second, third and fourth terms represent the luminosity function, the spectral class equation and the correction for atmospheric dispersion, respectively. The second and third terms have a double sign, since the effect of the magnitude and spectral class equations at different positions of the telescope (to the east or west) with reference to the column is reversed. In order to give d, d' and l, l' the proper sign to be used in correcting the coordinates measured on plates obtained at the normal position of the telescope (to the west of the column), in equation (2) it is necessary to use a plus sign if the telescope is to the east of the column and a minus if it is to the west of the column.

We assume the dependence of the atmospheric dispersion on the color index to be linear:

$$\rho = \Delta\beta (C - C_0), \qquad (3)$$

where $\Delta\beta$ is the required coefficient of the atmospheric dispersion, C is the color index of the star being measured, C_0 is the mean color index of the reference stars.

O.A. Mel'nikov showed in [5,6] that the color index and the effective wavelength which are means for a given spectral class are insufficient criteria for calculating the value of the refractive /65
index; for this reason we take a color index for *each* star from the catalog [4], while we determine the effective wavelength from the

same plates which were used to determined the atmospheric dispersion coefficient.

The atmospheric dispersion coefficients were found from seven pairs of plates: I (2933-2932), II (2934-2932), III (2936-2932), IV (2921-2919), V (2935-2919).

On each plate we measured 23 stars. For each star we compiled the differences of its coordinates on the first and second plates of the pair. Since all the plates were obtained with the telescope facing west of the column, in the differences of the coordinates of the same star, the second and third terms of formula (2) will disappear; only the differences of the last terms will remain, as well as the usual terms of linear formulas which allow for the difference between the scales of the plates, their mutual orientation and the difference of the origins of the measured coordinates. Thus,

$$\Delta x = ax + by + c + \rho(\tan z_1 \sin p_1 - \tan z_2 \sin p_2),$$
$$\Delta y = a'x + b'y + c' + \rho(\tan z_1 \cos p_1 - \tan z_2 \cos p_2). \qquad (4)$$

The subscripts 1 and 2 refer to the first and second plates of the pair respectively. The linear coupling constants of the plates were determined from seven reference stars (m 9.4^m, C = 0.1^m) for which we assume that $\rho = 0$. After substituting the constants a, b, c and a', b', c' in the provisional equations for each of the other fifteen stars (one star was not processed, since all the coordinates refered to it) we find the value of ρ for all plate pairs.

The products tan z sin p, tan z cos p were found graphically for each star. First they were determined for each plate at nine points with measured coordinates:

x	−70	−70	−70	00	00	00	+45	+45	+45
y	−95	0	+50	−95	0	+50	−95	00	+50

These values of tan z sin p, tan z cos p were plotted on graphs. Figure 1 presents such a graph for plate 2835 (curves 1, 2, 3 are tan z sin p, curves 4, 5, 6 are tan z cos p; curves 1 and 4 are for y = -95, curves 2 and 5 are for y = 0, while curves 3 and 6 are for y = +50). Then the appropriate values of tan z sin p and tan z cos p were taken for each star from its coordinates on the graph.

In determining separate values of ρ, their spread for the same star on different plate pairs proved to be quite large. In any case, it was greater than the error corresponding to the differences of the coordinates, since the coefficient of ρ in formulas (4) is less than one. /66

The values obtained were subsequently averaged for each star for all pairs and both coordinates. Here each coordinate was assigned a weight, depending on the value of the coefficient of ρ.

Then the 15 stars under consideration were divided into groups by their approximate color index values. The first group consisted of 9 stars with a mean color index of $+1.06^m$ ($+0.84^m$ C $+1.40^m$), the second consisted of 5 stars with a mean color index of $+0.28^m$ ($+0.10^m \leq C \leq +0.56^m$). One star with a color index of -0.39^m was considered separately. Thus we obtained three values of ρ for three color index values. By plotting them graphically (Fig. 2) we obtained three points lying almost on a straight line. By adding another point corresponding to the reference stars (mean color index of 0.10^m), for which ρ is equal to zero, we can fairly reliably construct a straight line. Each point here was given a weight corresponding to the number of stars for which this value of ρ was found.

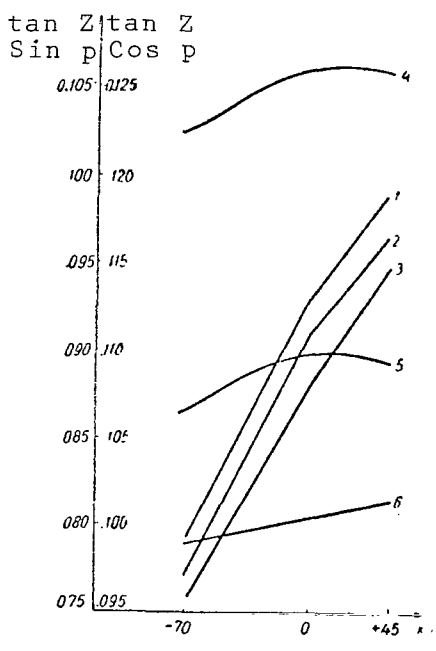

Fig. 1.

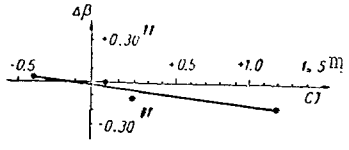

Fig. 2.

The atmospheric dispersion coefficient Δβ for the two groups of stars with the given color indices can be defined as the ratio $\frac{\rho_1 - \rho_2}{C_1 - C_2}$. Thus, we found the approximate relationship between the atmospheric dispersion coefficient and the difference of the color indices of the stars being measured. The error was estimated from the deviation of the points from the straight line.

The atmospheric dispersion coefficient for stars with color indices differing by one stellar magnitude at a zenith distance of 45° is equal to 0.17" ± 0.03" (probable error). This /67 agrees completely with the results of other authors [7-9]. A.M. Lozinskiy [9], on 16"-astrograph at Moscow obtained a shift of stars of type Z with reference to stars of type K due to atmospheric dispersion which was equal to 0.17". If we consider that the stars we used lie on the main sequence, then a color index equal to zero would belong to stars of spectral type A5, while a color index equal to one would characterize stars of type K2, i.e. our result is practically the same as on the Moscow astrograph.

The value of the atmospheric dispersion coefficient determined by us was compared with its theoretical values found from the difference of the refractive indices for effective wavelengths corresponding to the star groups being compared. The value $(1-n_\lambda)$ (the value of the refractive index expressed in radians) was taken from

the tables in the Geophysics Handbook [10] according to the λ_{eff} of a given group of stars for a temperature of +15°C, which is close to the temperature of observation. The values of λ_{eff} were determined from the ratio

$$\lambda = \frac{r(a+b)}{f},$$

where r is half the distance between first order companions of the first magnitude, f is the focal length of the instrument, a, b are grid constants. Since the diffraction companions can not be measured

TABLE 2

$\bar{m}$	C	λ_{eff}, mm	β_λ	$\Delta\beta_c$	$\Delta\beta_0$	$O-C$
10.3 (6)^m	+1.06^m	421	57.87″			
10.8 (4)	+0.33	412	57.79	−0.08″	−0.10″	−0.02″
8.9 (1)	−0.39	406	57.67	−0.12	−0.12	0.00

on all stars, the mean effective wavelengths are determined from a somewhat smaller number of stars than ρ. Values for them are given in Table 2 (in parentheses is the number of stars used for determining λ_{eff}). The fourth column of Table 2 gives the theoretical values of the refractive index found according to tables in [10] and adjusted to a pressure of 750 mm, at which the observations were carried out. The difference of the adjacent values of the refractive index gives the value of the atmospheric dispersion for the corresponding groups of stars $\Delta\beta_c$, while $\Delta\beta_0$ is the value of the atmospheric dispersion obtained from observations. /68

As is evident from Table 2, the observed and the theoretical values of the atmospheric dispersion agree very well. This fact has great significance for practical research. It permits the introduction of appropriate theoretical corrections into the measured relative coordinates of stars of different color, and this would improve the relative positions obtained on several plates. However, in any case we must determine the values of the effective wavelength for the objects being measured. And nonetheless, significant deviations of the results of separate plates from one another are still possible, due to atmospheric dispersion and a magnitude equation of meteorological origin.

The luminosity function and the spectral class equation were determined, allowing for the obtained value of the atmospheric dispersion. For this purpose we used four plates of which two were obtained at one position of the telescope with reference to the column and two at the other position. The description of the plates is given in Table 1. These plates were composed into three pairs: I (2810 - 2835), II (2898-2818), III (2898-2835). A pair consists of plates photographed at close hour angles and at similar zenith

distances, but as has already been said, at different telescope positions.

The measurements were taken on the KIM-3 at two positions differing by 180°. We measured 138 stars on each plate. For calculating the linear coupling constants of the plates we used the central images of 11 reference stars ($\bar{m}$ = 9.72^m, $\bar{C}$ = +0.12^m). After calculating the constants of the relationship of the plates for the remaining stars, we formulated the differences

$$\Delta x_{0-c} = \Delta x_0 - \Delta x_c, \tag{5}$$

where $x_0 = x_1 - x_2$ is the difference of the measured coordinates of the star on the first and second plates of the pair, $x_c = ax + by + c$ is the calculated value of this difference. Analogous differences were established for y. Then the mean value of the difference (5) was taken for each star on all the plate pairs, which in accordance with (2) was expressed in the form

$$\Delta x_{0-c} = 2d(m-m_0) + 2l(C-C_0) + 2\beta(C-C_0)(\tan z_1 \sin p_1 - \tan z_2 \sin p_2)$$

and

$$\Delta y_{0-c} = 2d'(m-m_0) + 2l'(C-C_0) + 2\beta(C-C_0)(\tan z_1 \cos p_1 - \tan z_2 \sin p_2), \tag{6}$$

where x_1, y_1 are the coordinates measured on the plate taken with the telescope to the east of the column, x_2, y_2 are the coordinates measured on the plate taken with the telescope to the west of the column. /69

There were 127 equations of the type of (7). The results of solving them by the Cauchy method and the probable errors came out to be:

$$\begin{aligned} d &= +0.014'' \pm 3, & l &= -0.013'' \pm 10; \\ d' &= +0.015'' \pm 3, & l' &= -0.009'' \pm 10. \end{aligned} \tag{7}$$

Thus, it is possible to ignore the spectral class equation since it is on the order of magnitude of the error, which coincides with the result of E.A. Gurtovenko [13]. The luminosity functions is a completely real value, identical over x and over y, but its value sharply differs from the result of E.A. Gurtovenko, who obtained

$$\begin{aligned} \Delta x &= -0.031''(m-m_0), \\ \Delta y &= +0.064''(m-m_0). \end{aligned} \tag{8}$$

This discrepancy can be explained by a shift of the lenses in the interval of time between the two investigations or else by the fact

that our photographs were obtained with an objective grid which changes the character of the luminosity distribution in the central image. The latter possibility seems more probable, but in order to justify it, subsequent investigation of this problem would be necessary. It is advisable to survey the results of previous investigations in the light of the results obtained in this article. In particular, the author of article [3] indicates that the atmospheric dispersion for the red and blue ends of the first order spectral companions is equal to 1.4". Based on the chromatic curve of the astrograph's lens [11] and on the curve of the spectral sensitivity of unsensitized plates [12], we can take as effective wavelengths of the red and blue ends of the spectrum 3900 Å and 4800 Å. This, naturally, is just an approximation, since the appropriate wavelengths still are a function of the transmission coefficient of the atmosphere, of the stellar magnitude and the energy distribution in the star's spectrum, but in the present case this may be used. According to the tables in reference [10] the atmospheric dispersion would be $\Delta\beta = 0.78''$ for the values taken by us for the effective wavelengths, i.e. a value half of that obtained by us.

However, the value 1.4" was obtained when we introduced the correction (8) for the luminosity function into the mean differences of the coordinates of the central images and the mean coordinates of the first order companions. We again calculated the atmospheric /70 dispersion coefficient after introducing the corrections in (7) for the images with the grid.

Every other line of Table 3 gives the directly measured differences of the coordinates, and under them are the values of the measured coordinate differences, corrected for the magnitude equation in accordance with (7). We determined the values of $\Delta\beta$ from the corrected coordinate differences, assuming that

$$\Delta x = \frac{1}{2}\Delta\beta \tan z \sin p,$$
$$\Delta y = \frac{1}{2}\Delta\beta \tan z \cos p. \qquad (9)$$

The values of $\Delta\beta$ found for each plate were averaged. Each result on the x-coordinate was attributed a weight proportional to the value of the product $\tan z \sin p$. Thus plate 1411 was given the weight 0.2, 1412 had a weight of 0.1, 1420 a weight of 0.6, plate 1429 a weight of 0.2. The results obtained on the y-coordinate were attributed a weight of 1. The recalculated value of $\Delta\beta$ proved to be equal to 0.80", which agrees very well with the initially calculated value.

TABLE 3

Plates	$x - \frac{x_S - x_N}{2}$	$y - \frac{y_S - y_N}{2}$
1411	−0.052	−0.127
	−0.102	−0.173
1412	−0.127	−0.472
	−0.177	−0.222
1420	+0.105	−0.472
	+0.055	−0.518
1429	−0.210	−0.277
	−0.160	−0.323

It is necessary to emphasize once more that the luminosity function defined in this article is a systematic part of the error depending on the lens. Random errors of this type, depending on observational conditions, can be significantly greater than the values found here. It is necessary to take the usual precautions in order to avoid them.

Since in photography with an objective grid atmospheric dispersion can significantly (by almost half a second) shift the mean location of the spectral companions with reference to the central image (this shift is equal to $\frac{1}{2}\Delta\beta$, i.e. 0.4″), it is necessary very cautiously to apply an objective grid for reducing luminosity with the given instrument, and possibly with other photographic refractors, especially with the 16″ astrograph at Moscow, whose atmospheric dispersion coefficient is the same as for the Goloseyevo astrograph.

References

/71

1. Kozarenko, B.I.: Soobshcheniya Gos. Astr. Inst. Shtern., No. 104, pp. 42-54, 1961.
2. Onegina, A.B.: Izv. Gl. Astr. Obs. Academy of Sciences of the Ukr. SSR., Vol. 3, No. 1, pp. 116-118, 1960.
3. Onegina, A.B.: Izv. Gl. Astr. Obs. Academy of Sciences of the Ukr. SSR, Vol. 4, No. 2, pp. 24-31, 1963.
4. Voroshilov, V.I. et al.: Katalog fotograficheskikh, fotovizual'nykh i fotokrasnykh velichin 22000 zvezd (Catalog of Photographic, Photovisual and Photored Magnitudes of 22,000 Stars). Academy of Sciences of the Ukr. SSR Press, Kiev, 1962.
5. Mel'nikov, O.A.: Izv. Gl. Astr. Obs. in Pulkovo, Vol. 20, No. 4, pp. 1-32, 1957.
6. Mel'nikov, O.A.: Astr. Zhur., Vol. 32, pp. 266-273, 1956.
7. Bulatova-Kalikhevich, F.F.: Astr. Zhur., Vol. 35, pp. 925-930, 1958.
8. Lavdovskiy, V.V.: Izv. Gl. Astr. Obs. in Pulkovo, Vol. 146, pp. 120-124, 1951.
9. Lozinskiy, A.M.: Soobshcheniya Gos. Astr. Inst. Shtern., Vol. 20-21, pp. 3-13, 1948.
10. Spravochnik po geofizike (Geophysics Handbook). "Nauka" Press, Moscow, p. 341, 1965.
11. Gurtovenko, E.A.: Izv. Gl. Astr. Obs. Academy of Sciences of the Ukr. SSR., Vol. 2, No. 2, p. 124, 1958.
12. Meyklyar, P.V.: Kurs astrofiziki i zvezdnoy astronomii (Course in Astrophysics and Stellar Astronomy). Vol. 1, State Technical and Theoretical Press, Moscow, Leningrad, p. 144, 1951.
13. Gurtovenko, E.A.: Izv. Gl. Astr. Obs. Academy of Sciences of the Ukr. SSR, Vol. 2, No. 1, pp. 95-111, 1957.

A STUDY OF STAR IMAGE FLICKERING BASED ON OBSERVATION OF TRACES CARRIED OUT ON THE AZT-7 TELESCOPE (200-mm REFLECTOR) IN 1963

G.V. Moroz

ABSTRACT: Star image flickering was investigated in 1963 in Goloseyevo (Kiev suburb) by the trace method on the 200-mm Maksutov reflector (AZT-3). The results of measuring 267 traces obtained during 20 nights show that the r.m.s. value of the oscillations are proportional to (sec z)$^{0.5}$, which is in agreement with earlier results of I.G. Kolchinskiy. On different nights the value of the exponent lies between 0.0 - 0.9. The r.m.s. of image motion at the zenith for each night lies between 0.3 - 0.5".

The flickering of star images in telescopes depending on zenith distance, the meteorological conditions and the character of the locality has been investigated by many scientists. Star image flickering has been studied in order to select a location for astronomical observations and in order to clarify the optical properties of the atmosphere. /72

I.G. Kolchinskiy [1] carried out a comprehensive investigation of star image flickering at the Main Astronomical Observatory of the Academy of Sciences of the Ukrainian SSR. One of the conclusions to which I.G. Kolchinskiy came is that the amount of flickering of the image is directly proportional to (sec z)$^{0.5}$, which agrees very well with the theoretical law derived by V.Z. Krasil'nikov [2]. However, in many cases, deviations from this law are detected. If according to I.G. Kolchinskiy, expressing his observations by the formula

$$\sigma = \sigma_0 (\sec z)^{\alpha}, \qquad (1)$$

α = 0.53 and σ_0 = 0.31", then the visual observations of flickering in Abastumani in 1932-1933 best satisfied the formula

$$\sigma = a \log \sec z + b$$

where a = 3.6", b = 0.40" [3].

As a result of measuring star traces obtained in observations in the region of the Great Lake of Alma-Ata, it was found that the mean flickering amplitude was completely independent of the zenith distance [4].

Stellar flickering was observed in 1960 in a number of regions of Kazakhstan in investigation of the astroclimate [5]. There it was established that the dependence of the flickering on the sec z or on the "air mass" L varied on different days: in many cases it was found to be linear, while for a number of days, it was clearly non-linear, although its non-linear character proved to be different from that described by I.G. Kolchinskiy.

The problem of the dependence of star image flickering in telescopes on the zenith distance has both theoretical and practical importance. In this connection, the Main Astronomical Observatory of the Academy of Sciences of the Ukrainian SSR carried out an investigation of stellar flickering from longer series of observations covering several years. It was proposed to pinpoint the type of dependence of the flickering on the zenith distance on the topography of the locality. /73

Observations of stellar flickering were carried out during 1963-1964 on an AZT-7 telescope. The present article presents the results of processing the star traces obtained in 1963.

The shed in which the instrument was set up is located to the south of the main building of the observatory on a field where isolated bushes and trees grow. To the south of the shed there is

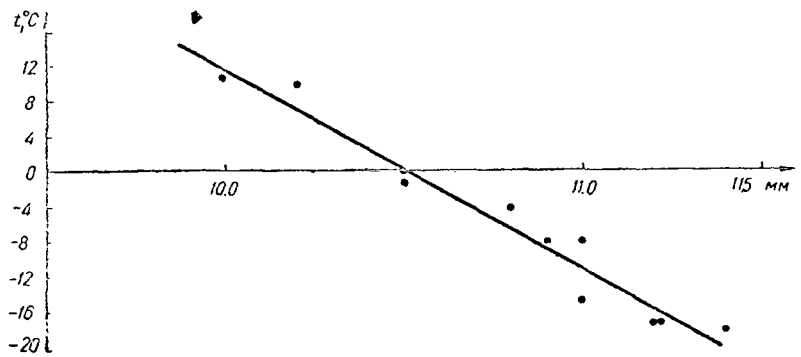

Fig. 1.

a wooded area sloping down into a small hollow. The field on which the observatory is located is surrounded on all sides by the forest of Goloseyevo; behind it to the north is the city of Kiev; on the south, west and east are separate tracts of forest and small settlements.

The shed is a round tower constructed of brick with a metal dome 5.5 m in diameter. The dome has sliding flaps and turns by means of an electric motor. The instrument is placed on a concrete pedestal 2 m in height.

The AZT-7 telescope (D = 200 mm) was erected at the end of 1962. Observations on the instrument were begun in February, 1963. Photography of the stars was carried out with a 10-meter equivalent focus with a disconnected hour mechanism on plates of dimensions 4.5 × 4.5 mm. The traces on the plates came out very clearly. In the course of observations it was noted that the instrument's focus depends substantially on the temperature, which forces us to investigate this dependence and construct its graph (Fig. 1). We should point out that the millimeter graduation of the focal scale /74 is insufficient and a vernier is necessary, since a change of the focus by only 0.5 mm significantly decreases the sharpness of the traces. Since the instrument's focus depends on the temperature, ventilation of the shed has a strong influence on the quality of the trace image. Traces on plates taken on summer nights are at first wider and more washed out, but then they become narrower and sharper, although the temperature in the shed has decreased at the most by 1.0 - 1.5° C and the focus has not changed substantially.

First we took photographs on Agfa Astro plates and then on Kodak plates. Traces on the Kodak plates come out better, possibly because these plates are sensitive to red light and the red stars near the horizon come out very clearly. In correcting for all the enumerated peculiarities of the instrument, the quality of the traces becomes very good. On certain nights when large stellar flickering is observed, the traces consist of separate beads. In observations of binary stars it can be observed that sometimes the oscillations of the separate components are not correlated; in certain cases they may be moving in opposite directions.

The stars were photographed at all azimuths and at all zenith distances. At the moment of passage through the vertical cross hair located in the center of the eyepiece, which corresponded to the center of the trace on the plate, the sidereal time was recorded with an accuracy of up to 0.1 min.

In all, 267 traces obtained in the course of 20 nights in 1963 were processed. The traces were processed by the same procedure as I.G. Kolchinskiy [1] used. The traces were measured on a MIR-12 microscope, on which a micrometer with a rack, two horizontal and one vertical cross hair was mounted. The horizontal cross hairs were shifted by means of a small drum on which the amount of shift of the cross hairs could be read off. The plate with the traces (5-10 traces) was placed under the microscope in such a manner that the trace was positioned along the horizontal pair of movable cross hairs, while the vertical cross hair coincided with the beginning of the trace. Then the stage on which the plate was lying moved along the guiding cross hairs by means of a micrometer screw, stopping every 50 μ, while the horizontal cross hairs were moved by the drum to the darkest part of the trace at the given point, after which the reading was taken from the drum. Initially, the length of the entire trace contained 800 points. Approximately 60 traces were of this type. As the research was very time-consuming, we

subsequently decided to take 200 points, since this number of points was sufficient to determine the amount of flickering. For each plate we determined the scale value of the ocular micrometer, which /75 on the average was equal to 0.6×10^{-3} mm.

The flickering values were determined analogously to the method used in reference [1], i.e., from the measured points by the method of least squares, we found the straight line equation; then the flickering value was found as the mean square value of the deviation of the individual points from the straight line:

$$\sigma = \sqrt{\frac{\Sigma v^2}{n}}, \tag{2}$$

where v are the deviations of the points of the trace from the line, n is the number of points. For stars having a slope greater than 14° (with a trace length of 40 mm) and for stars having a declinations greater than 40° (with a trace length of 10 mm) corrections for the curvature of the parallel were introduced according to the formula

$$\Delta m_k'' = \frac{15^2}{2} \cdot \frac{F_k^2}{206265} \cdot \tan \delta, \tag{3}$$

where F_k is the distance from the center of the plate to the k-th point in seconds of arc; δ is the declination; Δm_k is the correction for the curvature at the k-th point [7].

Thus,

$$\Delta m_k'' = 0{,}0005454\, F_k^2 \tan \delta. \tag{4}$$

The correction in millimeters will be

$$\Delta m_k = 0{,}0000264\, F_k^2 \tan \delta, \tag{5}$$

where F_k is the distance from the center of the trace to the k-th point, expressed in seconds of time.

The calculated correction Δm_k is for the deflection of the trace ACB in comparison to the end points A and B (Fig. 2). For reasons of convenience the correction for the curvature was introduced simultaneously with the calculation of the deviation of the points of the trace from the straight line, whose angular coefficients were determined from the points which were not corrected for curvature. Therefore, it is obvious that the obtained straight

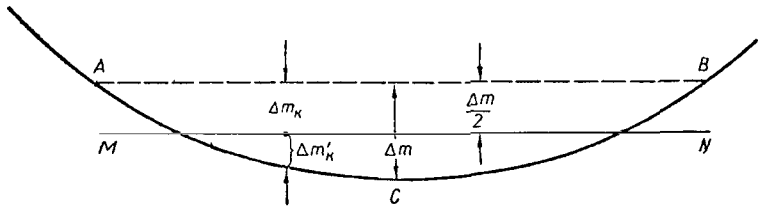

Fig. 2.

line will pass through the middle of the deflection, and the correction for the k-th point with reference to this straight line will assume the form: /76

$$\Delta m'_k = \Delta m_k - \frac{\Delta m}{2}, \qquad (6)$$

where Δm_k is the correction with reference to the calculated straight line MN, Δm_k is the correction with reference to the straight line AB, Δm is the greatest deflection of the trace with reference to the straight line AB.

We must point out that, due to its optical scheme, the AZT-7 instrument with a 10-meter focus produces an erect image.

The value of Δm_k can easily be found by means of a slide rule. First we find the value of F^2 where Δm_k varies per unit, and then from the table for F^2 we determine the number of the corresponding point.

In this manner we calculated 267 values of the mean square deviation. This value was taken in proportion to the flickering at a given zenith distance. The results are given in Table 1.

TABLE 1

Date	Azimuth	z	sec z	σ	log sec z	$1+\log\sigma$
Feb. 11—12	S	33°59′	1.206	0.518″	0.081	0.714
	S	58 38	1.921	0.629	0.284	0.799
	S	58 37	1.920	0.585	0.283	0.767
	S	67 02	2.563	0.848	0.409	0.928
	S	68 39	2.747	0.596	0.439	0.776
	S	45 22	1.423	0.584	0.153	0.766
	S	42 01	1.346	0.718	0.129	0.856
Feb. 12—13	S	33 59	1.206	0.423	0.081	0.626
	S	59 07	1.948	0.580	0.290	0.763
	S	44 41	1.406	0.382	0.148	0.582
	S	45 03	1.415	0.400	0.151	0.602
	S	70 21	2.974	0.705	0.473	0.848
	S	45 04	1.416	0.460	0.151	0.663
	S	22 17	1.081	0.346	0.034	0.539
Feb. 24—25	W	15 26	1.038	0.408	0.016	0.611
	W	11 28	1.020	0.466	0.008	0.668
	W	50 08	1.560	0.532	0.193	0.726
	S	47 00	1.466	0.390	0.166	0.591

TABLE 1 (cont'd)

Date	Azimuth	z	sec z	σ	log sec z	1+log σ
Feb. 24—25	S	47 07'	1.469	0 .611"	0.167	0.786
	S	66 14	2.481	0 .660	0.395	0.820
	S	45 08	1.418	0 .468	0.152	0.670
	S	68 18	2.705	0 .631	0.432	0.800
	S	45 55	1.438	0 .623	0.158	0.794
	S	55 46	1.778	0 .666	0.250	0.823
Feb.-Mar. 28—1	W	42 03	1.347	0 .481	0.129	0.682
	W	36 20	1.241	0 .264	0.091	0.422
	W	15 04	1.036	0 .287	0.015	0.458
March 4—5	N	52 06	1.628	0 .600	0.212	0.778
	N	67 26	2.606	0 .563	0.416	0.751
	N	45 48	1.434	0 .563	0.157	0.751
	N	59 14	1.955	0 .338	0.291	0.529
	E	36 50	1.249	0 .532	0.097	0.726
	E	75 56	4.114	0 .456	0.614	0.659
	E	66 25	2.499	0 .703	0.398	0.847
	S	80 21	5.966	0 .860	0.776	0.934
	S	42 16	1.351	0 .384	0.131	0.584
	S	38 15	1.273	0 .520	0.105	0.716
	S	59 33	1.973	0 .487	0.295	0.688
	W	56 05	1.792	0 .518	0.253	0.714
	W	70 48	3.041	0 .433	0.483	0.636
	W	61 00	2.063	0 .825	0.314	0.916
	W	53 28	1.680	0 .658	0.225	0.818
June 7—8	E	57 46	1.875	0 .553	0.273	0.743
	E	22 56	1.086	0 .425	0.036	0.628
	E	37 54	1.267	0 .384	0.103	0.584
	N	59 57	1.997	0 .759	0.300	0.880
	N	33 43	1.202	0 .468	0.080	0.670
	N	73 10	3.453	0 .736	0.538	0.867
	N	51 52	1.619	0 .514	0.209	0.711
	W	44 18	1.397	0 .776	0.145	0.890
	W	44 41	1.406	0 .497	0.148	0.696
	W	57 42	1.871	1 .176	0.272	1.061
June 14—15	W	41 38	1.338	0 .520	0.126	0.716
	W	17 18	1.047	0 .485	0.020	0.686
	W	72 32	3.332	0 .998	0.523	0.999
	N	58 10	1.896	1 .040	0.278	1.017
	W	57 52	1.880	1 .118	0.274	1.048
June 24—25	E	15 03	1.036	0 .451	0.015	0.654
	E	54 09	1.707	0 .497	0.232	0.695
	E	41 50	1.342	0 .415	0.128	0.618
	N	80 11	5.865	0 .996	0.768	0.998

TABLE 1 (cont'd)

Date	Azi-muth	z	sec z	σ	log sec z	1 + log σ
June 24–25	N	63 05′	2.209	0″.571	0.344	0.757
	W	76 01	4.138	1 .147	0.617	1.060
	W	23 02	1.087	0 .439	0.036	0.642
	S	42 45	1.362	0 .600	0.134	0.778
June 25—26	S	42 45	1.362	0 .778	0.134	0.891
	E	16 29	1.043	0 .464	0.018	0.667
	E	57 11	1.845	0 .557	0.266	0.746
	E	43 45	1.384	0 .394	0.131	0.596
	N	57 08	1.843	0 .687	0.266	0.837
	W	58 49	1.931	0 .458	0.286	0.661
	W	23 25	1.090	0 .417	0.037	0 620
	S	42 52	1.364	0 .388	0.134	0.529
June 26—27	N	75 22	3.958	1 .099	0.597	1.041
	N	63 58	2 278	0 .427	0.359	0.630
	N	61 17	2.081	0 .390	0.318	0.591
	W	26 57	1.122	0 .359	0.050	0.555
June 28—29	E	44 13	1.395	0 .707	0.145	0.849
	E	20 57	1.071	0 .476	0.030	0.678
	E	46 48	1.461	0 .703	0.165	0.847
	N	67 47	2.645	0 .755	0.422	0.878
	N	61 21	2.086	0 .468	0.319	0.670
	W	55 55	1.784	0 .771	0.251	0.887
	W	74 16	3.688	0 .406	0.567	0 609
	W	22 28	1.082	0 .400	0.034	0.602
July 5—6	S	41 40	1.339	0 .897	0.127	0.953
	S	7 29	1.009	0 .538	0.004	0.731
	E	47 33	1.482	0 .780	0.161	0.892
	E	36 53	1.250	0 .681	0.097	0.833
	N	74 33	3.754	1 .860	0.574	1.270
	N	64 26	2.317	0 .703	0.365	0.847
	N	61 58	2.128	0 .905	0.328	0.957
	W	61 11	2.296	1 .101	0.351	1.042
	W	29 04	1.144	0 .613	0.058	0.787
	W	29 29	1.149	0 .825	0.050	0.916
July 8—9	E	39 55	1.304	0 .547	0.115	0.738
	N	76 25	4.258	1 .073	0.629	1.031
	N	61 20	2.085	0 .664	0.319	0.822
	N	63 40	2.254	0 .621	0.353	0.793
	N	60 27	2.028	0 .534	0.307	0.728
	W	62 17	2.150	0 .536	0.332	0.729
	W	27 23	1.126	0 .427	0.042	0.630
	S	6 12	1.006	0 .400	0.003	0.602
	S	44 26	1.400	0 .520	0.146	0.716
	S	38 06	1.271	0 .507	0.104	0.705

TABLE 1 (cont'd)

/79

Date	Azimuth	z	sec z	σ	log sec z	1+log σ
July 11—12	S	42 02'	1.346	0 .551"	0.129	0.741
	S	5 43	1.005	0 .353	0.002	0.548
	W	60 26	2.027	0 .524	0.307	0.719
	W	25 56	1.112	0 .452	0.046	0.654
	N	62 07	2.138	0 .792	0.330	0.899
	N	42 58	1.367	0 .406	0.136	0.609
	N	65 44	2.433	0 .545	0.386	0.736
	N	69 36	2.869	0 .922	0.458	0.965
	E	52 59	1.661	0 .683	0.220	0.834
	E	27 17	1.125	0 .417	0.051	0.620
Aug. 1—2	E	19 51	1.063	0 .402	0.027	0.604
	E	43 43	1.381	0 .928	0.141	0.968
	E	60 11	2.011	0 .661	0.303	0.822
	E	74 34	3.758	0 .829	0.575	0.919
	S	24 51	1.102	0 .625	0.042	0.796
	S	71 29	3.119	0 .833	0.498	0.920
	S	35 39	1.231	0 .386	0.080	0.587
	W	61 55	2.124	0 .662	0.327	0.821
	W	30 24	1.159	0 .431	0.064	0.634
	W	54 01	1.702	0 .631	0.231	0.800
Aug. 11—12	S	35 02	1.221	0 .481	0.087	0.682
	S	26 51	1.121	0 .619	0.050	0.792
	S	40 41	1.319	0 .633	0.110	0.801
	W	49 18	1.534	0 .668	0.186	0.825
	W	49 33	1.541	0 .703	0.188	0.847
	W	49 52	1.551	0 .889	0.191	0.949
	W	50 11	1.562	0 .730	0.194	0.863
	W	50 33	1.574	0 .646	0.197	0.810
	W	50 52	1.584	0 .565	0.200	0.752
	W	51 14	1.597	0 .747	0.203	0.873
	W	51 34	1.609	0 .594	0.207	0.774
	W	51 54	1.621	0 .672	0.210	0.827
	W	52 14	1.633	0 .646	0.213	0.810
	W	52 42	1.650	0 .705	0.217	0.848
	W	52 58	1.660	0 .660	0.220	0.820
	W	53 17	1.673	0 .619	0.224	0.792
	W	53 40	1.688	0 .899	0.227	0.954
	W	54 02	1.703	0 .530	0.231	0.724
	W	54 24	1.718	0 .699	0.235	0.844
	W	54 45	1.733	0 .617	0.239	0.790
	W	55 04	1.746	0 .587	0.242	0.768
	W	55 26	1.763	0 .501	0.246	0.700
	W	55 46	1.778	0 .551	0.250	0.741
	W	56 06	1.793	0 .584	0.254	0.766
	W	56 27	1.809	0 .551	0.257	0.741
	W	56 48	1.826	0 .559	0.262	0.747

TABLE 1 (cont'd)

/80

Date	Azimuth	z	sec z	σ	log sec z	1+log σ
Aug. 11—12	W	57°10'	1.814	0 .528"	0.266	0.723
	W	57 34	1.865	0 .714	0.271	0.854
	W	57 59	1.886	0 .582	0.276	0.765
	W	58 21	1.906	0 .815	0.280	0.911
	W	58 40	1.923	0 .460	0.284	0.663
	W	59 00	1.942	0 .584	0.288	0.766
	W	59 20	1.961	0 .699	0.292	0.844
	W	59 44	1.984	0 .664	0.298	0.822
	W	60 09	2.009	0 .767	0.303	0.885
	W	60 29	2.030	0 .538	0.308	0.731
	W	60 51	2.053	0 .483	0.312	0.684
	W	61 14	2.078	0 .584	0.318	0.766
	W	61 36	2.102	0 .617	0.323	0.790
	W	61 56	2.125	0 .732	0.327	0.865
	W	62 18	2.151	0 .526	0.333	0.721
	W	62 43	2.182	0 .731	0.339	0.866
	W	63 03	2.206	0 .720	0.344	0.857
	W	63 16	2.223	0 .771	0.347	0.887
	W	63 51	2.269	0 .691	0.356	0.839
	W	64 16	2.303	0 .953	0.362	0.979
	W	64 38	2.334	0 .534	0.368	0.728
	W	64 58	2.363	0 .664	0.373	0.822
	W	65 21	2.398	0 .578	0.380	0 762
	W	33 24	1.198	0 .443	0.078	0.646
	N	54 09	1.707	0 .398	0.232	0.600
	N	73 10	3.453	0 .594	0.538	0.774
	N	6 37	1.007	0 .328	0.003	0.516
	N	46 30	1.453	0 .507	0.162	0.705
Sept. 26—27	S	42 15	1.351	0 .512	0.131	0.709
	S	41 39	1.338	0 .664	0.126	0.823
	W	17 23	1.048	0 .487	0.020	0.688
	E	43 42	1.383	0 .320	0.141	0.487
	E	59 34	1.974	0 .314	0.295	0.497
	E	27 29	1.127	0 .340	0.052	0.531
	W	67 31	2.615	0 .516	0.417	0.713
	W	49 59	1.555	0 .355	0.192	0.550
	W	39 03	1.288	0 .423	0.110	0.626
Oct. 3—4	W	41 36	1.337	0 .288	0.126	0.459
	W	18 53	1.057	0 .307	0.024	0.487
	W	19 30	1.061	0 .314	0.026	0.497
	W	20 39	1.069	0 .229	0.029	0.360
	W	21 21	1.074	0 .291	0.031	0.464
	W	22 19	1.081	0 .293	0.034	0.467
	W	22 58	1.086	0 .320	0.036	0.505
	W	23 35	1.091	0 .305	0.038	0.484

TABLE 1 (cont'd)

Date	Azimuth	z	sec z	σ	log sec z	1 + log σ
Oct. 3—4	W	24°38'	1.100	0".307	0.041	0.487
	W	25 10	1.105	0 .392	0.043	0.593
	W	25 53	1.112	0 .322	0.046	0.508
	W	26 38	1.119	0 .307	0.049	0.487
	W	27 14	1.125	0 .251	0.051	0.400
	W	28 31	1.138	0 .344	0.056	0.537
	W	29 07	1.145	0 .377	0.059	0.576
	W	29 47	1.152	0 .355	0.061	0.550
	W	30 21	1.159	0 .394	0.064	0.596
	W	31 37	1.174	0 .501	0.070	0.700
	W	32 10	1.181	0 .437	0.072	0.640
	W	32 52	1.191	0 .456	0.076	0.659
	W	33 35	1.200	0 .437	0.079	0.640
	W	34 09	1.208	0 .402	0.082	0.604
	W	34 47	1.218	0 .340	0.086	0.531
	W	35 22	1.226	0 .419	0.088	0.622
	W	36 02	1.237	0 .336	0.092	0.526
	W	42 22	1.353	0 .417	0.131	0.620
	W	42 58	1.367	0 .369	0.136	0.567
	W	43 29	1.378	0 .427	0.139	0.630
	W	44 01	1.391	0 .456	0.143	0.659
	W	44 31	1.402	0 .458	0.147	0.661
	W	45 08	1.418	0 .402	0.152	0.604
	W	45 44	1.433	0 .349	0.156	0.543
	W	46 18	1.447	0 .388	0.160	0.589
	W	47 03	1.468	0 .351	0.167	0.545
	W	47 36	1.483	0 .452	0.171	0.655
	W	48 10	1.499	0 .351	0.176	0.545
	W	48 34	1.511	0 .384	0.179	0.584
	W	49 05	1.527	0 .377	0.184	0.576
Oct. 7—8	E	75 36	4.021	0 .714	0.604	0.854
	E	67 40	2.632	0 .489	0.420	0.689
	E	63 05	2.209	0 .747	0.344	0.873
	E	47 36	1.483	0 .489	0.171	0.689
	E	13 35	1.029	0 .470	0.012	0.672
	E	60 24	2.025	0 .501	0.306	0.700
	E	64 08	2.292	0 .683	0.360	0.834
	E	79 34	5.522	0 .806	0.742	0.906
	N	60 39	2.040	0 .516	0.310	0.713
	N	70 32	3.001	0 .482	0.477	0.684
	N	55 19	1.753	0 .584	0.244	0.766
	N	66 26	2.051	0 .755	0.398	0.878
	N	45 07	1.417	0 .646	0.151	0.810
	W	23 27	1.090	0 .487	0.037	0.688
	W	61 50	2.118	0 .850	0.326	0.929
	W	63 03	2.206	0 .654	0.344	0.816

TABLE 1 (cont'd)

/82

Date	Azimuth	z	sec z	σ	log sec z	1+log σ
Oct. 7 8	W	41 18′	1.397	0 .670″	0.145	0.826
	W	31 03	1.167	0 .627	0.067	0.797
	W	19 28	1.061	0 .648	0.026	0.812
	W	34 34	1.214	0 .381	0.084	0.584
	S	33 57	1.206	0 .536	0.081	0.729
	S	61 51	2.123	0 .602	0.327	0.780
	S	71 50	3.207	0 .759	0.506	0.880
Oct. 17—18	S	39 24	1.294	0 .371	0.112	0.569
	S	36 22	1.197	0 .392	0.078	0.593
	W	53 46	1.692	0 .357	0.228	0.553
	W	20 42	1.069	0 .361	0.029	0.558
	W	73 02	3.427	0 .681	0.535	0.837
	W	47 07	1.469	0 .384	0 167	0.584
	W	48 17	1.503	0 .542	0.177	0.731
	N	21 22	1.074	0 .359	0.031	0.555
	N	54 39	1.728	0 .474	0.238	0.676
	N	51 35	1.609	0 .553	0 207	0.743
	N	72 56	3.407	1 .017	0.532	1.007
	E	48 29	1.509	0 .437	0.179	0.640
	E	29 04	1.144	0 .507	0.058	0.705
	E	59 20	1.961	0 .677	0.292	0.831
	E	73 08	3.417	0 .800	0.537	0.903
	E	81 45	6.969	0 .520	0 813	0.716
	E	55 41	1.774	0 .538	0.249	0.731

The values of sec z and of σ are given for each star, and from these values we constructed graphs of the dependence of σ on sec z. In all, 18 graphs were constructed. It was impossible to construct graphs for two days, due to the small number of observations. Several of the constructed graphs represent straight lines; for instance, those for February 11-12 and 12-13 and July 8-9. In other cases the graph is not a straight line and the growth of flickering with an increased zenith distance slows down as a rule; then, starting from $z = 50 - 60°$, the graph becomes almost a straight line with a more or less constant slope, and sometimes is even parallel to the sec z-axis (Fig. 3). The point of intersection of the graph with the σ-axis for most days lies in the range of 0.3 - 0.5″.

From Table 2, which gives the range of flickering for each day, it can be seen that in the summer, the scatter of the flickering is greater than during the rest of the year. Subsequently, the results of the observations were expressed by formula (1) or the formula

$$\log\sigma = \log\sigma_0 + \alpha \log \sec z. \qquad (7)$$

From the values of log σ and log sec z given in Table 1, we constructed graphs for each day of the observations. Then we calculated the values of α and log σ_0 for each graph by the method of least squares. The results of the computations are given in Table 2. From both the graphs and the tables it is evident that for the various days α has values in the range of 0.0 - 0.9. The values of log σ_0 lie in the range $\bar{1}.5 - \bar{1}.8$.

/83

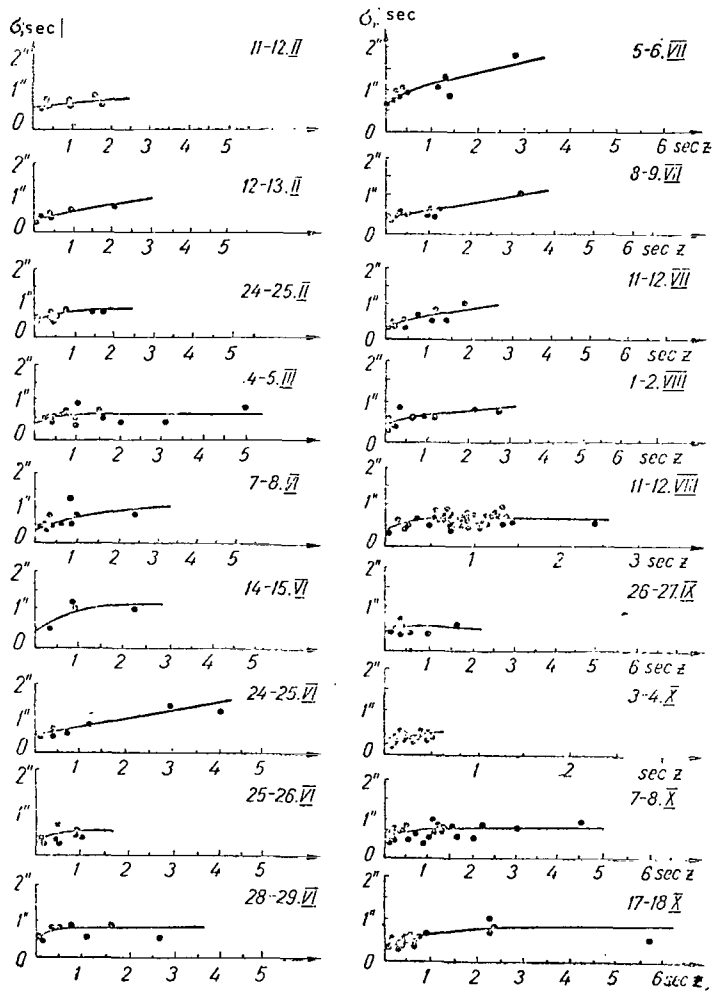

Fig. 3.

/84

All the flickering values were divided into four groups by their azimuths: the group of southern stars (azimuths from 315° to 45°); western stars (azimuths 45 - 135°); northern stars (azimuths 135 - 225°); eastern stars (azimuths from 225 to 315°). The only star traces excluded from these groups were those of α Agl. observed on August 11-12 and α Lyr observed on October 3-4. (On these days, only one star was observed the entire time). Thus, approximately 40 to 50 stars appeared in each group.

For each group we calculated the value of α and log σ and constructed the corresponding graphs of the dependence of log σ on log sec z (Fig. 4: (a) is from observations of eastern stars; (b) is from observations of southern stars, (c) is from observations of western stars and (d) is from observations of northern stars). The

TABLE 2

Date	No. of Stars	α	$1+\log\sigma_0$	σ_0	Flickering Range
February 11—12	7	0.22	0.74	0.55″	0.5″—0.8″
February 12—13	7	0.70	0.53	0.36	0.3—0.7
February 24—25	10	0.44	0.64	0.45	0.4—0.7
February--March 28—1	3	—	—	—	0.3—0.5
March 4—5	15	0.17	0.68	0.38	0.3—0.8
June 7 8	10	0.61	0.60	0.34	0.4—1.2
June 14—15	5	0.73	0.71	0.47	0.5—1.1
June 24—25	8	0.56	0.62	0.43	0.4—1.1
June 25—26	8	0.42	0.63	0.40	0.3—0.7
June 26—27	4	0.87	—	0.35	0.4—1.0
June 28—29	8	0.01	0.75	0.38	0.4—0.8
July 5—6	10	0.68	0.78	0.64	0.5—1.9
July 8—9	10	0.58	0.61	0.42	0.4—1.1
July 11—12	10	0.70	0.59	0.38	0.4—0.9
August 1—2	10	0.65	0.68	0.42	0.4—0.9
August 11—12	51	0.28	0.72	0.38	0.3—1.0
September 26—27	9	—0.02	0.63	0.35	0.3—0.7
October 3—4	38	0.70	0.49	0.28	0.3—0.5
October 7—8	24	0.22	0.71	0.46	0.4—0.8
October 17—18	17	0.39	0.60	0.40	0.4—1.0

values of α, log σ_0 and their mean square errors are given in Table 3.

/85

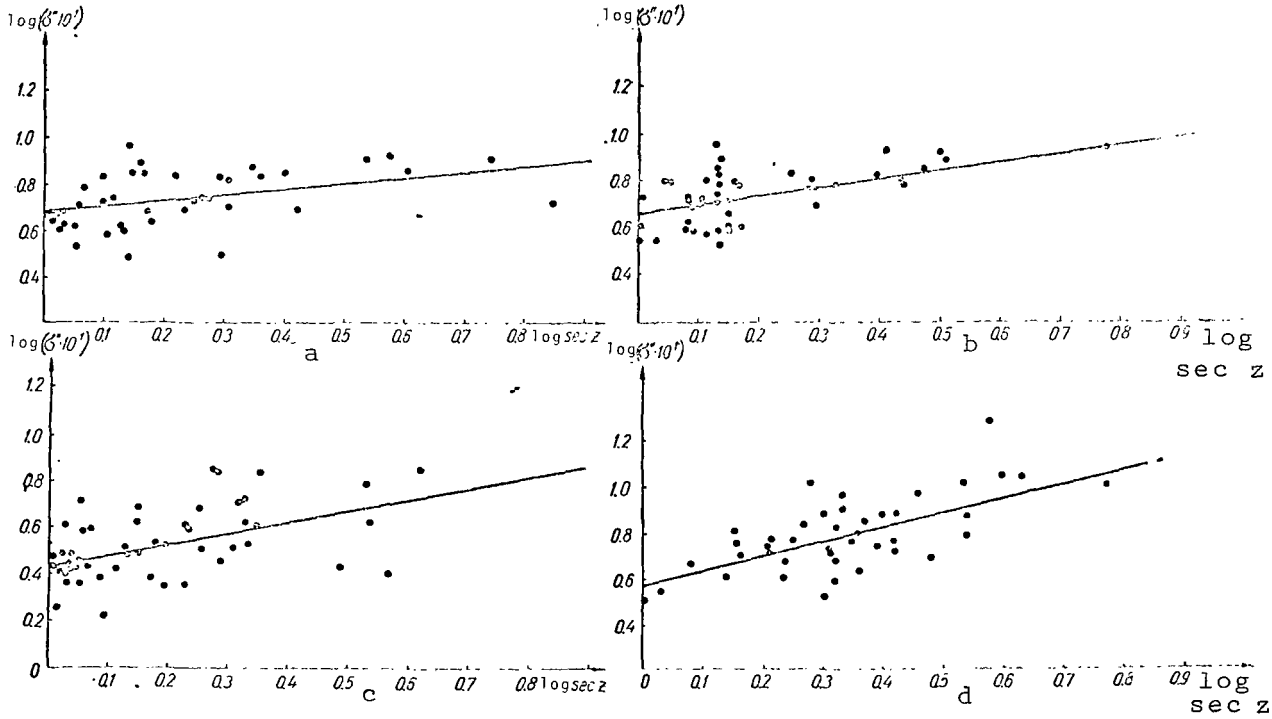

Fig. 4.

TABLE 3 /86

Azimuth	α	$\log \sigma_0$	σ_0
Southern Stars	0.41 ± 0.06	$\bar{1}.66 \pm 0.07$	$0.46'' \pm 0.07$
Western Stars	0.48 ± 0.09	1.64 ± 0.11	0.44 ± 0.11
Northern Stars	0.65 ± 0.10	$\bar{1}.57 \pm 0.09$	0.37 ± 0.08
Eastern Stars	0.23 ± 0.05	$\bar{1}.68 \pm 0.09$	0.48 ± 0.10

The southern and western stars have values of α which approximate the theoretical values and those found by I.G. Kolchinskiy in reference [1]. In the case of northern stars α is greater. This may be explained by the fact that Kiev is located to the north of the observatory. Here we constantly observed large flickering and poor image quality. The eastern stars gave values of α lower than the theoretical values. If we superimpose the graphs of the southern and eastern stars on one another, we can see that basically their points coincide, and only four or five are located significantly lower than the others. This also appeared in the values of α of the eastern stars. The graphs of the northern and western stars also converge and their flickering scatter is greater than in the preceding two groups.

Finally, the values of α and σ_0 were calculated for all stars during one year. Their values were the following:

$$\alpha = 0.51 \pm 0.07, \quad \sigma_0 = 0.42'' \pm 0.08''.$$

A general graph constructed for all points is given in Figure 5.

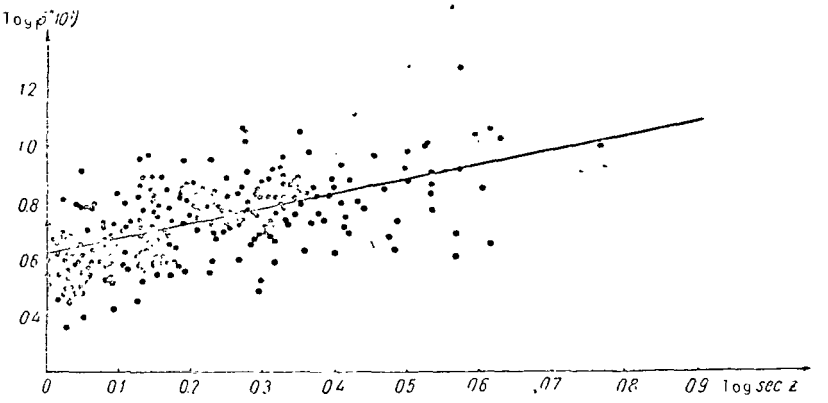

Fig. 5.

In this manner, the value of α obtained from the aggregate of /87 all observations of 1963 in Goloseyevo proves to agree very well with the analogous results of I.G. Kolchinskiy, which are close to

the theoretical value. It is also interesting that in the observations of 1963, the value of α depends on the azimuth.

References

1. Kolchinskiy, I.G.: Izv. Gl. Astr. Obs. Academy of Sciences of the Ukr. SSR, Vol. 3, p. 2, 1961.
2. Krasil'nikov, V.A.: Academy of Sciences of the SSSR, New Series, Vol. 65, p. 3, 1949.
3. Kharadze, Ye.K.: Byull. Abastumanskoy observatorii, No. 21, 1937.
4. Fesenkov, V.G.: Izv. Astrofiz. in-ta, Vol. 1, Nos. 1-2, 1955.
5. Issledovaniye astroklimata i opticheskikh svoystv atmosfery v Kazakhstane (Investigation of the Astroclimate and the Optical Properties of the Atmosphere in Kazakhstan). Trud. Astrofiz. in-ta, Vol. 4, 1964.
6. Gaze, V.G.: Izv. Krymskoy astrofiz. observatorii, Vol. 3, 1948.
7. Podobed, V.V.: Fundamental'naya astrometriya (Basic Astrometry). Fizmatgiz, Moscow, 1962.
8. Maksutov, D.D.: Astronomicheskaya optika (Astronomical Optics). Association of State Presses, Moscow, 1946.

DEPENDENCE OF STAR IMAGE FLICKERING ON METEOROLOGICAL CONDITIONS

G.V. Moroz

ABSTRACT: Meteorological conditions and their influence on the dependence of the amount of image flickering on zenith distances are studied. It was established that under anticyclone conditions image flickering is nearly constant at all zenith distances and decreases slightly at the zenith. If the atmosphere over the point of observation has the characteristics of an unstable air mass, the image flickering increases regularly with the zenith distances.

The dependence of image flickering on various meteorological conditions has been investigated by a number of authors, but no unambiguous conclusions have been reached. Certain investigators consider that it is necessary to study the general state of the air mass above the point of observation. Thus, I.G. Kolchinskiy [1] showed that in groups of observations carried out at the same wind velocity, there is a tendency for flickering to increase in the case when temperature inversions have occurred on a level 0 - 300 m from the Earth's surface. A comparison of flickering at the zenith with the parameter $\Delta T/v^2$ used by T.A. Vorontsov, showed that large oscillations sometimes arise under conditions of significant atmospheric stability, while small oscillations may be observed under non-stable conditions as well. /88

N.I. Kucherov [2] examined the influence of synoptic fronts on the quality of images for certain points of the northern Caucasus and Crimea. In 75% of all cases, an increase in the angle of turbulence was caused by the passage of fronts. G.I. Bol'shakova and Sh.P. Darchiya [3] at two high-altitude points of Pamir and Dagestan noticed deterioration of image quality with the passage of fronts in only 50% of all cases.

Article [4] determines the flickering of stellar images for 20 nights in 1963 and their dependence on the zenith distance according to the formula

$$\bar{\sigma} = \sigma_0 (\sec z)^n,$$

where σ is the flickering value for a given zenith distance, σ_0 is the flickering at the zenith, sec z is the amount proportional to the thickness of the air mass through which the ray passes in

the Earth's atmosphere, α is the exponent. On the average the value of α was obtained equal to 0.5, but for separate days it varied within the limits 0.0 to 0.9. The values of σ_0 varied within the range of 0.3 - 0.6. So much scatter of the values of the parameters is obviously explained by the difference in the optical values of the atmosphere during the observations. In the present article we have attempted to determine the effect of synoptic conditions on the value of σ_0 and α. For this purpose, we divided all the days of observation into four groups, and then studied the characteristics of the conditions of the air mass for each group: group I: $\alpha < 0.5$, $\sigma_0 > 0.4$; group II: $\alpha < 0.5$, $\sigma_0 < 0.4$; group III: $\alpha > 0.5$, $\sigma_0 < 0.4$; group IV: $\alpha > 0.5$, $\sigma_0 > 0.4$. The graphs of the dependence of the star image flickering on the air mass for each group are given in Figure 1. In group I, graph 1 is constructed /89

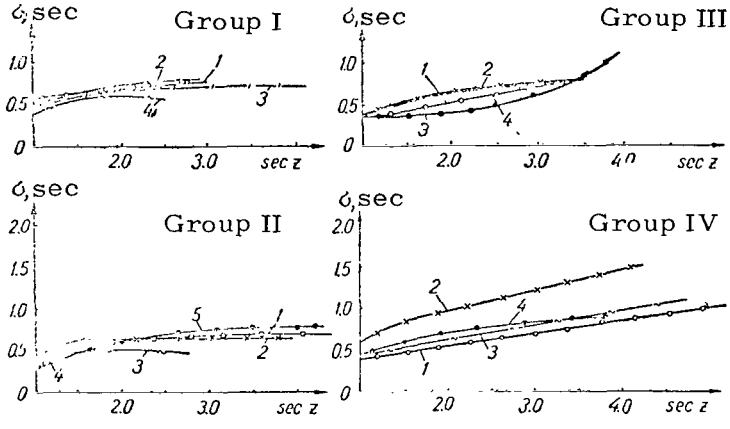

Fig. 1.

for February 11-12, graph 2 for February 24-25, graph 3 for October 7-8 and graph 4 for June 25-26; in group II, graph 1 is for March 4-5, graph 2 for June 28-29 and August 11-12, graph 3 for September 26-27, graph 4 for October 3-4, graph 5 for October 17-18. The graphs of the third group depict the following: 1 is February 12-13, 2 is June 7-8, 3 is June 26-27 and 4 is July 11-12. The fourth group contains the graphs: 1 for June 24-25, 2 for July 5-6, 3 for July 8-9 and 4 for August 1-2.

In order to determine the state of the air mass on every day of observation we used the results of aerological sounding of the atmosphere. Radiosondes were sent out from a platform located in the vicinity of the Main Astronomical Observatory and separated from it by a wooded elevation. The distance between these points is approximately 5 km; the meteorological data for their ground

layers differ from one another. The summer temperatures (evening and night) at the Main Astronomical Observatory, located in the forest, are several degrees lower than those on the platform for sending out sondes, which is located inside the city limits and on certain days at the Main Astronomical Observatory we observed greater humidity and even a small amount of ground mist. However, it can be considered that these differences exist up to a height of 50 - 100 m, while above that the state of the air masses is identical. The soundings were carried out in the evening at 20 - 21 hrs. and in the morning at 2 - 3 hrs. Moscow time, while the photographs of star traces were taken in the interval between soundings. For each night of observations we constructed two stratification curves (curves of temperature distribution with height) from the data of the evening (Curves 1) and the morning (Curves 2) soundings (Cf. Figs. 2,3,4,5) and the corresponding curves of the dew points by means of which it was possible to observe the curve of humidity with height. The evening dew points are described by Curves No. 3, while the morning dew points are given in Curves 4. For the purpose of comparing the data of the observations with the synoptic conditions, next to the stratification curves for each day we give the appropriate section copied from the weather maps located in the Synoptic Bulletin of the Central Weather Institute for 1963. On these maps the point of observation is designated by a small circle, and the figures around the circle correspond to the temperature at the surface, the dew point and the barometric tendency during the last three hours. The maps depict weather conditions at 3 A.M. Moscow time; therefore for each observation we gave the map for the beginning of the second day, as this is closest to the moment of observation. /90

We shall consider the synoptic conditions for the days of group I, which are characterized by equal flickering at all zenith distances (cf. Fig. 1).

February 11-12 (Fig. 2). The point of observation lies on the south-western periphery of a Siberian anticyclone, in a zone of weak barometric gradients. From 0.5 km to a height of 1-2 km, there extends an inversion consisting of two less powerful inversion layers with air moisture which sharply decreases with the height. At a height of 0.5 km, in the evening the wind becomes stronger by up to 10-11 m/sec, while in the morning it increases by 17-18 m/sec. At the surface, the wind is weak and inversion mist is observed.

February 24-25. The point of observation is located in a laterally extended high-pressure zone with the center of the anticyclone over south-eastern Europe. The inversion here descends to a height of 0.5 - 1.0 km; there is mist at the Earth's surface; the wind is weak.

June 25-26. An anticyclone has extended from the north to

the point of observation. An incoming air mass from the north is less stable. There is an isothermal layer at an altitude of 2.5 - 3.0 km. The wind becomes weaker with height. At night a low radiation inversion formed at the Earth's surface. Apparently, it was strong on the territory of the Main Astronomical Observatory, since the temperature at the surface reached the dew point, ground mist was observed and stars near the horizon were not visible.

October 7-8. A weakly expressed offshoot of a high-pressure area extended to the point of observation. The horizontal barometric gradients are small. Inversion is at the height of two km; towards morning it becomes stronger and drops to 1.5 km. The wind is weak; there is nocturnal radiation inversion at the Earth's surface.

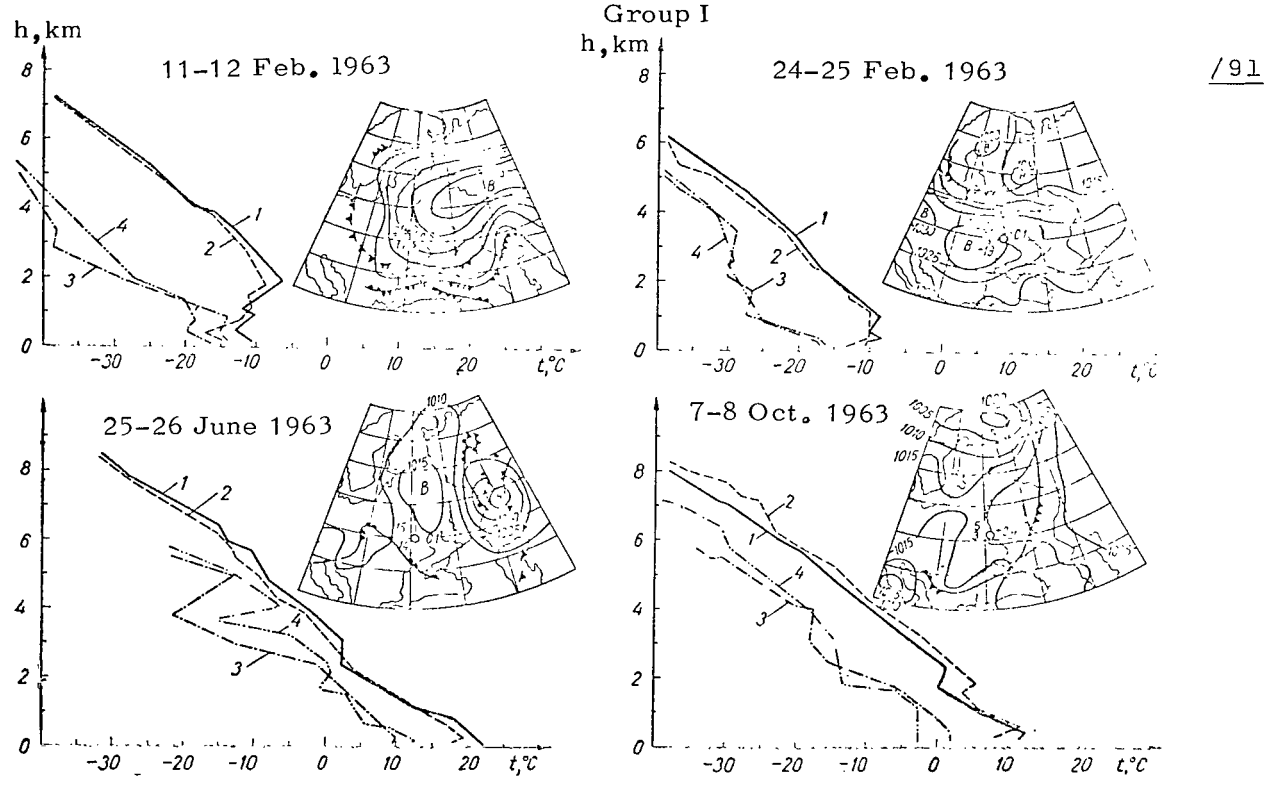

/91

Fig. 2.

Thus, the general characteristics of the weather of the first group of days are weather of high-pressure areas and their peripheries, the presence of dry intercepting layers with temperature inversion or isothermy, with weak winds.

Let us consider the properties of the synoptic conditions in the second group of days, for which the change of image flickering in dependence on sec z is shown in Figure 1, while the weather maps are given in Figure 3.

March 4-5. A high-pressure offshoot extends to the point of observation. A diffuse front passes through the offshoot over western Europe. On the morning of March 4 the weather was hazy, but the region of high pressure extended to the east, including Kiev, and in the evening clear weather prevailed. The stratification curve has an isothermal layer at a height of 2 km. The wind becomes stronger and changes direction at higher altitudes.

June 28-29. A high-pressure area extending to the Ukraine from the south is moving to the east. Kiev appears to be on the eastern periphery of a European cyclone. A warm front passes through; it becomes warmer. Strong wind is observed at a height of 2.5 km, becoming gradually weaker above and below this height. In the morning, on the other hand, the wind in this stratum becomes weaker and at the Earth's surface becomes somewhat stronger.

August 11-12. A region of high pressure has settled over the point of observation. A cold front has passed through the offshoot from the south-west. On the evening stratification curve, isothermy appears at a height of 2 km, while under this stratum an increase in the wind is observed.

September 26-27. Kiev is behind a warm front formed in a low pressure trough. The stratification curve has layers with increased moisture and a large temperature gradient. The wind is not strong, but a wind shift in the 0 - 3 km stratum was observed at the time of the evening sounding. At night at the Earth's surface there is strong radiation inversion. Ground mist was observed at the Main Astronomical Observatory.

October 3-4. The weather was characterized by the passage of the periphery of a cold front. There is inversion at a height of 0.5 - 1 km. In the 0.5 - 1.5 km stratum we observed a strong wind which became weaker toward morning.

October 17-18. A high-pressure area was located over Kiev, but its center very rapidly moved away to the south-east, the wind changed direction, and the pressure dropped. The stratification curve at a height of 1 - 2 km shows a stratum of warm dry air, but due to the strong wind at this height, inversion develops towards morning. The wind at the Earth's surface is strong, but /93

decreases with height.

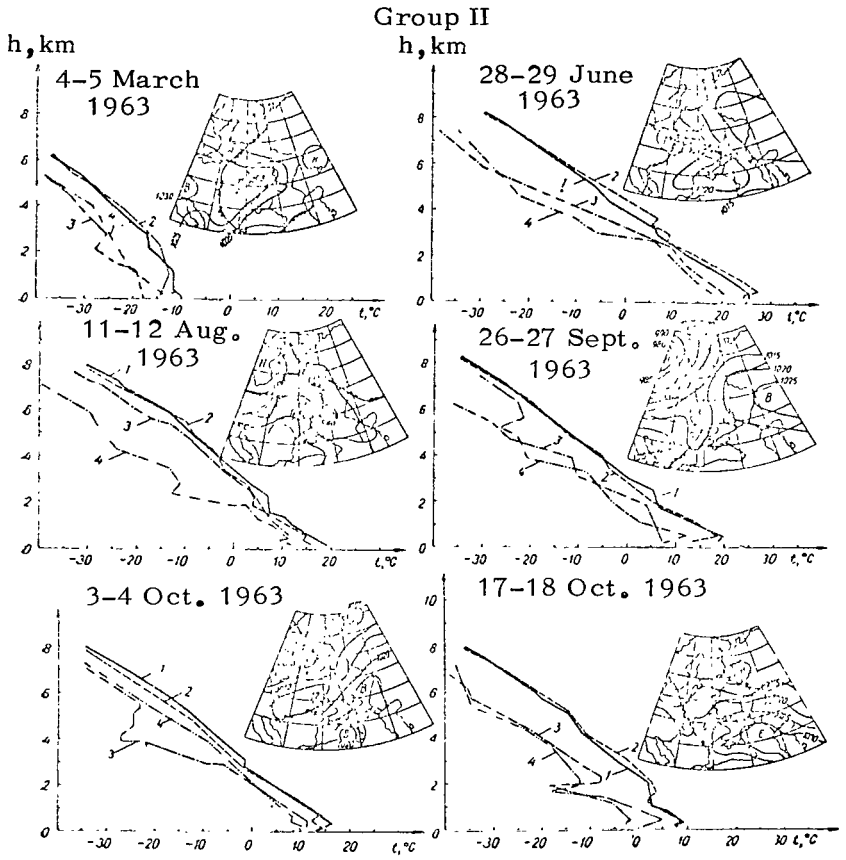

Fig. 3.

If we compare the weather characteristics of the first two groups, for which the dependence of flickering on the air mass is less strongly expressed ($\alpha < 0.5$) and which differ only in the amount of flickering at the zenith, we may say that the general features of these two groups are anticyclonic activity, the presence of descending air currents and the formation of warm and dry inversion layers. However, if in group I these are stable air masses of stationary anticyclones or ridges formed in homogeneous air with weak winds, then in group II, the weather changes quickly, which is characteristic for regions laying on the border between high and low pressure areas. /94

The graphs of image flickering referring to group III are given in Fig. 1. Oscillations at the zenith are comparatively small, but then they increase gradually and smoothly all the way to the horizon. Let us consider the characteristics of the weather on these days (Fig. 4).

February 12-13. The meteorological conditions were analogous to those studied in group I on February 11-12. However, the continuing departure of the ridge of the Siberian anticyclone to the east is accompanied by an increase of wind. The anticyclone at the Earth's surface is gradually filled by a warmer air mass, the inversion mist disappears and a strong moist interlayer is detected at an altitude of approximately 4 km.

June 7-8. A non-stable air mass in a diffuse baric field is distributed over the point of observation. An insolation type of weather settles. (In the air warmed during the day the vertical temperature gradient increases, ascending currents and cumulus clouds appear; at night the lowest strata cool off, the stability of the air mass at the surface increases, radiation inversion appears, the clouds dissolve.)

June 26-27. Also an insolation type of weather, but a front passes through the point of observation. (It rained in Kiev during the day on the 26th.) In the evening the wind was weak, but it became stronger towards morning.

July 11-12. A small anticyclone had settled over the point of observation, but then the air mass, characterized by isothermy in the evening, is converted to a non-stable insolation mass.

The fourth group is distinguished by large oscillations at all zenith distances (cf. Fig. 1). The stratification curves of this group and the weather maps are given in Figure 5.

June 24-25. During the day of June 24 a warm and a cold front (diffuse occlusion front) joined together over the point of observation. At a height of 3 km there is frontal isothermy of the warm front with a strong wind, but in the morning the eastern sector of an anticyclone with inversion on its periphery is found here. At the Earth's surface the wind gradually becomes stronger with height, while the temperature gradient approximates the adiabatic gradient.

July 5-6. The weather maps indicate the presence of a diffuse baric field over the point of observation. The stratification curve up to 3 km is directed along the dry adiabat, while above this there is a strong moist intercepting layer. The wind increases with height.

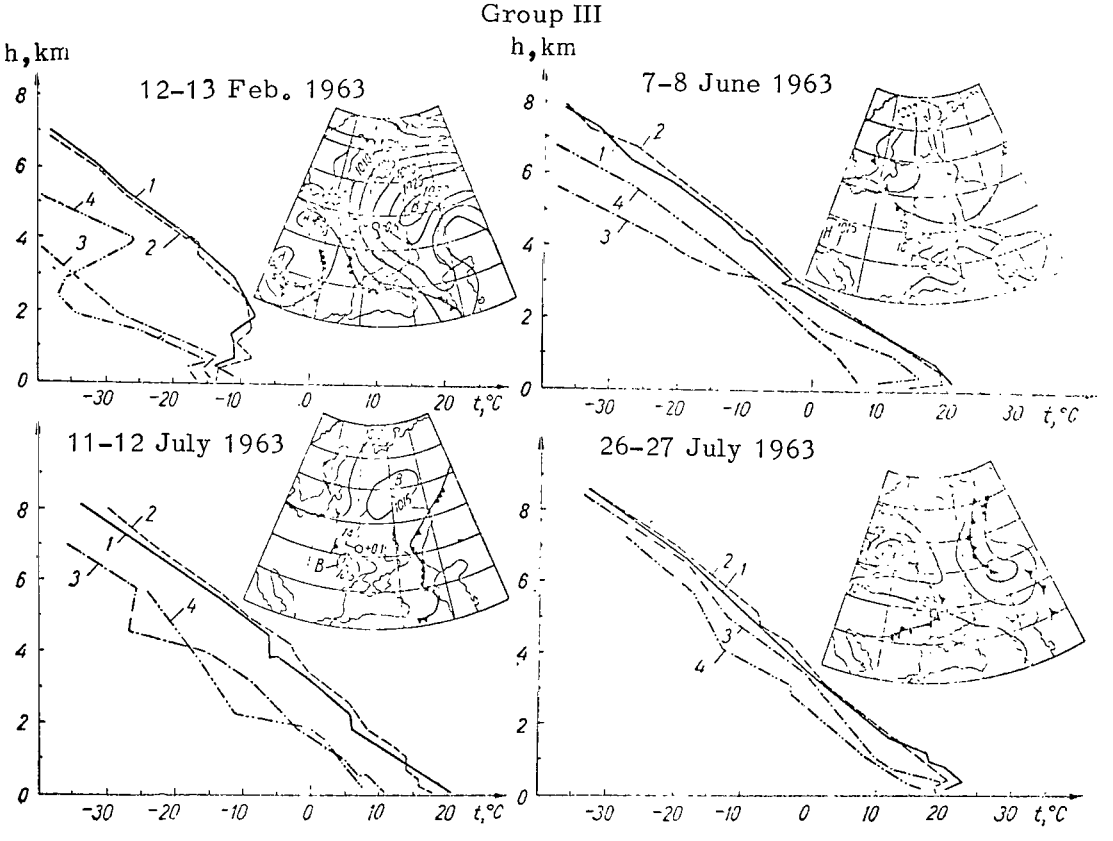
Group III
h,km
12-13 Feb. 1963
7-8 June 1963
11-12 July 1963
26-27 July 1963
t,°C

Fig. 4.

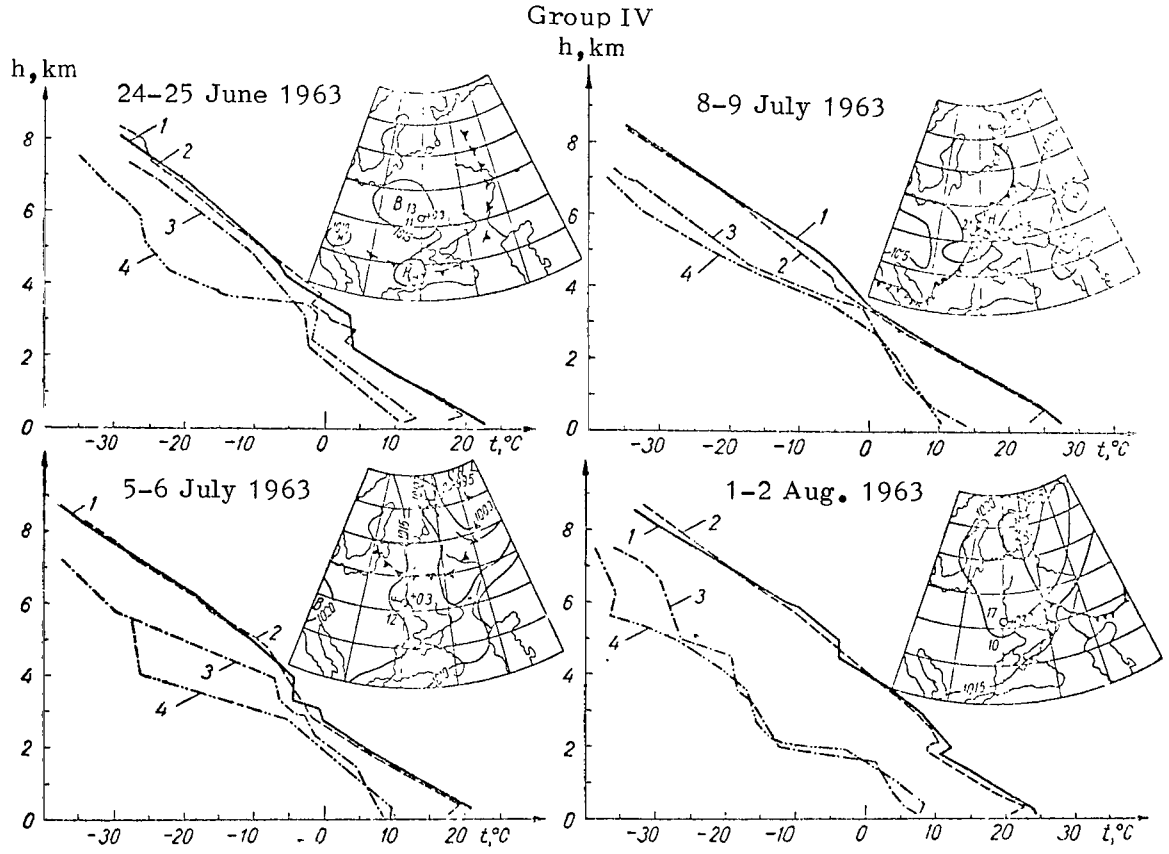
Group IV
h, km
24–25 June 1963
8–9 July 1963
5–6 July 1963
1–2 Aug. 1963
h, km
t, °C
1
2
3
4

Fig. 5.

July 8-9. The weather is that of a non-stable air mass: a diffuse baric field and an approaching cold front. There is a moist layer at a height of 4 km. The lowest atmospheric layers are stratified, as in the preceding cases. The wind increases with height. /97

August 1-2. Observations were carried out in an air mass on the southern periphery of an anticyclone. These days, characterized by very low moisture of the air mass, differ from the preceding days, but also share some common characteristics: a temperature in the stratum up to 2 km which approximates the adiabatic gradient; the existence of an inversion layer at a height of 2 km, in which the moisture increases; moderate wind, increasing with height.

If we compare the atmospheric conditions for the last two groups, their common characteristics appear to be the presence of air mass instability in the stratum up to 3 km; in stable air masses a tendency to disrupt the stability and to create conditions for the appearance of vertical motions is observed. The difference between these groups consists of the following. In group III the daily variation of the temperatures in the lowest stratum (up to 1.5 - 2 km) is clearly expressed, which is characteristic for the insolation type of weather with strong warming during the daytime and cooling at night. The passage of the fronts is related to the convective activity, which increases by day and decreases by night. The temperature gradient, which is greatest at the surface, decreases gradually with height. No daily variation is observed in group IV. The evening curve up to 3 km coincides almost completely with the morning curve. The radiation inversion is less than in group III. The temperature gradient approximates the adiabatic gradient up to a height of 2 - 3 km, but above this there is an inversion layer with increased moisture. In this layer the wind becomes stronger, cloudiness appears; here can also be found a type of atmospheric mist, like the fumulus which were observed over the Ukraine and described in article [5]. All this can serve as the cause of image quality deterioration and increased flickering.

In concluding this survey, we must say that in view of the small number of days of observation, the conclusions we have reached must be considered provisional. They can not be verified at this time by more extensive material.

The basic conclusion which may be drawn from this investigation is that star image flickering and the character of its dependence on zenith distance is determined by the general state of the air mass up to a great height, rather than by its surface layer alone. /98 The type of curves characterizing the increase of flickering with the zenith distance depends primarily on whether or not we are concerned with a stable air mass with descending motions or with

non-stable masses in which convective currents arise. In the first case the flickering does not depend on the zenith distance and becomes only somewhat smaller at the zenith. In the case of non-stable air masses, the amount of flickering increases constantly as the zenith distance increases.

Furthermore, the following circumstance, related to the amount of dispersion of the points of the obtained curves (cf. article [4], Fig. 3), was observed. The least scatter of the points is observed with quiet dry air at the Earth's surface (curves for July 8-9, February 12-13). Increase in the wind at the surface layer increases the dispersion of the points, without changing the slope of the curve (August 11-12, October 17-18). Especially large scatter of the points is characteristic of days with high moisture, when nocturnal cooling leads to the formation of ground mist (March 4-5, June 25-26, September 26-27). However, if in windless weather the air on the observation platform does not cool uniformly, and local temperature inhomogeneities form, there may be wide divergence of isolated points from the mean curve on the graphs (June 7-8, August 1-2).

For the indicated consultation on meteorology given during the writing of the present article, the author expresses his deep gratitude to L.Z. Prokh, a candidate of geographical science.

REFERENCES

1. Kolchinskiy, I.G.: Opticheskaya nestabil'nost' zemnoy atmosfery po nablyudeniyam zvezd (Optical Instability of the Earth's Atmosphere in Stellar Observations). "Naukova dumka", Press, Kiev, 1967.
2. Kucherov, N.I.: In the book: Opticheskaya nestabil'nost' zemnoy atmosfery (Optical Instability of the Earth's Atmosphere). "Nauka" Press, pp. 49-59, 1965.
3. Bol'shakova, G.I. and Sh.P. Darchiya: In the book: Opticheskaya nestabil'nost' zemnoy atmosfery (Optical Instability of the Earth's Atmosphere). "Nauka" Press, pp. 68-82, 1965.
4. Moroz, G.V.: "Issledovaniye drozhaniya izobrazheniy zvezd na teleskope AZT-7" (Investigation of Star Image Flickering on the AZT-7 Telescope). Present Collection, p. 72.
5. Prikhot'ko, G.F. and L.Z. Prokh: In the Collection: Tr. Ukr. Nauchno-issl. geol.-razv. inst., Vol. 7, 1957.
6. Tverskoy, P.N.: Kurs meteorologiii (Course in Meteorolgy). Hydrometeorological Press, Leningrad, 1962.

SOME RESULTS OF OBSERVATIONS OF SPECTRA OF STARLIGHT SCINTILLATION CARRIED OUT ON THE 200-mm MAKSUTOV REFLECTOR AZT-7 AT GOLOSEYEVO (KIEV SUBURB)

E.M. Diamant, I.G. Kolchinskiy and Yu.K. Filippov

ABSTRACT: Some results of observations of starlight scintillation carried out with the 200-mm Maksutov reflector at Goloseyevo in 1965-67 are given. The spectra were recorded with a heterodyne-type analyzer in the frequency band of 0.5 - 70 Hz.

At present we have every reason to believe that starlight /100
scintillation, i.e. the random fluctuation of stellar luminosity, observable by the naked eye and objectively recordable by means of quick-response photoelectric apparatus, is a random process.

In investigating scintillation as a random process, we can obtain a frequency spectrum from observations, or more precisely, we can determine the spectral density in the frequency function. Observations of this type are carried out using apparatus intended for analysis of the spectra of random processes: spectroanalyzers.

Observations of scintillation spectra were carried out at the beginning of the 1950's in the Washington Naval Observatory by A. Mikesell, while in 1957-58, three colleagues from the Institute of Electromechanics of the Academy of Sciences USSR, I.P. Rozhnova, R.G. Vinogradova and L.N. Tikhomirova collaborated on research at the Crimean Astrophysical Observatory [1,2,9].

The Washington observations were carried out by the method of recording the star signal on magnetic tape and then analyzing it on "playbacks". The technique was very complex, but the results were found to be interesting: a very close correlation between the wind speed in the region of the tropopause and the intensity of scintillation was observed at high frequencies (> 100 Hz).

The observations at the Crimean Astrophysical Observatory were carried out using a standard ASChKh-1 heterodyne type analyzer, in which the spectrum can be observed on a screen, as well as very simple parallel action analyzers with *RC*-filters having a small number of channels (no more than eight). The range of the ASChKh-1 analyzer does not permit observation of processes with frequencies less than 20 Hz. Comparatively few observations were made at the Crimean Astrophysical Observatory. The observers received an impression of the general character of scintillation spectra, which is necessary for developing photoelectric automatic guidance systems.

Systematic prolonged observations of scintillation spectra are important for obtaining information on characteristics of the astroclimate. By comparing them with aerological data we can obtain definite information on wind conditions in the troposphere. We hope that from such observations scientists will succeed in determining the location of the atmospheric strata causing scintillation.

The data on spectral scintillation densities under various meteorological conditions can be used in planning photoelectric tracking systems and various apparatus related to lasers, in which radiation passes through a turbulent medium. All this has attracted great interest to observations of scintillation spectra. /101

Research of starlight scintillation is carried out on the following circuit (Fig. 1).

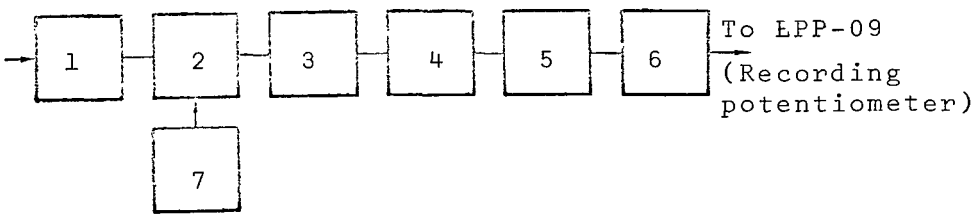

Fig. 1. 1. Input Filter; 2. Ring Modulator; 3. Wide-Band Filter; 4. Tuning Fork Filter; 5. Amplifier; 6. Averager; 7. Tunable Heterodyne.

An image of the objective lens illuminated by starlight is formed on the cathode of the photomultiplier. The signal is amplified from the photomultiplier by the direct current amplifier and enters the analyzer. Both parallel and series action analyzers can be used. An oscillograph for visual observation of the signal under investigation is connected parallel to the analyzer. The harmonics are recorded by an electronic tape recorder.

In observations at the Main Astronomical Observatory of the Academy of Sciences Ukrainian SSR we used analyzers of both types in combination with a mirror-lens AZT-7 telescope, whose main spherical mirror is equal to 21.3 cm in diameter. With the introduction of an extension into the optical circuit, the focal length of the telescope is 10 m. The image of the objective forms on FEU-17 photocathode by means of a Fabry lens. The signal is amplified from the photomultiplier by a direct current amplifier, contained in the same unit as the photomultiplier.

For a signal amplifier we used a wide-band amplifier with an electrometer tube. The first two stages are a binary electrometer tetrode and a binary triode with regulating resistors in the anode and cathode circuit. Application of such a circuit

permits us to decrease the zero drift of the current, caused by fluctuations of the grid current. The third stage is the cathode, connected to the feedback circuit. The photomultiplier is fed from a stabilized 1100 V rectifier and from a standard stabilized rectifier of the VES type.

For the purpose of investigating scintillation spectra in 1964-65, we first decided to apply a multichannel parallel action analyzer with *RC*-filters. The circuit of such an analyzer was developed on general lines at the Institute of Atmospheric Physics of the Academy of Sciences USSR and applied there for solving various problems related to observation of the spectra of random processes, i.e., spectra of surges in wind velocity, spectra of the flickering of a ground light source et al.[3]. A detailed description of such an analyzer is given in [4]. An analogous analyzer constructed at the Main Astronomical Observatory of the Academy of Sciences, Ukrainian SSR has the following characteristics: the range of analyzable frequencies is 0.3 - 200 Hz; the filter transmission band varies from 0.34 to 10 Hz; the minimum distinguishable signal is 1 V; the dynamic range is 20 db; the frequency reading error is 0.5 - 0.7 Δf and the amplitude reading error is 20 - 50%. /102

In practice, for investigation of spectra the effective range of the analyzer was restricted to 100 Hz, since at greater frequencies, the signal amplitude was close to zero. This is related to the fact that, in the first place, scintillation intensity decreases as it passes from the low-frequency to the high-frequency region of the spectrum and secondly, the observations were carried out with the objective lens of the AZT-7 telescope fully open.

Thus, due to the effect of integration of the objective len's area, high frequencies were repressed as well. The time of analysis was chosen equal to 60 sec. This is greater than the time of establishing transition processes in the lowest-frequency channels and at the same time is sufficient for averaging the statistical characteristics of the process.

Close examination of the analyzer showed a number of disadvantages: on the one hand, those characteristic of all analyzers of this type, and on the other hand, those caused by the particular working conditions of the given analyzer.

The voltage taken from the integrators of each channel and determined by the recorder is proportional to the amplification coefficient of the channel, the integral transmission band of the channel and the spectral density of the signal at the filter's output. Therefore, at low frequencies on the range the signal is small. It is not always possible to use the preamplifier, due to the limited dynamic range of the analyzer. *RC*-filters, although to a lesser degree than *LC*-filters, are subject to aging, heating and

the influence of meteorological factors (since the equipment is performing under the conditions of the microclimate of the telescope tower during the entire year). Measurements taken in calibration of the apparatus showed that these changes may reach 200%, although the analyzer was constructed with high-accuracy and high- /103
grade elements. These changes have a random character; they may be corrected for by calibration, but calibration at such low analysis frequencies is a laborious and time-consuming process, and reliable generators of such low-frequency sound do not exist as yet.

The detector-integrator unit is the least stable component of the analyzer. Calibration by sinusoidal voltage of a single frequency and amplitude show that the transmission coefficient of the unit for different channels varies randomly even in a single night of observations; in our case these changes reached 30%. All this complicates processing the obtained results (which under conditions of mass observations has a resolving value), and also reduces the accuracy of the obtained results.

For the indicated reasons, in the summer of 1965, we constructed another heterodyne analyzer (whose diagram is given in Fig. 2) for the purpose of observing scintillation spectra. Its principle of construction does not differ from that of analyzers of similar type already described in references [5,6]. The analyzer of the

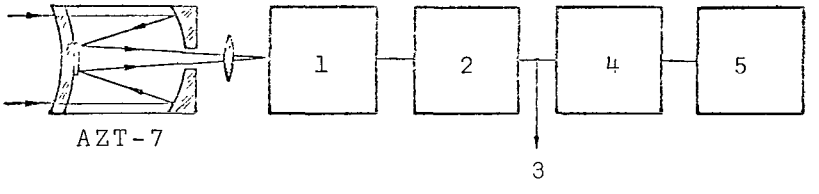

Fig. 2. 1. PM-17; 2. Direct Current Amplifier; 3. To the Oscillograph; 4. Analyzer; 5. EPP-09 (Recording Potentiometer).

Main Astronomical Observatory of the Academy of Sciences of the Ukrainian SSR has a very low analysis frequency (0.5 Hz); the circuit is formed with semiconducting triodes. Its schematic diagram is given in Figure 3. The technical characteristics of the analyzer (series action) are: the range of analyzable frequencies is 0.5 - 75 Hz; the filter transmission band remains constant for the entire range at 0.5 Hz; the minimum distinguishable signal is 0.2 V; the dynamic range is 40 db- the frequency reading error is 0.25 Hz in the range 0.5 - 40 Hz and $\leq$ 1 Hz in the range 40 - 70 Hz; the amplitude reading error is 5%; the time of analysis is 7.5 min; the dimensions are 120 × 190 × 550 mm; the combined power supply is 220 V or a battery supply of 12 V with internal stabilization of 10.5 V.

In contrast to the diagrams obtained on the parallel action

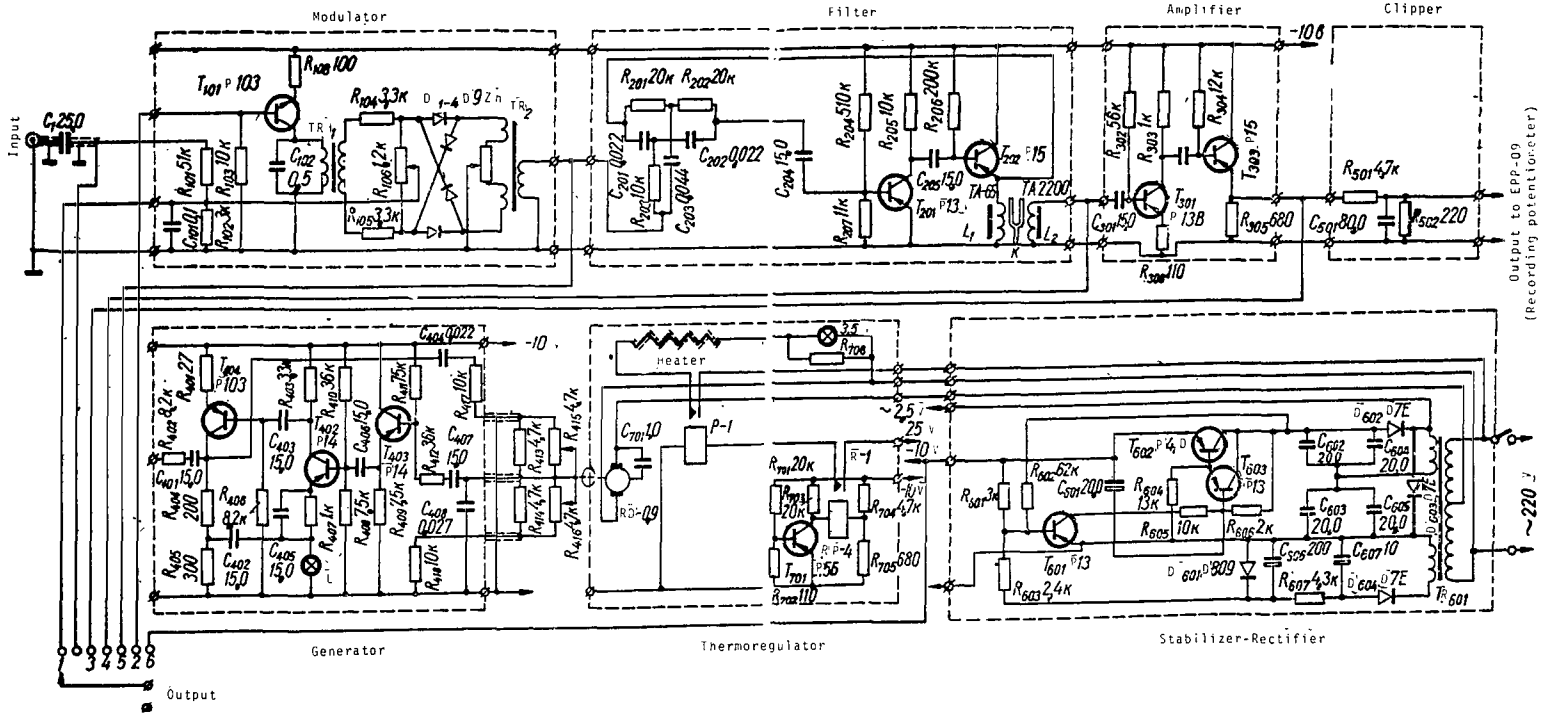
Modulator
Filter
Amplifier
Clipper
Input
Output
Output to EPP-09
(Recording potentiometer)
Generator
Thermoregulator
Stabilizer-Rectifier
Heater
-106
-10
~25 V
~220 V

Fig. 3.

analyzer, which require subsequent deciphering, the new analyzer immediately gives the amplitude spectrum of the signal. Restricting the analysis band to 75 Hz and increasing the time of analysis to 7.5 min does not prove to be a disadvantage of the apparatus, since stellar spectra with one-minute averaging over a period of 8 - 10 min differ little from one another. The differences between them do not exceed the analyzer's errors. Therefore, within known limits it is possible to speak of scintillation as of a stationary random process, in which connection the time of analysis may be increased to 10 min.

Let us consider the basic units of the series action analyzer.

Input Filter. In order to avoid overloading the analyzer with the components of the higher harmonics of frequencies not included in the analyzer's range, and for protection from possible mirror-induced noise, a low-frequency *RC*-filter which weakens all frequencies outside the analyzer's range is placed at the analyzer's input.

The Modulator. The signal, having passed through the input filter, falls on the mixer, where it is combined with the signal from the separate heterodyne. At the output of this stage the signals $f_{het} + f_{sig}$ and $f_{het} - f_{sig}$ form. The modulator is constructed according to a annular circuit with transformer input and output, which permits it to be easily correlated with the preceding and following stages. The annular circuit is characterized by minimal non-linear distortions, by a minimal number of combined frequencies and almost complete suppression of the frequencies of the signal and the heterodyne. To ensure more thorough balancing of the mixer, the winding of the transformer Tr_2 consists of two halves between which a low-resistance variable resistor with grounded midpoint is inserted. Diodes of the D9Zh type are carefully selected by the size of the direct current and the back resistance, for which reason no compensating resistors are included. With the indicated nominal values of the components and with the amount of voltage from the heterodyne on the winding of the transformer Tr_1 equal to 10 V, the modulator is linear for input signals from 0.01 to 1.0 V, which guarantees a large dynamic range of the instrument (40 db). /105 /106

The Preamplifier. From the output of the modulator the signals $f_{het} + f_{sig}$ and $f_{het} - f_{sig}$ enter the input of the selective amplifier, constructed with triodes T_{201} and T_{202} with negative feedback through a binary balanced *T*-network with *RC*-elements. A characteristic of this amplifier is the series connection of the signal with the balanced *T*-network. With small internal signal source resistance such a circuit allows the *RC*-filter to acquire a resonance characteristic similar to that of the *LC*-filter, with a drop of the slopes to zero. [4]. Thus, the following tuning-fork filter, which determines the selectivity of the analyzer, is

protected from any spurious signals falling on its input.

The Tuning-Fork Filter. Use of a tuning-fork filter as the selective element permitted us with small dimensions to obtain a circuit with great equivalent quality and stability, with characteristics similar to the characteristics of the *LC*-filter. The frequency of the tuning-fork selected by us is sufficiently high, much higher than the upper frequency of analysis and its harmonics, and at the same time it is low enough to guarantee the required stability and selectivity. The mutual arrangement of the tuning fork and the exciting coils, based on the electromagnetic system of telephone earphones of the TA-65 and TA-2000 type, can be used to change the quality of the circuit in a wide range. In our equipment they are arranged in such a manner that a tuning fork frequency of 440 Hz guarantees a quality of Q = 1000 (the band $\Delta f_{0.7}$ = 0.44 Hz).

The Intermediate Frequency Amplifier. The signal isolated by the tuning-fork filter with an intermediate frequency of 440 Hz is amplified by a single-stage aperiodic amplifier (on the T_{301} triode), and passing through the emitter follower (on the T_{302} triode), enters the input of the rectifier, constructed according to the system of voltage stress.

The Heterodyne of the Analyzer. This is assembled on the system of the two-stage *RC*-amplifier with positive feedback through a phasing *RC* ladder network. In order to increase the stability in the heterodyne we used silicon transistors and cathode at the input and output. The amplitude of the heterodyne is stabilized by the usual system of a non-linear element (an incandescent light of 24 V 0.15 α) attached to the feedback supply system. The heterodyne's small range of frequency tuning and the measures taken for /107 stabilization ensure the constancy of the frequency and amplitude of the heterodyne signal.

As in all generators of this type, the frequency scale of the heterodyne is non-linear; it is compressed in the upper part of the range and expanded towards the bottom. In the present case this disadvantage proves to be very convenient, since it permits us to maintain a sufficient amount of time for analysis at low frequencies. For a scanning motor we used a synchronous motor of the *RD*-09 type with a 1:1280 reducer and with limit switches which reverse the motor at the ends of the range. Since it is proposed to use the analyzer under different temperature conditions, in addition to internal thermostabilization of each stage, a general thermostabilization is carried out for the entire apparatus, including the heating element and the semiconducting thermorelay which maintains the temperature within the casing at 23 $\pm$ 3°C.

In general the voltage of the charge capacitor is determined by the formula

$$U_{\text{outp.}} = k\sqrt{F(\omega)},$$

where k is the constant allowing for the system amplification coefficient and the frequency characteristic of the tunable filter. This voltage is recorded by an EPP-09 recording potentiometer. The corresponding recording U_{outp} (which depends on the frequency) will henceforth be called the frequency spectrum.

For purposes of comparison, it was convenient to introduce certain numerical characteristics of the obtained scintillation spectra. Since in our research we did not measure the value of the constant component corresponding to the mean luminosity of the star, we were unable to determine the modulation index of the fluctuations and were restricted to relative characteristics only. We assumed such a characteristic to be K, equal to the areas under the spectral curves S_1 and S_2 in the ranges 0.5 Hz - f_1 and f_1 - f_2, where f_1 and f_2 were fixed values. Thus,

$$K = \frac{S_1}{S_2}.$$

Here f_1 = 9 Hz and f_2 = 50 Hz.

The values of the areas S_1 and S_2 obtained from spectrum recordings are proportional to the square roots of the strength of the processes in the indicated range frequencies. Furthermore, we used the characteristics K_1 and K_2, which represent the ratio of the ordinate of the leveled spectral curve at a determined frequency to the ordinate at zero frequency. We assumed these frequencies to be 9 and 30 Hz respectively. /108

Certain Observational Results

Observations on a series action analyzer were begun in September, 1965. We investigated the spectra of bright stars obtained at various zenith distances from 10 to 80°. A list of the observed stars is given below.

Star	*Stellar Magnitude*
Sirius	-1.58
Vega	0.14
Capella	0.21
Arcturus	0.24
Rigel	0.34
Procyon	0.48
Altair	0.89

Star	*Stellar Magnitude*
Betelgeuse	0.92
Spica	1.21
Antares	1.22
Deneb	1.33

The observations consisted of continuous registration of the spectra of certain stars (with two to four sequential recordings) at various zenith distances z. From September, 1965 to June, 1967, observations were carried out over 70 nights, and more than 1000 spectra were obtained.

Figures 4 and 5 give recordings of stellar scintillation spectra. It is evident that the scintillation intensity decreases as it passes from the low-frequency region of the spectrum to the high-frequency range. With our equipment, in practice the curve decreases to zero in the frequency range around 50 Hz. Doubts may arise as to the expedience of observations of scintillation spectra in the comparatively narrow range from 0.5 to 50 Hz. In fact, certain observers established interesting correlations between wind conditions in the region of the tropopause and the character of the scintillation spectra in the frequency range above 100 Hz. However, the contribution of these frequencies to the complete range of scintillation spectra is comparatively small. Theoretical considerations have as yet not given grounds for assuming that precisely the indicated high frequency region is where all the variations of the scintillation characteristics relative to changes in atmospheric conditions are concentrated. On the other hand, spectral analysis in the high frequency range requires significantly more complex apparatus, which at the given stage of our research was impossible to achieve. For this reason we considered it advisable, until the construction of more modern equipment, to carry out observations of scintillation spectra in the frequency range 0.5 - 50 Hz, after which we attempted to compare the results of these observations with aerological data.

Figure 4 gives the scintillation spectra of Vega for various z in the course of a single night of observation (October 4, 1966). As a rule, when z increases, the intensity of the high-frequency range of the spectrum decreases.

A survey of all the material at our disposal showed that the character of the spectra changes substantially with time. Figure 5 gives a number of recordings of the scintillation spectra of Arcturus, taken at $z = 40 - 60°$ in the periods: a. July 4-8, 1966 and b. June 18-21, 1966. Within each period the spectrum type changes little, in contrast to the spectra obtained in different cycles, which show notable differences.

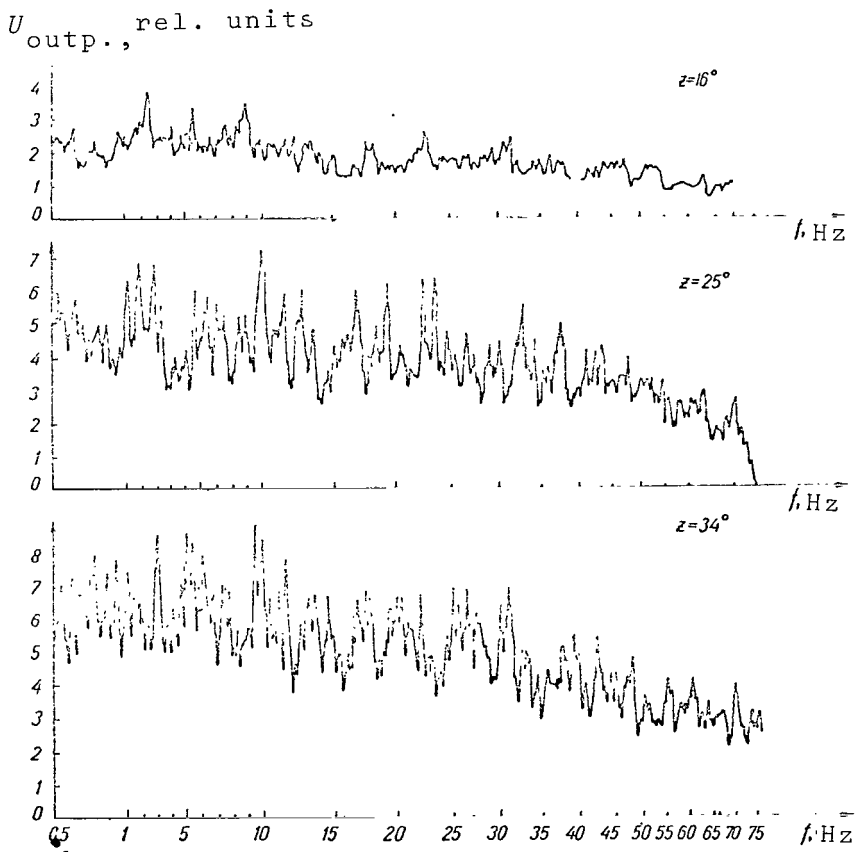
$U_{outp.}$, rel. units
z=16°
z=25°
z=34°
f, Hz
0,5 1 5 10 15 20 25 30 35 40 45 50 55 60 65 70 75

Fig. 4.

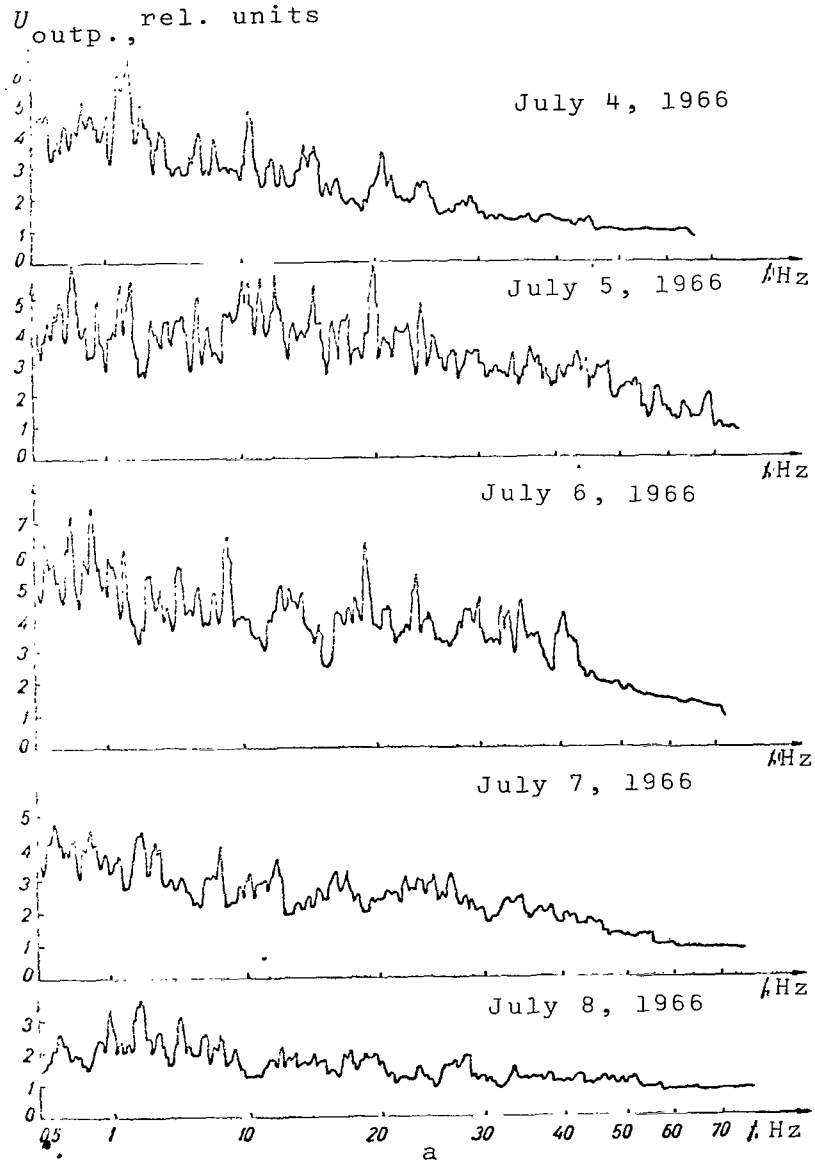
$U_{outp.}$, rel. units
July 4, 1966
July 5, 1966
July 6, 1966
July 7, 1966
July 8, 1966
f, Hz
0.5
1
10
20
30
40
50
60
70
a

Fig. 5a.

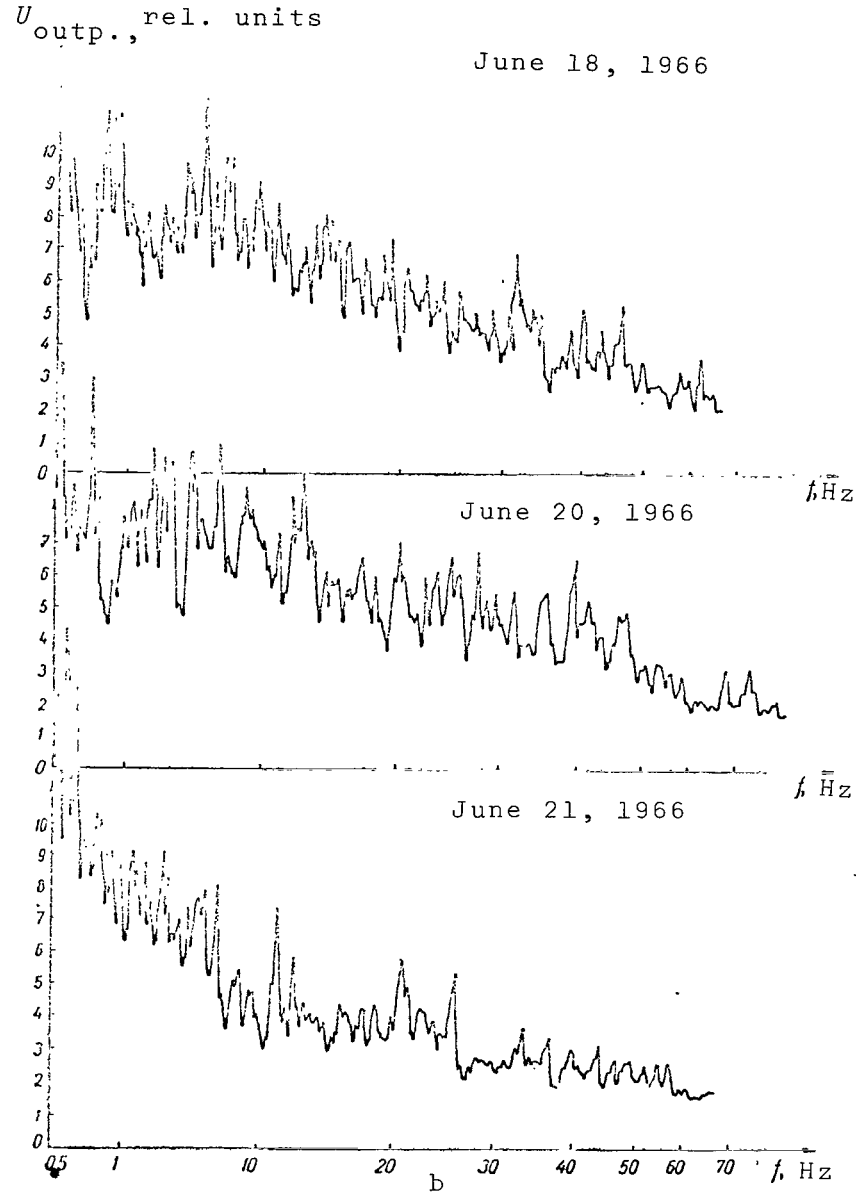
$U_{outp.}$, rel. units
June 18, 1966
f, Hz
June 20, 1966
f, Hz
June 21, 1966
0.5
1
10
20
30
40
50
60
70
f, Hz
b

Fig. 5b.

Since changes which would lead to relative redistribution of the energy in the spectrum can not occur in the apparatus, we must assume that variations in the spectrum type from cycle to cycle are related to specific changes in meteorological conditions in the atmospheric strata which cause stellar scintillation. /112

In order to obtain more concrete data, it is logical to compare the obtained spectra with the results of aerological observations on corresponding nights. We used data on temperature, pressure and relative humidity obtained by radiosonde observations at a point located 5 km to the north-east of the observatory (Bagrinov mountain). For purposes of comparison we selected the soundings taken in intervals of time close to the moments of observation.

Graphs of the Heteorological Conditions at the Time of the Observations

In these graphs we shall not concern ourselves with the general synoptic situation, but shall consider only aerological data referring to the individual nights. The distribution of the nights of observation by month is:

I	II	III	IV	V	VI	VII	VIII	IX	X	XI	XII
2	1	4	6	15	19	12	—	5	6	—	—

Here 48 nights out of 70 (68%) were characterized by the presence of temperature inversion in the stratum between 0.2 and 1 km. In the other cases, isothermy or temperature decrease with height was observed. The mean temperature gradients by height were distributed in the following manner:

Stratum, Km	Gradient, degrees/Km
0 - 3	5.2
4 - 7	6.5
8 - 11	6.3

The height of the tropopause varied from 8 to 14 km, and in 67% of the cases it was 10-11 km. /113

The data on the mean wind speeds and on the relative air moisture by strata are given in the table.

For comparison with the aerological data we chose observations of one star: Vega. In order to avoid the influence of the effect of the zenith distance, the observations were divided into three groups by z intervals: 10 - 40, 40 - 60, 60 - 86°. The aerological data were averaged over the layers 0.2 - 0.5, 1 - 3, 4 - 7, 8 - 11, 12 - 15 km.

Height, km	Mean Wind Velocity v, m/sec	v_{max}	v_{min}	Relative Moisture, % Mean Moisture U	U_{max}	U_{min}
0.2—0.5	7	18	2	66.0	93	42
1—3	9	18	3	66.2	90	29
4—7	12	34	3	50.0	88	6
8—11	14	53	4	49.0	87	10
12—15	13	40	4	44.9	73	8

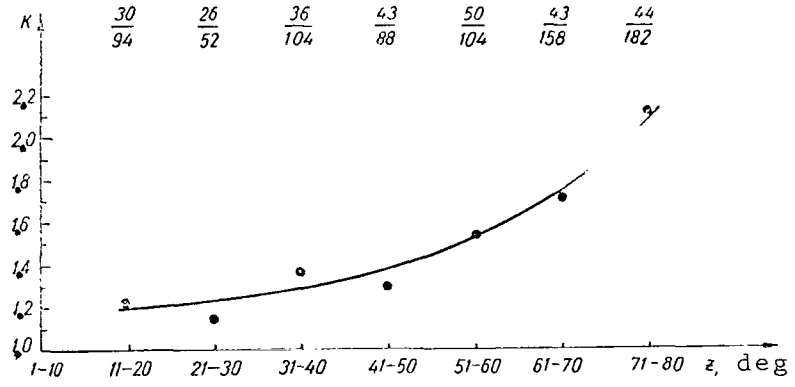

Fig. 6.

Regardless of the considerable scatter of the points, the following conclusions can be reached.

(1) The mean values of K in the specified zenith distance zones are approximately doubled in transition from z = 0 - 20° to z = 70 - 80°. This is evident from Figure 6, where the values of z are plotted by zones on the x-axis. Here and in the following graphs, the figures at the points indicate: in the numerator: the number of nights of observation; in the denominator: the over-all number of spectra obtained on these nights in a given z zone. Thus, the proportion of high frequencies decreases with an increase in z, which was shown by other observers as well [1,8]. The indices K_1 and K_2 decrease when z increases which likewise testifies to the decrease in the proportion of high frequencies. K_1 decreases insignificantly, while K_2 in the zone around 80° is 40% of its value in the 11 - 20° zone (Fig. 7).

(2) Comparison of the mean values of K with the wind speeds in the specified intervals showed a decrease of this index with an increase of the wind speed. The reduction is especially

noticeable in the 4 - 7 and 8 - 11 km strata (Fig. 8). This conclusion agrees very well with the results obtained in [9].

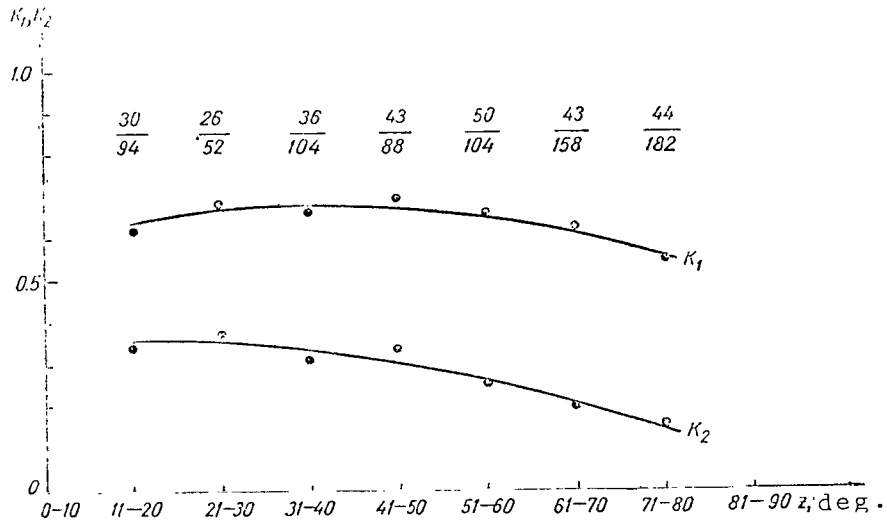

/114

Fig. 7.

Consequently, in the comparatively low-frequency region investigated by us, the proportion of higher frequencies in scintillation increases with increased wind speed. The indices K_1 and K_2 increase with an increase in wind speed, which agrees with the behavior of K (Fig. 9). /115

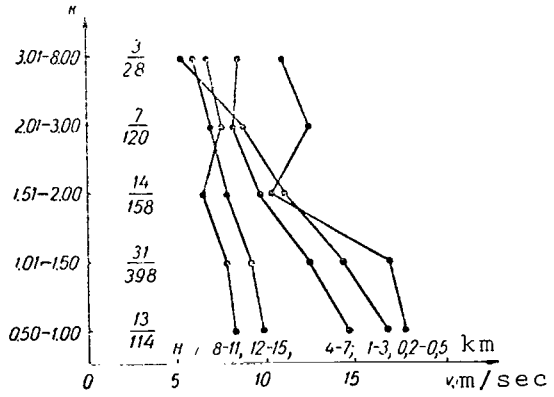

Fig. 8.

(3) It is impossible to reach any definite conclusions concerning the effect of the relative air moisture U on the indices K, K_1, K_2 in the separate strata on the basis of our observations. We can only say that a general property of all the mean curves we have constructed is the correlation of small values of K_1 and K_2 to small values of U, i.e. in dryer air the high-frequency spectral region becomes weaker

(Fig. 10). However, this conclusion would have to be proved by a significantly greater number of observations. /116

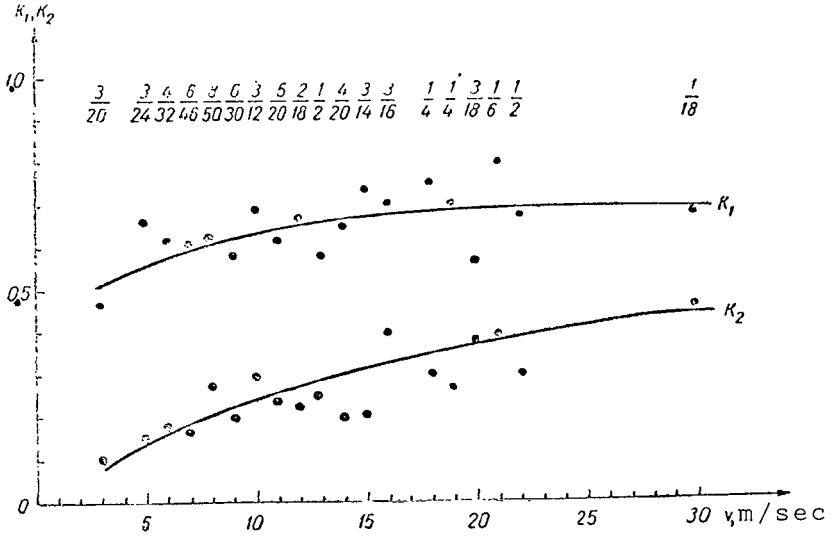

Fig. 9.

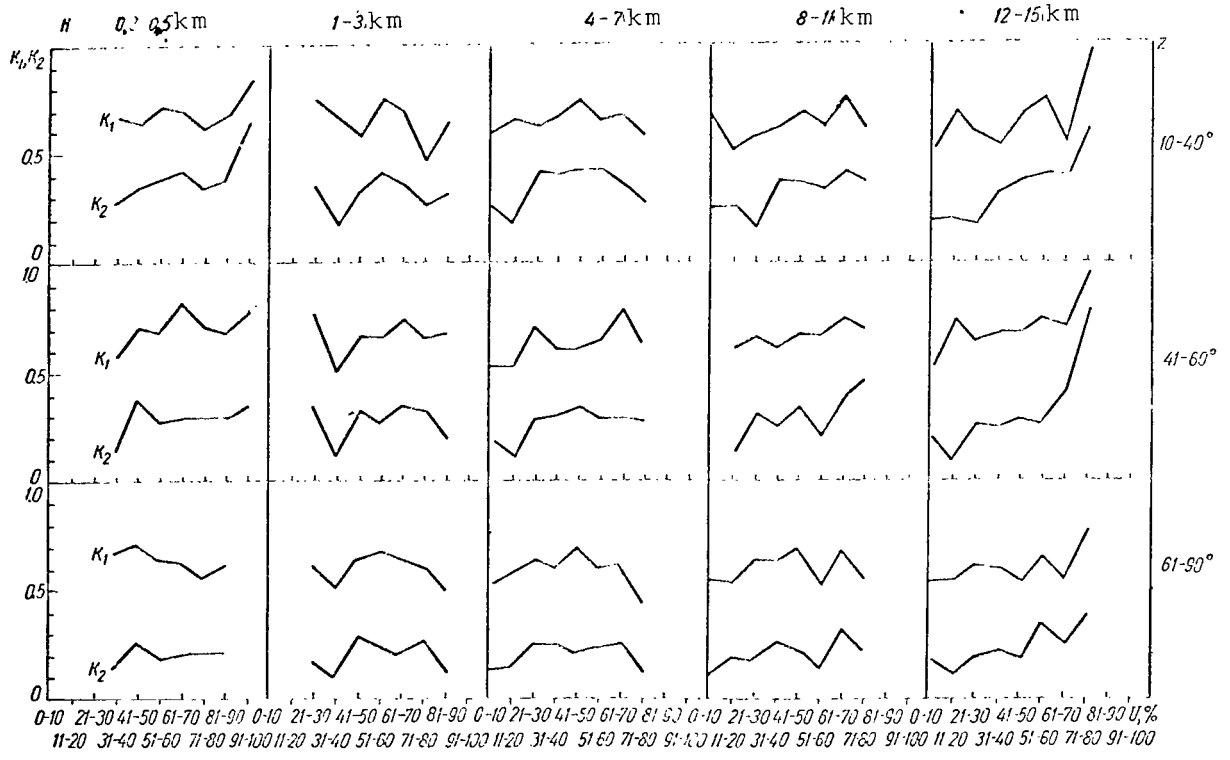

/117

Fig. 10.

REFERENCES

1. Vinogradova, R.G.: In the Book: Trudy soveshchaniya po issledovaniyu mertsaniya zvezd (Transactions of the Conference on Investigation of Starlight Scintillation). Academy of Sciences SSSR Press, Moscow, Leningrad, pp. 135-144, 1959.
2. Vinogradova, R.G., I.P. Rozhnova and L.N. Tikhomirova: In the book: Sbornik rabot po voprosam elektromekhaniki (Collection of Articles on Problems of Electromechanics). Vol. 4, Academy of Sciences SSSR Press, Moscow, Leningrad, pp. 276-281, 1960.
3. Gurvich, A. S.: In the Book: Trudy Instituta fiziki atmosfery, 4. Atmosfernaya turbulentnost' (Transactions of the Institute of Atmospheric Physics, 4. Atmospheric Turbulence). Academy of Sciences SSSR Press, Moscow, pp. 101-143, 1962.
4. Bovsheverov, V.M., A.S. Gurvich et al: In the Book: Trudy soveshchaniya po issledovaniyu mertsaniya zvezd (Transactions of the Conference on Investigation of Stellar Scintillation). Academy of Sciences SSSR Press Moscow, Leningrad, 1959.
5. Stopskiy, S.B.: Analizatory spektra zvukovykh i infrazvukovykh chastot dlya akusticheskoy spektrometrii (Analyzers of Sonic and Infrasonic Frequency Spectra for Acoustical Spectrometry). Gosenergoizdat, Moscow, Leningrad, 1962.
6. Kriksunov, V.G.: Avtomaticheskiye analizatory spektrov elektricheskikh signalov (Automatic Analyzers of Electrical Signal Spectra). "Tekhnika" Press, Kiev, 1965.
7. Kozina, O.G. and A.A. Fransuzov: Radiotekhnika, No. 12, 1958.
8. Mel'nikov, O.A., I.G. Kolchinskiy and N.I. Kucherov: In the Book: Trudy soveshchaniya po issledovaniye zvezd (Transactions of the Conference on Stellar Research). Academy of Sciences SSSR Press, Moscow, Leningrad, 1959.
9. Mikesell, A.H.: The Scintillation of Starlight Publ. of the U.S. Naval Observatory, Second Series, XVII, Part IV, Washington, 1955.

ON THE ASTROCLIMATE OF TWO POINTS IN THE TRANSCARPATHIAN AND ODESSA REGIONS OF THE UKRAINIAN SSR

L.R. Lisina and E.S. Kheylo

ABSTRACT: Astroclimatic conditions of two points in the Ukrainian SSR (Dubrovka in the Transcarpathian and Zhovtnevoye in the Odessa region) are compared. The observations were carried out during the summer of 1961. Data on image quality and flickering and atmospheric transmission were obtained.

The Main Astronomical Observatory of the Academy of Sciences /118
of the Ukrainian SSR is investigating the astroclimate of certain regions of the Ukraine, for the purpose of selecting a site which would be suitable for establishing an astrophysical branch of the Main Astronomical Observatory. We present the results of examination of two points, one of which is located in the village of Dubrovka in the Uzhgorod sector of the Transcarpathian region, and the other in the vicinity of Zhovtnevoye village in the Bolgrad sector of the Odessa region. Research at the first point was carried out from May 16 to August 16, 1961, and at the second point from May 25 to August 31, 1961. Investigations in the village of Zhovtnevoye were carried out in conjunction with the Odessa Astronomical Observatory.

General description of the points of observation. Dubrovka village is located five kilometers from the large village of Sredneye through which the Uzhgorod - Mukachevo highway passes. The site chosen for investigation is located in a hilly region on a flat-topped hill two kilometers to the west of Dubrovka. The city of Uzhgorod is located 25-30 km to the north-west of the point of observation, while Mukachevo is 20 km to the south-east. Uzhgorod is hidden behind two low mountain passes, while in the direction of Mukachevo the district is open. To the west the horizon is open; on the south it is blocked by a mountain up to a height of 3° (with an azimuth of 10°). The horizon to the north and east is hidden by mountains up to 7-10° above it. The soil in the region under investigation contains a large amount of clay. When it is not raining, the lowest atmospheric strata absorb a large amount of dust. There are no large bodies of water in the vicinity. A brook with a width up to 5 m runs through Dubrovka, while nearby there is a canal approximately 10 m wide. During the months of research that were spent in this area, there was no fog over these waterways.

The observational point in the Odessa region was located near the village of Zhovtnevoye, which is in a gully 3 km to the west of the point of observation. Bolgrad is in the same direction, at a distance of 10 km. The locality is level, the soil is "black

earth". Seven kilometers to the south-east there is a fresh-water inlet. There are no other bodies of water. The horizon is open on all sides.

The program of observations consisted of two parts: astronomical and meteorological. The astronomical part included: (1) a visual estimate of the quality of star images according to the stability of the diffractional pattern; (2) investigation of atmospheric stability through visual and photographic observations of the flickering amplitude of stellar images and the limbs of planetary disks; (3) an estimate of daytime atmospheric stability from observations of oscillation of the limb of the solar disk (visual); (4) photoelectric determination of the atmosphere's transmission coefficient. /119

We planned to begin the first series of astronomical observations half an hour after sunset, the second at midnight and the third half an hour before sunrise. But in the short June nights, only two series of observations were carried out.

Meteorological observations were carried out every four hours and included only measurement of air temperature in the shade, an approximate determination of the direction of the wind and an estimate of cloudiness on a 10-point scale (0 is completely clear, 10 is dense cloudiness).

Equipment of the outpost. The Transcarpathian outpost was supplied with an AZT-7 reflector with a D.D. Maksutoy system (mirror diameter = 20 cm), which was set up on a parallactic APSh-40 base with an AChM-3 clock drive mechanism. In addition the following were involved in assembly of the apparatus: a standard AFM-3 electrophotometer, an optical extension and a plate-holding device. The extension allowed us to increase the equivalent focal distance of the telescope to 10 m, while without the extension it was only 2 m.

The observations at the Odessa outpost were carried out on several instruments. In order to determine the quality of the star images we used a refractor with a "Merts" objective with a diameter of 150 mm, and focal distance of 2900 mm and a C-10 eyepiece, such that the magnifying power of the telescope was equal to 290. The telescope tube was placed on a parallactic base with a clock drive mechnaism.

Image flickering was observed on a horizontal telescope with an ATsU-2 coelostat device. The telescope tube was constructed in Odessa University laboratories. The diameter of the telescope's objective is 100 mm, the focal distance is 4000 mm. The observations were carried out at a magnification of 500. The horizontal telescope was set up on brick supports. The observations for determining the transmission coefficient were carried out by means of an electrophotometer, constructed at the Main Astronomical Observatory by the engineer K. Ye. Skorik, and placed in the focus

of a school refractor (objective diameter 80 mm and focal distance 800 mm).

In the focus of the telescope's objective was placed a mirror slit whose plane is inclined toward the focal plane at an angle of 45%. Behind it were the shutter, the light etalon (luminophor) and the light filter. The light receiver was a photomultiplier FEU-19M, whose current was amplified by a two-stage amplifier and was fed to a measuring device. The electrophotometer was charged by a high- /120
voltage battery and an L-6 runner with generator.

Method of observation and processing. According to the observational program, the image quality was estimated on the five-point Danjon and Coudere system [1]. Stars at various zenith distances and at various azimuths were chosen. Ten to twelve stars were observed in a single series. Processing of the observations consisted of calculating the value of the angle of turbulence $t''(z)$ characterizing atmospheric instability at a given moment of time and in a given direction. The value of the angle of turbulence was determined from the appearance of the star images. For each series of observations, graphs of the dependence of the value of the angle of turbulence on sec z were constructed. From these graphs the value of the turbulence at the zenith was determined as the ordinate of a point with abscissa equal to one ($z = 0°$).

Since atmospheric stability was estimated from the value of the amplitude of stellar flickering (or of oscillation of the limb of the solar disk) on different instruments in the Transcarpathian and Odessa outposts, it was impossible to use the same methods in both places.

Capron cross-hairs are stretched in the eyepiece of the AZT-7: three in one direction and three perpendicular to the first, with the same distance (3.2″) between them.

On the horizontal telescope, there were two pairs of cross-hairs: movable and fixed. The first pair shifted position by means of a micrometer screw with a numbered drum. The scale value of the drum was obtained from observations of the passage of stars through the telescope's field of vision with the clock mechanism shut off. The angular distance between the cross-hairs of the movable pair was equal to 3.2″, as on the AZT-7.

The flickering amplitude was estimated from the visible deviations of the image of a star (or of the limb of the disk of a planet or the Sun) from the cross-hairs, in the distance intervals between them. In processing these observations, the flickering amplitudes were calculated in angular measure and graphs of the dependence of this balue on the time were constructed for various zenith distances. On the Transcarpathian expenition these groups were divided into observations for which the mean value of the zenith distances were approximately 20, 40, 60° respectively. On the Odessa expedition

the mean values of the zenith distances of the groups were approximately 30, 40, 60°.

From these data we constructed graphs of the dependence of the mean value of amplitude flickering on z. The values of the flickering at the zenith were found by dividing the flickering at a given /121 zenith distance by the value of sec z.

Photographic observations of flickering were carried out only in Dubrovka. The plate holders of the AZT-7 telescope fit 4.5 × 4.5 cm plates and encompass a field through which an equatorial star in its diurnal motion passes in 2.5 min.

Due to the small relative aperture of the telescope with the ten-meter focus (1:50), only the bright stars Vega, Arcturus, Altair and Deneb were photographed.

In order to obtain the flickering values, the star traces were measured under the microscope. The deviations from the mean direction of the trace were determined for several tens of points and the mean square values of the deviations for a given trace were found in linear units and then converted to angular units. The values of the flickering amplitude at the zenith, as in the case of visual observations, were obtained by assuming the flickering to be proportional to sec z. The transmission coefficient p was obtained from the ratio

$$\log P_\lambda = \frac{\log E - \log E_0}{M},$$

where E is the recorded brightness of the star, E_0 is its extra-atmospheric brightness, expressed in units of the instrument's scale, M is the atmospheric mass corresponding to a given zenith distance, λ is the wavelength. In this case both expeditions used identical photomultipliers and SZS-9 light filters, such that the effective wavelength was 430 mμ.

In the observations, we took three readings of the etalon's brightness, then three readings from the star and again three from the etalon, in order to check the constancy of the instrument's performance. For the same reason, we continually checked the "zero constancy", since with a completely darkened photocathode the reading on the instrument's scale must be equal to zero. For the purpose of processing the observations we constructed graphs of the dependence of log E on M. For nights characterized by the straight-line graph of this dependence, log E_0 were found as the ordinate of the point of intersection of the straight line with the log E axis. The values obtained for E_0 were averaged and from them we calculated P_λ for all observations, after which we constructed graphs of the variation of P_λ with time.

The observational results. In Dubrovka the estimated values of image quality ranged from two to five with a mean value of four. In Zhovtnevoye these estimates varied from one to five with a mean value of two.

We found the single-valued correlation between the values of the estimates of image quality in points and the value of the angle of turbulence in seconds of arc, based on which we obtained the mean value of the angle of turbulence at the zenith: at Zhovtnevoye 0.20″; at Dubrovka, o.52″. /122

Figure 1 shows the change of the angle of turbulence in the course of a night. As can be seen, this angle changes very little during the night at both locations. Thus it follows from the obtained data that at Zhovtnevoye the angle of turbulence is significantly smaller than at Dubrovka.

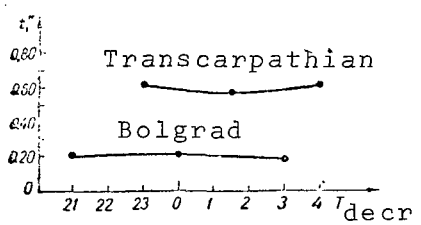

Fig. 1.

The mean values of the flickering amplitude for the groups, according to visual observations, are given in Table 1. The graphs of the variation of the flickering amplitude from night to night during July and August in Zhovtnevoye are given in Figure 2, and for June, July and August in Dubrovka in Figure 3.

If we consider that the flickering amplitude is proportional to sec z, then at $z = 0°$, in Zhovtnevoye $\Delta = 0.30''$, and in Dubrovka $\Delta = 0.60''$.

TABLE 1

Point of Observation	20°	30°	40°	60°
Zhovtnevoye	—	0.36″	0.30″	0.60″
Dubrovka	0.60″	—	0.90″	1.00″

The flickering amplitudes according to photographic observations in Dubrovka are given in Table 2. We must point out that visual estimates give a somewhat greater value to the flickering amplitude. This is natural, since a photograph records all deviations of the star image from the mean location, while visually, only deviations of great amplitude are noticed. Thus, with respect to the amount of amplitude flickering as well, the point in Zhovtnevoye is the better of the two.

The value of the transmission coefficient appeared to be equal to 0.60 at both sites. The curve of the change of this coefficient with time during June-August in Zhovtnevoye is shown in Figure 4, and for August in Dubrovka, in Figure 5.

An important aspect of the astroclimate is the number of clear /123 nights and the stability of clear weather. We agreed to consider clear nights those in which the sky remained completely free of

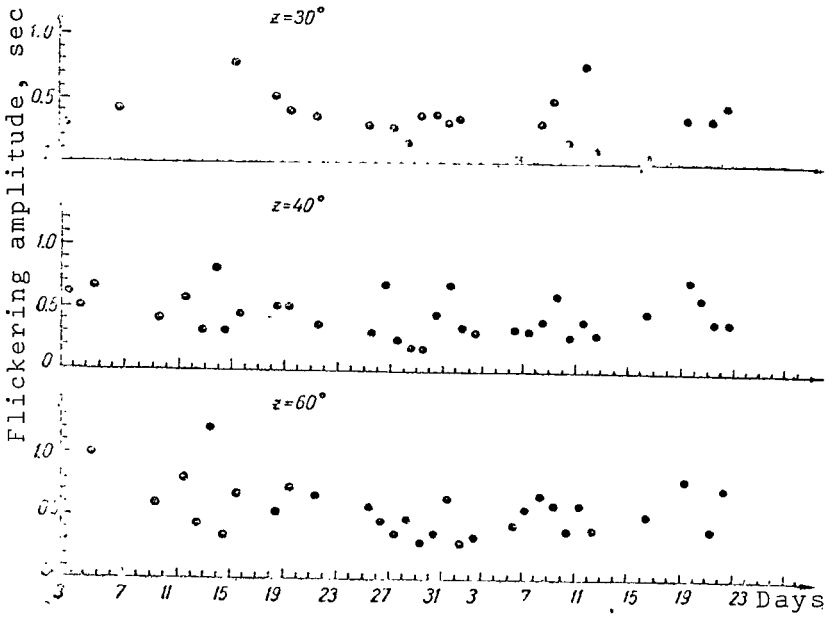

Fig. 2.

clouds, and nights suitable for observation, those in which it was possible to carry out even one series of observations. The number of "clear" and "observational" nights and their percentage with

TABLE 2

Date	No. of Plates	Δ_z	z	$\Delta_0 (z=0'')$
June 24	7	0.32″	14.5°	0.31″
29	15	0.41	38.2	0.32
July 3	21	0.30	3.8	0.30
3	21	0.50	25.1	0.48
4	23	0.55	13.1	0.54
4	23	0.28	20.4	0.26
6	24	0.50	40.5	0.38
Average	—	—	—	0.37

respect to the total number of days of research of the expeditional outposts are given in Table 3. We must point out that in Zhovtnevoye the weather remained clear eight days in a row.

The mean value of the temperature between noon and midnight in Zhovtnevoye was approximately 10° C, in Dubrovka, approximately 15°C.

/124

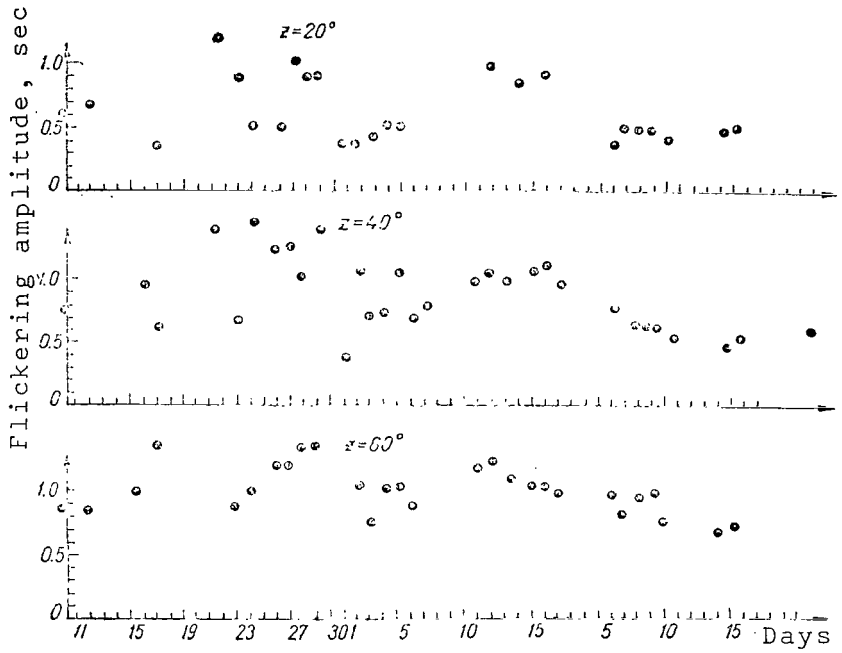

Fig. 3.

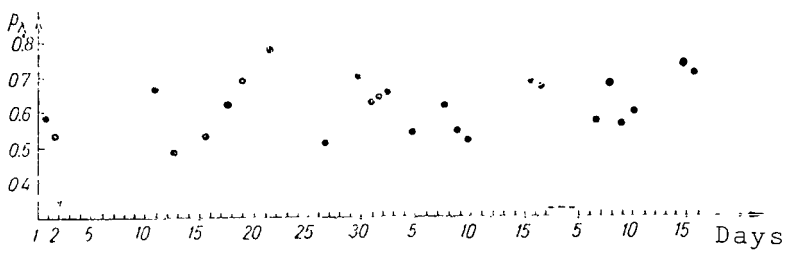

Fig. 4.

/125

TABLE 3

Point of Observation	Number of Days of Research	Observational Nights		Clear Nights	
		Number	%	Number	%
Zhevtnevoye	87	57	66	41	47
Dubrovka	77	49	64	15	19

Zhovtnevoye was characterized by the presence of wind, generally abating towards night. The sky in Dubrovka is noticeably illuminated by the lights of Uzhgorod and Mukachevo, while in Zhovtnevoye it is sufficiently dark. Furthermore, during all the time of observations in Dubrovka there was not a single cloudless day, and there was

always mist at the horizon, sometimes reaching as high as 15-20° above the horizon.

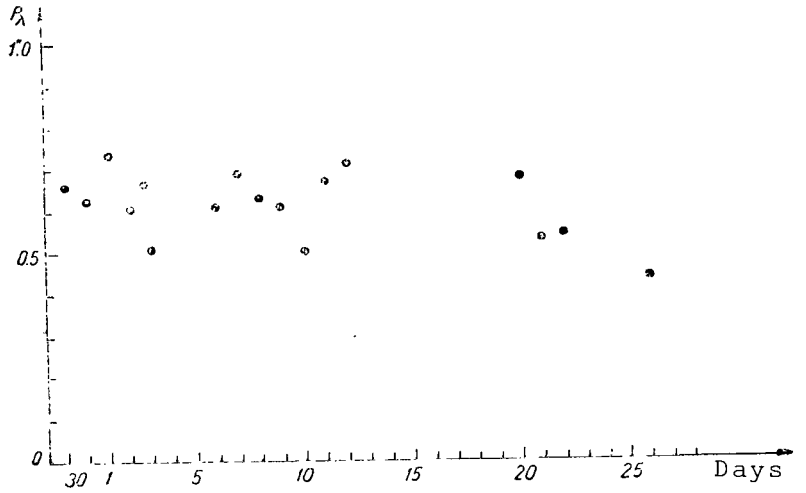

Fig. 5.

References

/126

1. Danjon, A. and A. Coudere: Astr. Zhurn., Vol. 17, p. 1, 1940.
2. Kurs astrofiziki i zvezdnoy astronomii (Course in Astrophysics and Stellar Astronomy). Ed. A.A. Mikhaylova. Gostekhizdat, Moscow, Leningrad, pp. 497-503, 1951.

INVESTIGATION OF FLICKERING AMPLITUDE COMPONENTS BY TRACES OF ARTIFICIAL SATELLITES: THE BEADED STRUCTURE OF STAR TRACES

I.V. Shvalagin and Ya.M. Sinichenko

ABSTRACT: The article proves that image motion determined from the traces of stars and artificial satellites and obtained at roughly the same time is approximately equal. The beaded structure of satellite traces is studied. The mean value of the interval between the beads is 0.91 sec.

Investigation of the Dependence of the Flickering Amplitude on the Direction of the "Unfolding" of a Trace

/127

Deviations of the image of a heavenly object in the focal plane of a telescope from a determined mean location, which arise as a result of the optical instability of the Earth's atmosphere, have a random character. The methods for determining flickering from the traces of star images provides an opportunity to obtain a single flickering component, namely that perpendicular to the direction of the star's "unfolding", i.e. the direction of the motion of the star image across the plate when the telescope tube is motionless.

If, as was noted in reference [1], the "unfolding" of the trace is accomplished by means of a special plate holder in which the plate may shift through various angles to the horizon, while remaining in the focal plane, then the mean flickering amplitude does not depend on the direction of the "unfolding". However, this problem may be considered as not yet investigated [2]. Reference [3] emphasizes the necessity of investigating the components of flickering in the direction of the diurnal motion of star images: in the direction of the trace itself.

It is possible to investigate the dependence of the flickering amplitude on the direction of "unfolding", from the traces of the moving images of slow, fairly bright satellites, since in this case the direction of "unfolding" depends on the elements of the satellite's motion and can be varied [4].

In order to solve this problem, observations were carried out in the following manner: the visible motion of the satellite was observed in the telescope's guide. A section of the sky with a star of 2.5-3.5 stellar magnitude was chosen along the presumed route of the moving object before its appearance. For twenty seconds after fixing the main tube of the telescope on this section of the sky, the trace of the satellite and simultaneously the trace of the star were photographed. However, due to the difference of the visible speeds of the satellite (v_{sat}) and the star (v_{st}), the star's

trace proved to be significantly shorter than that of the satellite. Thus, for instance, for an equatorial star in the focal plane of the AVR-2 telescope (F = 3000 mm), v_{st} = 0.2 mm/sec; however, if the visible speed of the satellite ω = 0.1 degree/sec, then v_{sat} = 5 mm/sec in the focal plane. On a 9 × 12 cm photographic plate /128 with an exposure time of 18 sec, the trace of the satellite was 9 cm, while the trace of an equatorial star was 3.6 mm long. For every 0.1 mm along the star's trace, only 36 deviations could be measured. Therefore, after the satellite had passed through the field of vision of the telescope's main tube, the exposure to the star was continued. As a result, in 7-8 min we obtained a star trace which also covered the entire length of the plate. In this case it is impossible to find a correlation between the simultaneous deviations along the full length of the traces of the star and the satellite. From the traces of the star and the satellite it is possible to determine only the mean square value of the flickering amplitudes σ_{st} and σ_{sat} respectively. Therefore, if there were no stars of 2.5 to 3.5 magnitude in the area of the satellite's motion, we photographed 5-7 stars at various zenith distances, separated from one another by 10-15°.

The results of processing the plates are given in Table 1, in which ϕ is the angle between the diurnal circle and the visible path of the satellite, i.e. on the photographic plate this is the angle between the track of the star image and the track of the satellite image. The angle ϕ was determined directly from the plate.

It follows from Table 1 that $\sigma_{st} \approx \sigma_{sat}$. The mean square value of the differences of $\sigma_{st} - \sigma_{sat}$ is ± 0.06".

In motion of the star image on the plate, the main component of its displacement along the trace is caused by its diurnal motion. In motion of the satellite;s image, this main component of displacement is determined by the angular shift of the satellite on the celestial sphere. However, due to image flickering, in the case of stars, as in the case of a satellite, supplementary displacements arise along the trace. The mean square value of these displacements

TABLE 1

Z	φ	σ_{st}	σ_{sat}	Z	φ	σ_{st}	σ_{sat}
89	00	0.86	0.90	69	38	0.82	0.89
21	00	0.93	0.92	48	36	0.46	0.56
50	00	0.51	0.46	35	35	0.37	0.42
71	00	0.64	0.69	29	28	0.31	0.38
21	00	0.34	0.34	27	20	0.32	0.34
22	00	0.30	0.25	66	45	0.71	0.65
38	80	0.46	0.45	56	36	0.52	0.55
46	80	0.53	0.59	37	33	0.30	0.34
68	31	0.62	0.63	41	84	0.69	0.59
70	32	0.68	0.76	56	75	0.48	0.44
				63	75	0.54	0.43

is designated by σ_x. From the data in Table 1 it is evident that, /129 regardless of the value of the angle ϕ, the value of σ_y is the same for both the star and the satellite, in other words, it can be considered that in general $\sigma_x \approx \sigma_y$. Thus, the complete displacement of the image $\sigma = \sqrt{2}\sigma_y$.

For the Uzhgorod station, $\sigma_y = 0.28''$ at $Z = 0°$; hence $\sigma = 0.39''$ at the same Z.

The Bead Structure of Star Traces

In detailed examination of star traces it was observed that they do not have identical darkening along their full length. Clumps and gaps are observed, i.e. the so-called bead structure. A number of authors have written on this, but this phenomenon was most closely investigated by Ye.Ya. Boguslavskaya [4] and I.G. Kolchinskiy [2]. Ye.Ya. Boguslavskaya from observations on the large astrograph at Moscow, found that the mean distance between the beads $\tau = 0.3$ sec., while on a wide-angle astrograph $\tau = 0.37$ sec, and on a coronograph $\tau = 0.34$ sec. I.G. Kolchinskiy found that the distance between beads ranged between 0.33 sec. and 0.86 sec.. I.G. Kolchinskiy indicated that the bead structure is related to the low-frequency scintillation component.

Since we did not devote particular attention to investigation of scintillation, we decided to estimate it by using the beaded structure of star traces.

Out of 295 traces examined, the bead structure was observed in 214 cases, and primarily at large zenith distances $Z > 50°$. In general all the traces can be divided into the following groups: (1) traces with very sharply defined structure; beads are clustered in groups along the trace, but there are also single beads (38 traces); (2) traces with clearly evident beads, but whose borders are not sharply defined (37 traces); (3) traces with a weakly expressed bead structure (136 traces); (4) traces with no beads whatsoever (84 traces).

It is very difficult to say anything about the appearance of the beads. We observed beads in the form of separate points on the trace, sometimes having a completely round shape, sometimes in the form of dashes, and also in the form of "rice grains" of irregular form, inclined towards the trace line.

In order to determine the interval between the beads, 15 traces with sharply defined bead structure were processed. Intervals 20 mm long were measured on each trace. As an example in Table 2 we give the results of processing of a trace obtained at $Z = 66°$.

TABLE 2 /130

τ_1, sec	τ_2, sec	τ_3, sec	τ_1, sec	τ_2, sec	τ_3, sec
1.22	0.72	0.59	1.34	0.42	0.72
1.01	0.55	0.57	0.86	0.45	0.58
0.80	0.59	0.55	0.95	0.52	0.72
0.66	0.62	0.18	0.76	0.48	0.28
0.85	0.40	0.38	1.35	0.55	0.91
0.79	0.53	0.42	1.80	0.36	1.34
0.82	0.46	0.36	0.46	0.62	0.46
1.00	0.49	0.46	0.67	0.57	0.40
0.86	0.46	0.41	1.06	0.51	0.56
			0.88	0.16	0.32

The second column gives the intervals between the beads τ_1, the third column contains the lengths of the beads τ_2 and the fourth column gives the length of the gaps between the beads τ_3.

In Table 3 we give the mean values of τ_1, τ_2 and τ_3 for 15 star traces.

TABLE 3

Z	δ	τ_1, sec	τ_2, sec	τ_3, sec
45°	+10°	0.73	0.51	0.60
65	−16	0.85	0.62	0.47
66	−16	0.90	0.51	0.47
42	+05	0.56	0.34	0.23
73	−29	0.78	0.50	0.38
67	−18	0.90	0.66	0.49
70	−18	0.85	0.49	0.39
48	+01	0.82	0.52	0.29
75	−28	0.92	0.50	0.46
80	−30	0.92	—	—
64	−06	1.06	—	—
67	− 8	0.96	—	—
74	−25	1.10	—	—
69	−18	1.10	—	—
72	−18	1.25	—	—

Thus, the mean value of the interval between the beads, according to our investigations, is equal to τ_1 = 0.91 sec. We point out that the mean value of the interval between the beads for Goloseyevo is τ = 0.53 sec [2].

For purposes of comparison with the data on the bead structure of traces obtained by I.G. Kolchinskiy in Kiev [2], in Table 4 we give analogous data for Uzhgorod. The mean value of the bead/gap ratio coincides approximately with the data of I.G. Kolchinskiy, /131 who obtained a value of 1.5 for this ratio [2].

TABLE 4

No. of Traces	Interval, sec		Bead/Gap Ratio	Bead-Gap Difference
	Beads	Gap		
1	0.66	0.49	1.34	0.17
2	0.49	0.39	1.25	0.10
3	0.52	0.29	1.79	0.23
4	0.62	0.47	1.30	0.15
5	0.34	0.23	1.48	0.11
6	0.50	0.48	1.04	0.02
7	0.51	0.47	1.08	0.04
8	0.50	0.46	1.09	0.04
Average	0.52	.41	1.30	0.11

References

1. Kolchinskiy, I.G.: In the book: Trudy soveshchaniya po issledovaniyu mertsaniya zvezd (Transactions of the Conferences on Investigation of Stellar Scintillation). Academy of Sciences USSR Press, Moscow, Leningrad, pp. 145-155, 1959.
2. Kolchinskiy, I.G.: Opticheskaya nestabil'nost' zemnoy atmosfery po nablyudeniyam zvezd (Optical Instability of the Earth's Atmosphere According to Observations of Stars). "Naukova dumka" Press, Kiev, 1967.
3. Vasil'yev, O.B.: In the book: Opticheskaya nestabil'nost' zemnoy atmosfery (Optical Instability of the Earth's Atmosphere). "Nauka" Press, pp. 40-48, 1965.
4. Bratiychuk, M.V. and I.V. Shvalagin: Byull. stantsiy opticheskogo nablyudeniya iskusstvennykh sputnikov Zemli. Vol. 49, pp. 18-22, 1967.
5. Boguslavskaya, Ye.Ya.: In the book: Trudy soveshchaniya po issledovaniyu mertsaniya zvezd (Transactions of the Conference on Investigation of Starlight Scintillation). Academy of Sciences USSR Press, Moscow, Leningrad, pp. 173-181, 1959.

Translated for the National Aeronautics and Space Administration by:
Aztec School of Languages, Inc.,
Research Translation Division (456)
Maynard, Massachusetts.
NASw-1692.

"The aeronautical and space activities of the United States shall be conducted so as to contribute . . . to the expansion of human knowledge of phenomena in the atmosphere and space. The Administration shall provide for the widest practicable and appropriate dissemination of information concerning its activities and the results thereof."

—NATIONAL AERONAUTICS AND SPACE ACT OF 1958

NASA SCIENTIFIC AND TECHNICAL PUBLICATIONS

TECHNICAL REPORTS: Scientific and technical information considered important, complete, and a lasting contribution to existing knowledge.

TECHNICAL NOTES: Information less broad in scope but nevertheless of importance as a contribution to existing knowledge.

TECHNICAL MEMORANDUMS: Information receiving limited distribution because of preliminary data, security classification, or other reasons.

CONTRACTOR REPORTS: Scientific and technical information generated under a NASA contract or grant and considered an important contribution to existing knowledge.

TECHNICAL TRANSLATIONS: Information published in a foreign language considered to merit NASA distribution in English.

SPECIAL PUBLICATIONS: Information derived from or of value to NASA activities. Publications include conference proceedings, monographs, data compilations, handbooks, sourcebooks, and special bibliographies.

TECHNOLOGY UTILIZATION PUBLICATIONS: Information on technology used by NASA that may be of particular interest in commercial and other non-aerospace applications. Publications include Tech Briefs, Technology Utilization Reports and Technology Surveys.

Details on the availability of these publications may be obtained from:

SCIENTIFIC AND TECHNICAL INFORMATION DIVISION

NATIONAL AERONAUTICS AND SPACE ADMINISTRATION

Washington, D.C. 20546